RAPID EXPOSURE ASSESSMENT OF COMPLEX ENVIRONMENTAL SAMPLES IN DISASTER RESEARCH USING TRADITIONAL AND NOVEL METHODS

A Dissertation

by

NOOR ALAA ALY

Submitted to the Graduate and Professional School of
Texas A&M University
in partial fulfillment of the requirements for the degree of

DOCTOR OF PHILOSOPHY

Chair of Committee,	Ivan Rusyn
Committee Members,	Weihsueh Chiu
	Thomas McDonald
	Erin Baker
Head of Department,	Ivan Rusyn

December 2021

Major Subject: Toxicology

ABSTRACT

Chemical contamination following environmental disasters profoundly effects the environment and human health. Exposure assessment is traditionally performed using Gas Chromatography-Mass Spectrometry (GC-MS) and Liquid Chromatography-Mass Spectrometry (LC-MS). While these methods are the accepted analytical techniques for exposure studies, they can take hours to process a single sample and often require unique sample preparation based on the target compounds. Limitations in the throughput of current analytical technologies is a critical gap in disaster research. Ion Mobility Spectrometry-Mass Spectrometry (IMS-MS) is a novel technology which is a rapid analytical method and can be used to detect a wide range of chemicals based on unique mass-to-charge (*m/z*) and collision cross section (CCS). This proposal's objective is to compare and develop methods for rapid exposure assessment of complex environmental samples in disaster research with the use of traditional and novel methods. Foremost, we will perform a series of studies using traditional analytical methods for exposure assessment of soil and water samples. We will test the hypothesis that spatial and temporal trends of common pollutants including PFAS, PAHs and metals can be determined using these methods. Then, we will use IMS-MS to characterize persistent organic pollutants and their metabolites and degradation products. We will test the hypothesis that IMS-MS can be used for the identification and detection of common environmental contaminants in a complex sample. Overall, this work will demonstrate IMS-MS can be used for environmental sample analysis and will aid in the critical need for increased throughput and response time in disaster research.

DEDICATION

I would like to dedicate my dissertation work to my family. I am especially grateful for my parents, Alaa and Ghada for all their love and support. My sister, Sarah, who has always wanted to be a dedicatee, I look up to you and I am thankful to have you by my side. Without all your lifelong guidance, I would not be where I am today. Thank you.

I would also like to dedicate this dissertation to my mentor, Dr. Ivan Rusyn. Your faith and encouragement in me have led me to grow and become the scientist I am today. Thank you for your guidance over the last three years.

ACKNOWLEDGEMENTS

First, I would like to thank my committee chair and mentor, Dr. Ivan Rusyn, for his leadership, guidance, and support throughout the course of my doctoral studies and research. Thank you for always holding me to the highest standard and inspiring me to strive to reach my full potential. I would also like to thank my committee members, Drs. Erin Baker, Thomas McDonald and, Weihsueh Chiu for their guidance, feedback, and support during my graduate education. Sincere thanks go to these and many other professors who have taught me, both professionally and personally, throughout my time at Texas A&M University.

Next, I would like to thank my colleagues and friends in the Rusyn lab and Interdisciplinary Toxicology program for their camaraderie and encouragement, and for making my experience at Texas A&M a meaningful and memorable one. Many thanks also go to the faculty and staff in the Department of Veterinary Integrative Biosciences, and especially to Kim Daniel, for being a consistent source of guidance, knowledge, and encouragement.

I would also like to thank my mom (Ghada), my dad (Alaa), and my sister (Sarah) who have always supported me to follow my dreams, encouraged me to strive for my best, and been there both to celebrate my successes and to help navigate the challenges.

Lastly, I would like to thank our collaborators, contributors, and funding sources, without whom this work would not be possible. Thank you to Dr. Terry Wade and Yina Liu (Texas A&M University Geochemical and Environmental Research Group) for chemical analysis of environmental samples collected in these studies. Many thanks also

go to Dr. Erin Baker and Dr. James Dodds (North Carolina State University), for their expertise and advice on Ion Mobility. I would also like to thank Drs. Yu-Syuan Luo, Gaston Casillas, James Kaihatu, and Fabian Grimm for your collaboration and efforts on the work presented herein. Many thanks also go to Dr. Elena Craft of the Environmental Defense Fund and Dr. Michael Honeycutt of the Texas Commission of Environmental Quality for their assistance in environmental sampling logistics and helpful discussion. I would also like to thank Entanglement Technologies and the Galveston Bay Foundation for assistance in collection of environmental samples.

CONTRIBUTORS AND FUNDING SOURCES

Contributors

This work was guided by a dissertation committee consisting of Drs. Ivan Rusyn, Weihsueh A. Chiu and Thomas J. McDonald, of the Department of Veterinary Integrative Biosciences at Texas A&M University and Dr. Erin S. Baker of the Department of Chemistry of North Carolina State University.

A portion of the sample collection in Chapter 2 was done by the Galveston Bay Foundation and Dr. Gaston Casillas of the Department of Veterinary Integrative Biosciences. The instrumental analysis of samples in Chapter 2 was conducted by the Texas A&M University Geochemical and Environmental Research Group. A portion of the models and visualization presented in Chapter 2 were created by Drs. Gaston Casillas and James M. Kaihatu of the Department of Veterinary Integrative Biosciences and Department of Civil and Environmental Engineering. A portion of data analysis in Chapter 2 were conducted by Drs. Sharmila Bhandari and Weihsueh A. Chiu of the Department of Veterinary Integrative Biosciences and Dr. Mikyoung Jun of the Department of Statistics. A portion of the sample collection in Chapter 3 was done by Dr. Gaston Casillas of the Department of Veterinary Integrative Biosciences. The instrumental analysis of samples in Chapter 3 was conducted by the Texas A&M University Geochemical and Environmental Research Group and TDI Brooks International. A portion of data analysis in Chapter 3 were conducted by Dr. Weihsueh A. Chiu of the Department of Veterinary Integrative Biosciences. All other work conducted for this dissertation was completed by Noor A. Aly independently.

Funding Sources

Doctoral studies were supported by the National Institutes of Health (NIH) T32 Ruth L. Kirschstein Institutional National Research Service Award "Regulatory Science in Environmental Health and Toxicology" Training Grant Number ES026568, funding for the Ivan Rusyn laboratory, and institutional support from Texas A&M University.

This work was also made possible in part by the U.S. Environmental Protection Agency (EPA) Science to Achieve Results (STAR) Research Program under Grant Number RD84003201, NIH P42 Hazardous Substances Basic Research Grants Program under Grant Number ES027704 and ES031009, and NIH P30 Center Core Grants Program under Grant Number ES029067 and ES025128. The contents of this work are solely the responsibility of the authors and do not necessarily reflect the official views of the NIH or EPA. The use of specific commercial products in this work does not constitute endorsement by the authors or the funding agencies.

NOMENCLATURE

ACS	American Chemical Society
AFFF	Aqueous Film Forming Foam
APPI	Atmospheric Pressure Photoionization
ASE	Accelerated Solvent Extraction
ATSDR	Agency for Toxic Substances and Disease Registry
BL	Bladen County
BPA	Bisphenol A
C_{BL}	Concentration of Metal in Bladen County
CCS	Collision Cross Section
CDC	Centers for Disease Control and Prevention
CERCLA	Comprehensive Environmental Response, Compensation, and Liability Act
DBOFB	4,4-dibromooctafluorobiphenyl
DCVC	Dichlorovinyl-L-cysteine
DCVG	Dichlorovinyl-L-glutathione
DDD	Dichlorodiphenyldichloroethane
DDE	Dichlorodiphenyldichloroethylene
DDMU	1,1-Bis(p-chlorophenyl)-2-chloroethene
DDT	Dichlorodiphenyltrichloroethane
DI	Deionized
DR2	Disaster Research Response
^{DT}IMS	Drift Time Ion Mobility Spectrometry
EPA	Environmental Protection Agency
ES	Extraction standard
ESI	Electrospray Ionization
ESRI	Environmental Systems Research Institute
FID	Flame Ionization Detection
FIMS	Flow Injection Mercury System
FTAB	Fluorotelomer Sulfonamidoalkyl Betaine
FTS	Fluorotelomer Sulfonate
FTSAS	Fluorotelomer Thioether Amido Sulfonate
GB	Galveston Bay
GC-MS	Gas Chromatography - Mass Spectrometry
GIS	Geographic Information Systems
GPS	Global Positioning Systems
GULT	Glutathione S-transferases
HDPE	High-Density Polyethylene
HI	Hazard Index

HQ	Hazard Quotient
HRMS	High Resolution Mass Spectrometry
HSC	Houston Ship Channel
IARC	International Agency for Research on Cancer
ICP-MS	Inductively Coupled Plasma -Mass Spectrometer
IMS-MS	Ion Mobility Spectrometry - Mass spectrometry
IS	Injection Standard
ITC	Intercontinental Terminal Company
ITRC	Interstate Technology and Regulatory Council
LC-MS	Liquid Chromatography-Mass Spectrometry
LLOQ	Lower Limit of Quantitation
LOD	Limit of Detection
LOQ	Limit of Quantitation
MPFAC	Mass-Labelled PFCAs
NAC-DCVC	N-acetyl-S-(1, 2-dichlorovinyl)-cysteine
NAC-TCVC	N-acetyl-S-(1, 2-trichlorovinyl)-cysteine
NEPA	National Environmental Policy Act
NIEHS	National Institutes of Environmental Health Science
NOAA	National Oceanic and Atmospheric Administration
OH	Hydroxyl
PAH	Polyaromatic Hydrocarbon
PCB	Polychlorinated Biphenyl
PCE	Tetrachloroethylene
PCPP	Pharmaceuticals and Personal Care Products
PFAS	Per- and Polyfluoroalkyl substances
PFBA	Perfluorobutanoic acid
PFBS	Perfluorobutanesulfonic Acid
PFDA	Perfluorodecanoic Acid
PFHpA	Perfluoroheptanoic Acid
PFHxA	Perflurohexanoic Acid
PFNA	Perfluorononanoic Acid
PFOA	Perfluorooctanoic Acid
PFOS	Perfluorooctane Sulfonate
PI	Pyrogenic Index
PM	Particulate Matter
POP	Persisitent Organic Pollutant
QC	Quality Control
QTOF	Quadropole Time-of-flight
RBF	Radial Basis Functions
SCF	Supercritical Fluid Chromatography

SPE	Solid Phase Extraction
SRM	Standard Reference Material
SSL	Soil Screening Levels
SULT	UDP-glucuronosyltransferases
TCE	Trichloroethylene
TCEQ	Texas Commission of Environmental Quality
TCMX	2,4,5,6-tetrachloro-m-xylene
TCVC	Trichlorovinyl-L-cysteine
TCVG	Trichlorovinyl-L-glutathione
TEF	Toxic Equivalency Factors
USGS	United States Geological Survey
WAX	Weak Anion Exchange

TABLE OF CONTENTS

Page

LIST OF FIGURES

LIST OF TABLES

Page

CHAPTER I

1. INTRODUCTION

1.1. Disaster Research: Background and the current state of exposure assessment of complex environmental samples

Environmental emergencies and disasters including weather-related or anthropogenic events often occur unexpectedly and can have severe impacts on humans and the environment. Weather processes, such as hurricanes, tornadoes, wildfires, earthquakes, and volcanic eruptions, have operated throughout Earth's history and serve important ecological purposes. Similarly, tropical storms are one of the most common occurring weather events, and the large amounts of rainfall and flooding are associated with many positive outcomes, for example by helping with drought mitigation and assisting human agricultural activities. The movement of wind and waves can break up stagnant bacteria and red tide, a harmful algal bloom that kills fish and makes shellfish dangerous to consume[1]. This wind movement also redistributes the Earth's heat and creates a global heat balance, without tropical storms the equator would be significantly warmer and the poles would be significantly cooler. Storms also increase nutrient density in sand, sediments and soils which allows for new growth in coral reefs and inland plants.[2] Wildfires are another example of a climate related event that serve important ecological purposes. They remove dead and decaying plant matter which increases soil fertility and promotes new growth. Many plants also require fire to continue their life cycles. For example, pine tree seeds are located inside a pinecone, the outer layer of the pinecone must be melted by fire for the seed to be released.[3] Today, humans perform prescribed

burns where they control the spread of the fire to allow for the ecological benefits of fire but reduce their potential harm on surrounding populations. Unfortunately, these natural processes also impact humans and often result in loss of life and property as well as have lasting hazardous health effects. The wind and flooding associated with storms can disperse contaminants. Water's access to poorly ventilated locations can result in mold, which can increase severity of respiratory diseases. Fires also distribute airborne particulate matter which are known to have negative human health outcomes. The World Meteorological Association released a report that climate and weather-related disasters surged five-fold over the last 50 years due to climate change[4]. With the increasing occurrences of these events it is of vital importance for us to understand their impacts on humans and the environment.

In 2020 there were 22 weather and climate events across the United States, breaking the previous record of 16 events occurring in 2017. These included tropical cyclones, severe storms, a drought, and wildfire and are estimated to have incurred $95 billion in losses[5]. Not only do these events cause physical and financial damages, but they can also result in unique combinations of human exposures and hazards. In 2005 Hurricane Katrina, a category 4 hurricane made landfall in the US and affected over 1.5 million people. Many federal agencies including The Environmental Protection Agency (EPA), National Institute of Environmental Health Sciences (NIEHS) and the Centers of Disease Control and Prevention (CDC) as well as state environmental and public health agencies worked together to determine what immediate human health risks were. This required the monitoring of water quality, wastewater, and air quality. In many locations

floodwaters were severely contaminated and sediment testing showed that many heavy metals were at levels considered hazardous for human exposure. Petroleum hydrocarbons, polycyclic aromatic hydrocarbons and pesticides were also detected in sediments. With this information, personal protective equipment could be recommended to first responders and recommendations could be made to the public on safe drinking water [6-7]. Long-term health effects of these events are difficult to predict since exposures are often complex and several factors such as pre-existing conditions, and socioeconomic status play a role. Studies have been conducted trying to assess the long-term impacts of hurricanes on various health risks [8]. The literature suggests an association between upper respiratory symptoms and mold exposure in the months following a hurricane[9]. Hurricanes have also been associated with pregnancy complications such as gestational hypertension and pre-term delivery in the months following a storm [10].

Unlike climate related events, anthropogenic disasters serve no ecological benefit, and they often result in far more dangerous outcomes. Humans have had an impact on the environment since the rise of agriculture. The industrial revolution marked a turning point, since then anthropogenic events have increased in both frequency and magnitude. These disasters often pose serious risks to humans and the environment. They can result in complex exposures which may be difficult to characterize and evaluate the associated potential risks. One such example was the collapse of the World Trade Center on September 11th, 2001. The destruction released more than a million tons of debris and dust, the components of the debris and the potential health impacts this had on rescue

workers and the population of Manhattan have since been well studied. However, at the time of the disaster much was misunderstood or unknown. The dust had aerodynamic particulates ranging in size upward from about 2.5 micrometers (μm) and contained a blended mixture of concrete, gypsum, and synthetic vitreous fibers, with metals, radionuclides, ionic species, and asbestos[11]. Further organic analyses revealed polycyclic aromatic hydrocarbons, polychlorinated biphenyls, and other hydrocarbons. This full characterization took years to complete and at the time there was little toxicity data on many of these compounds. Further, it was believed that components in the fine particulates (PM2.5) would be too small to produce measurable effects. Thus, many of the adverse health outcomes were not predictable. Twenty years later we understand that exposure to dust and debris resulted in adverse outcomes in respiratory and reproductive health as well as increase in cancer incidence[12].

The Deepwater Horizon oil spill of 2010 in the Gulf of Mexico is another event that impacted the ecosystems and resulted in additional impacts to human health. Approximately 210 million gallons of crude oil were released because of the explosion and an estimated 1.8 million gallons of chemical dispersants were used in response efforts. Some key pollutants of concern were hydrocarbons, particulate matter (PM), ozone, carbon monoxide, sulfur oxides and nitrogen oxides as well as a mixture of surfactants used as chemical dispersants. As would be expected, the Gulf ecosystem suffered greatly: large areas of coastal vegetation were destroyed and many marine species had increasing death and injury rates. Human health impacts were also recorded, especially for impacted communities along the gulf. These communities were especially

vulnerable in that they had a historic burden of health disparities, persistent environmental health threats, and residence in a geographic area prone to both natural and technologic disasters. This event specifically brought to light the lack of standardized study protocols to assess baseline and collect critical acute exposure data in the aftermath of an environmental emergency. This was an important motivation to the creation of the Disaster Response Research Program (DR2)[13].

Starting in the late 1960s and lasting through the 1980s, the United States created a series of environmental acts and policies to control, reduce and mitigate human impacts on the environment. This movement began with President Nixon's enactment of the National Environmental Policy Act (NEPA) in 1969, which required federal agencies to go through a formal process before taking any action anticipated to have substantial environmental impacts, shortly thereafter the Environmental Protection Agency (EPA) was formed. During this period the Comprehensive Environmental Response, Compensation, and Liability Act of 1980, otherwise known as CERCLA or Superfund, was put into place. This act provides a Federal "Superfund" by imposing a tax on chemical and petroleum industries to clean up uncontrolled or abandoned hazardous-waste sites as well as accidents, spills, and other releases of pollutants and contaminants into the environment[14].

The National Institutes of Environmental Health Science (NIEHS) has developed a Disaster Research Response Program (DR2): an initiative created to provide a framework for research related to public health emergencies. The DR2 aims to combine knowledge and skillsets from unique disciplines of environmental health sciences to

coordinate disaster research through publicly accessible data collection tools, a network of trained research responders and stakeholders, an integration with emergency response, recovery, and mitigation activities[15]. Following Hurricane Harvey, a category 4 storm that made landfall in Houston, Texas in 2017, researchers, media, state and local agencies, and nonprofit organizations conducted environmental and biological sampling, community health assessments and survey, developed registries to track long-term health impacts and supported access to health care. DR2 resources and partnerships improved coordination, effectiveness, and efficiency and allowed for the collected data to assess potential health effects and inform the public[16].

1.2. Current challenges and gaps in Disaster Research Response

Natural and anthropogenic disasters such as large precipitation events or chemical spills have the potential to impact environmental and human health adversely. Climate change and shifts in domestic economic activity have markedly increased the risk of chemical contamination events resulting from weather-related or anthropogenic emergencies. Due to the sudden and often unexpected nature of these events, disaster research faces several challenges. First, research must begin quickly and efficiently so that critical information is not lost. This requires secure funding, protocols that are already in place, and personnel who are trained to collect samples and gather relevant information. Integration with emergency management, health authorities and community engagement may also pose a challenge. Finally, health and environmental risks in emergencies are difficult to quantify – there are few tools to evaluate the increasing number of chemicals, the potential health hazards and the extent of exposure in an

emergency-type situation. Specialized equipment which is expensive and cumbersome is needed which further limits the areas and subjects that can be monitored. Exposure characterization is not only a general challenge in environmental health and regulatory toxicology, but it also is a common primary element in decision contexts that are related to evaluation and management of chemically-contaminated sites. (e.g., National Priority List Superfund sites). The complex exposure types as a consequence of these contamination events may have significant human and ecological adverse health impacts, creating an urgent need to rapidly and comprehensively evaluate unknown hazards in order to determine the risks and minimize the impact of the event on the community and the environment. The immediate health impacts and long-term consequences are often not well understood and basic questions concerning the safety and health of impacted communities remain unanswered. Therefore, efficient characterization of chemical contamination related to environmental disasters is vital for understanding the potential hazards of exposures and communicating the risk to stakeholders and affected communities. Finally, these disasters bring to light that traditional exposure and risk assessment methods are slow and not able to elucidate the necessary information required in an emergency situation.

1.3. Exposure Assessment in the 21st Century

The exposome represents the totality of exposures throughout the lifespan. This is a cumulative measure of exposure to both chemical and nonchemical agents such as diet, stress and sociodemographic factors[17]. The growing need for a comprehensive quantitative and qualitative analysis of the exposome has resulted in the rapid evolution

of exposure science with a focus on solving the challenges of rapid detection of potentially harmful chemicals at low but biologically relevant concentrations. Monitoring tools and models, including analytical chemistry are the essential step preceding a quantitative risk assessment regarding public health. By characterization of complex samples, it provides information on the nature and extent of human exposure to chemicals. Exposure measurements useful for public health decision making can be made in multiple settings (e.g., environmental media, human biofluids, in vitro test systems), and at different levels of biological organization, (e.g., blood, tissues, cells, organelles). Exposure measures of these kinds are critical for identification of emerging health threats and monitoring of harmful substances in the environment, in the workplace, or in the household.

Several advances in exposure science have been made in the 21st century. Improvements in remote sensing, global positioning systems (GPS) and geographic information systems (GIS) have increased the capacity to assess human and ecological exposures and establish models to predict changes and conduct epidemiological studies. Advances in computational exposure assessments have allowed for conceptual, empirical, and predictive models that address data gaps where exposure assessments do not exist. Targeted analysis have long been the gold standard for conducting exposure assessments and comprise the vast majority of exposure assessments today. These analyses provide accurate high-resolution mass spectrometry, such as gas chromatography-mass spectrometry (GC-MS) and liquid chromatography-mass spectrometry (LC-MS), these are often used in tandem because of their complementary

nature when facing a broad range of organic pollutants of different polarity and volatility. Chemicals are identified and quantified based on a mass spectrum, elution time, detector signals or a combination of these measures. These methods have demonstrated great potential for obtaining information for a large number of organic compounds in the environment and human body[18-20]. Recent advances have increased the range of chemicals for which standards and methods are available[21-22]. While these studies are effective, they are limited to chemicals for which standards are available. Hence, untargeted analysis, which involves the detection of all chemicals present in a sample, has emerged as an approach to provide qualitative information on the uncharacterized exposome. This includes both endogenous chemicals and exogenous chemicals. While these studies are broader and encompass a wide range, they do not offer the same absolute quantification, and cannot be subject to toxicity testing as targeted analysis. A combination of the two methods will most likely be used moving forward in exposure assessments[23].

1.4. Novel Untargeted Methods

Our increasing need to understand the influences of environmental exposures on human health has made apparent that new approaches are needed to supplement traditional targeted analyses. Only a few hundred chemicals are routinely monitored through targeted methods, however, humans are exposed to thousands of chemicals every day. The development and applications of high-resolution mass spectrometry (HRMS) has shown potential and promise to greatly expand our ability to capture the broad spectrum of environmental chemicals in exposome studies. HRMS can perform

both untargeted and targeted analysis because of its capability of full- and/or tandem-mass spectrum acquisition at high mass accuracy with good sensitivity[24]. Several advances in HRMS including Fourier-transform MS[25], hybrid ion trap-orbitrap MS[26], quadrupole time-of-flight MS[27-28], allow for increased chemical detection and capture a wider, untargeted chemical space. In order to perform an untargeted analysis using HRMS the following workflow is generally conducted. First, an analytical untargeted method will be used for chemical detection, this generates large datasets of full mass spectra. Second, extraction of molecular features will be based on accurate mass identification. Third, data mining combined with statistical analysis are used to identify markers that can then become targeted analytes. This process, supplemented by reference standards, is used to confirm and quantify these specific markers, which can then be studied in relation to specific health outcomes[29].

Recently, ion mobility spectrometry (IMS) has been interfaced with HRMS to provide Collison Cross Section (CCS) measurements, an additional molecular descriptor based on the structural features of individual chemicals which can increase confidence of molecular identification for untargeted experiments. In a drift tube ion mobility (DTIM), ions transverse a uniform electric field region in the presence of a neutral buffer gas such as nitrogen, the ion-neutral interactions provide structurally-selective retention of analyte ions within the drift tube. The measured drift time is primarily a function of experimental parameters such as drift tube length, drift gas pressure, temperature, electric field strength, and masses of both buffer gas species and analyte molecule. Using these parameters, measured drift times in DTIM can be converted into a collision cross

section (CCS) value via the fundamental low field IM relationship, referred to as the Mason-Schamp equation as shown below in

$$CCS = \frac{(18\pi)^{1/2}}{16}\frac{ze}{(K_bT)^{1/2}}\left[\frac{1}{m_i}+\frac{1}{m_B}\right]^{1/2}\frac{t_AE}{L}\frac{760}{P}\frac{T}{273.15}$$

The parameters of this equation are: K_b - Boltzmann's constant, T - drift tube temperature, z – ion charge state, e - charge of an electron, m_i – ion mass, m_B - buffer gas mass, t_A - measured arrival time, E - electric field, L - drift tube length, P - drift tube pressure, and N - buffer gas number density at standard temperature and pressure[30]. CCS measurements are standardized and thus reproducible between laboratories, as well as have the capacity to distinguish isomeric species in complex mixtures.

These qualities along with information provided by HRMS makes IMS a promising tool for untargeted analysis. Previous studies in biological matrices have shown that by using collision cross section as additional metric for tentative identification, higher confidence in identifying molecular signatures can be gained in untargeted metabolomics [31].

1.5. Study Rationale

Development of analytical approaches to characterize external and internal human exposure to environmental and endogenous chemicals with speed and precision is now widely accepted as a necessary step in efforts to identify the environmental and genetic causes of disease. While traditional gas chromatography (GC)-MS, and liquid chromatography (LC)-MS–based analytical methods have successfully been applied for decades to characterize exposure, sample processing time and the need for chemical

derivatization limit their applicability for rapid global assessment of exposure in settings like natural disasters and industrial events. Large-scale exposure assessments for human cohorts nearing several thousands have the same challenge. The absence of ultra-fast methods that are appropriate for this scale of exposure or urgent exposure assessment in emergency settings requiring short turnaround times has been an obstacle to this initial step of the risk assessment paradigm. This study's objective is to develop and deploy sensitive ultra–high-throughput methods suitable for identifying and quantifying a diverse spectrum of chemicals.

Exposure assessment has traditionally been focused on a select and small subset of compounds largely selected from toxicology studies showing hazard. This study will advance non-targeted analysis of complex mixtures and pioneer new methods for identifying chemical features, using a combination of physico-chemical, chemical-specific collision cross-sectional area, isotopic signature, accurate mass-to-charge ratio. This expansion of exposure assessment will create unique opportunities to evaluate the toxicology and risk of more complete chemical mixtures and develop materials for reducing or mitigating exposures.

This research proposes to conduct exposure assessments following environmental disaster events using traditional methods (Specific Aims 1 and 2) as well as develop novel methods for the rapid identification of new chemical exposures during and after environmental emergency contamination events with Ion Mobility Separation Mass Spectrometry (IMS-MS) as a new approach that meets major requirements for exposome-scale analysis of human exposure to endogenous and exogenous chemicals

(Specific Aims 3 and 4). The features of this approach include high sensitivity, high-throughput, effective separation of isomeric compounds, applicability to a broad chemical space with little modification, ability to quantitate, and multi-dimensional identification of chemicals. This major innovation in analytical chemistry, RapidFire™ SPE-IMS-MS, offers single sample run times of 10 seconds with an up-front multi-cartridge solid-phase separation, allowing single samples to be analyzed after polar, nonpolar, mixed mode, and other initial separations.

1.6. Specific Aims

Environmental samples such as soil and water are complex matrices that may include many common environmental pollutants, these cover a broad range of chemical classes, such as polyaromatic hydrocarbons (PAHs), pesticides, as well as inorganic compounds. Specific protocols are available for chemical analysis of individual classes of compounds; however, these methods are time consuming and highly targeted. In disaster situations, where response time is important, there is a critical gap in rapid analytical methods which encompass a wide range of compounds. Exposure assessment is traditionally performed using GC/LC-MS, while these methods are widely used, they have limitations in throughput and can take hours to process a single sample. The overall goal of this research is to compare and develop methods of rapid exposure assessment of complex environmental samples in disaster research with the use of traditional and novel methods. The long-term goal is to show IMS-MS can be used for environmental sample analysis and will increase throughput and response time in disaster research. Therefore, this research will use both LC-MS (Specific Aim 1) and GC-MS (Specific Aim 2) to

analyze both water and soil samples respectively for contaminants. Next, this research aims to show how the novel analytical method IMS-MS can be used for detection of persistent organic pollutants and their metabolites and degradation products (Specific Aim 3). Finally, this research proposes to develop a database containing over 4,500 chemicals to be used as a tool for screening environmental samples using SPE-IMS-MS (Specific Aim 4).

1.6.1. Specific Aim 1: To conduct a temporal and spatial analysis of per- and polyfluoroalkyl substances (PFAS) in Houston ship channel following firefighting foam deployment at the Intercontinental Terminal Company (ITC) fire

The objective in this aim is to measure concentrations of PFAS using LC-MS methods in the Houston Ship Channel/ Galveston Bay (HSC/GB) and to determine if there are temporal and spatial trends. This research will test the hypothesis that PFAS detected in the HSC/GB following the ITC fire response will have the highest concentrations in the areas closest to the fires and immediately following incident and over-time their concentrations will decrease. We will determine the spatial and temporal trends of PFAS due to firefighting foam deployment as well as determine any potential human health hazards that may occur due to exposure.

1.6.2. Specific Aim 2: To conduct temporal analysis of contaminant distribution and potential human health risks of Hurricane Florence in North Carolina

The objective in this aim is to measure key environmental pollutants in areas

effected by hurricane Florence to determine whether damage to a coal ash facility resulted in release of contaminants. This research will test the hypothesis that detected organic and inorganic contaminants in soils from North Carolina following Hurricane Florence using GC-MS are due to damage to a coal ash facility and redistribution caused by hurricane Florence associated flooding. The research will determine concentrations of PAHs, pesticides, PCBs and metals to find the temporal and spatial trends following the hurricane as well as determine any potential human health hazards that may occur due to exposure.

1.6.3. Specific Aim 3: To characterize and detect persistent organic pollutants (POPs) and their metabolites and degradation products utilizing Ion Mobility Spectrometry – Mass Spectrometry (IMS-MS)

The objective in this aim is to determine both structural information and optimal ionization methods of persistent organic pollutants (POPs) and their metabolites/ degradation products. The research will test the hypothesis that both parent and metabolite/ degradation products can be identified using different IMS ionization techniques. In this aim the research will use IMS-MS to determine structural information of common POPs and metabolite/ degradation products and show how this information can be used for their identification in complex mixtures.

[1]CHAPTER II

2. TEMPORAL AND SPATIAL ANALYSIS OF PER AND POLYFLUOROALKYL SUBSTANCES IN SURFACE WATERS OF HOUSTON SHIP CHANNEL FOLLOWING A LARGE-SCALE INDUSTRIAL FIRE

2.1. Abstract

Firefighting foams contain per- and polyfluoroalkyl substances (PFAS) – a class of compounds widely used as surfactants. PFAS are persistent organic pollutants that have been reported in waterways and drinking water systems across the United States. These substances are of interest to both regulatory agencies and the general public because of their persistence in the environment and association with adverse health effects. PFAS can be released in large quantities during industrial incidents because they are present in most firefighting foams used to suppress chemical fires; however, little is known about persistence of PFAS in public waterways after such events. In response to large-scale fires at Intercontinental Terminal Company (ITC) in Houston, Texas in March 2019, almost 5 million liters of class B firefighting foams were used. Much of this material flowed into the Houston Ship Channel and Galveston Bay (HSC/GB) and concerns were raised about the levels of PFAS in these water bodies that

[1] *Reprinted with permission from "Temporal and spatial analysis of per and polyfluoroalkyl substances in surface waters of Houston ship channel following a large-scale industrial fire incident" by Noor A. Aly, Yu-Syuan Luo, Yina Liu, Gaston Casillas, Thomas J. McDonald, James M. Kaihatu, Mikyoung Jun, Nicholas Ellis, Sarah Gossett, James N. Dodds, Erin S. Baker, Sharmila Bhandari, Weihsueh A. Chiu, Ivan Rusyn, 2020. *Environmental Pollution*, Volume 265 B, Copyright [2020] by Elsevier.

have commercial and recreational uses. To evaluate the impact of the ITC incident response on PFAS levels in HSC/GB, we collected 52 surface water samples from 12 locations over a 6-month period after the incident. Samples were analyzed using liquid chromatography–mass spectrometry to evaluate 27 PFAS, including perfluorocarboxylic acids, perfluorosulfonates and fluorotelomers. Among PFAS that were evaluated, 6:2 FTS and PFOS were detected at highest concentrations. Temporal and spatial profiles of PFAS were established; we found a major peak in the level of many PFAS in the days and weeks after the incident and a gradual decline over several months with patterns consistent with the tide- and wave-associated water movements. This work documents the impact of a large-scale industrial fire, on the environmental levels of PFAS, establishes a baseline concentration of PFAS in HSC/GB, and highlights the critical need for development of PFAS water quality standards.

2.2. Introduction

Per and polyfluoroalkyl substances (PFAS) are synthetic molecules comprising a carbon chain with fluorines attached [32]. Their physicochemical properties make them an ideal component of numerous consumer and industrial products, including cookware, water and oil-resistant fabric, and aqueous film forming foams (AFFFs) that are used in fire suppression [32-34]. Due to their widespread use and persistence, PFAS have become an emerging public health challenge globally. Humans are exposed to PFAS by ingesting contaminated water and food, use of various household items (*e.g.*, food containers), by inhalation, and via occupational exposure [35-37]. It was reported by the Centers for Disease Control and Prevention's National Health and Nutrition

Examination Survey (2011-2012) [38] that PFAS were detected in serum of 97% of Americans [39].

Among the thousands of PFAS known to be produced, only a small number have been investigated in detail using human or animal models [40]. For example, an epidemiological study conducted by the C8 study panel in the Ohio River Valley that followed both residents and workers exposed to perfluorooctanoic acid (PFOA) from the DuPont chemical plant showed a link to kidney and testicular cancer, ulcerative colitis, thyroid disease, hypercholesterolemia and pregnancy-induced hypertension [41]. The National Toxicology Program has concluded that two of the most-studied PFAS, PFOA and perfluorooctane sulfonate (PFOS), present a hazard to immune system function in humans [42]. However, the full extent of the potential health effects of these substances is largely unknown and efforts to systematically review available evidence [43-44] and collect new toxicity data [40] are underway.

Considering the possible adverse health effects due to PFAS exposure, in the early 2000s the United States Environmental Protection Agency (U.S. EPA) published a drinking water advisory for PFOS and PFOA, which ultimately led to the reported discontinuation of production of these substances in the U.S. by some manufacturers [45-46]. However, production of other forms of PFAS is on the rise [47-48]. The U.S. EPA monitored for PFOS, PFOA, perfluorononanoic acid (PFNA), perfluorohexane-sulfonic acid (PFHxS), perfluoroheptanoic acid (PFHpA), and perfluorobutanesulfonic acid (PFBS) in drinking water between 2013 and 2015 [49]; however, there are no Maximum Contaminant Levels (MCLs) or regulations established for these chemicals that apply

across the U.S. A number of states have established or proposed MCLs for several PFAS. Recently, the U.S. Congress has indicated intent to strengthen regulation of PFAS under the pending decision of the National Defense Authorization Act. Congress proposes to designate all PFAS as hazardous substances under the Comprehensive Environmental Response, Compensation and Liability Act (known as Superfund), as toxic pollutants under the Clean Water Act, and to phase out military use of PFAS-containing AFFFs by 2025 [50].

PFAS are ubiquitous in the environment and their long-range transport is of interest to researchers and decision-makers [51]. Many studies have focused on characterization of legacy contaminated sites and the resulting presence of these substances in food, groundwater and air, as well as in human serum and urine. In the past two decades, almost 500 industrial facilities that may be discharging PFAS into the air and water have been identified in the US [44, 52-53]. Industrial releases and waste site leaching represent fixed long-term PFAS point sources exposure sites; however, far less is known about the extent of the environmental contamination during singular events. For example it has been documented that during the fire and collapse of the World Trade Center, PFAS were released into the environment [54-55], but other instances where PFAS are used such as during industrial fires may present unique one off releases where large concentrations of PFAS can enter the surrounding environment.

PFAS are used in fire-suppressing AFFFs, they can rapidly extinguish hydrocarbon fuel fires as well as form an aqueous film on the fuel surface to prevent evaporation and re-ignition [56]. AFFFs are a proprietary blend of surfactants, many

contain PFAS which can be created through electrochemical fluorination or telomerization [57]. Electrofluorination-based fluorochemicals possess fully fluorinated carbon chains with homologues of varying [CF_2] units. Telomerization-based fluorochemicals possess carbon chains that are not fully fluorinated and typically have homologues of varying [C_2F_4] units [58]. Noticeable differences in PFAS composition of AFFFs have been documented and most of AFFFs have proprietary formulations that make exposure assessment difficult [45, 59-60].

A recent example of a large-scale deployment of AFFF is the petrochemical fire that occurred in the Houston area in March of 2019. Millions of liters of Class B fire-fighting foams were deployed over several days to contain the fire [61]. Although there was a dike wall in place to prevent AFFFs from reaching public waterways, a breach occurred that caused the foams to escape into the Buffalo Bayou, part of the Houston Ship Channel (HSC) that is connected to Galveston Bay (GB). Our study hypothesized that this incident will result in large-scale PFAS contamination in HSC/GB, an area that also is used for recreation. To characterize the extent of the environmental release of PFAS from this disaster, the concentrations of these contaminants in surface water, and the duration of the elevated levels of PFAS, we conducted a temporal and spatial survey of the waters in the HSC/GB. Understanding the extent and spread of PFAS in the environment is important to determine the potential for human exposure during major incidents. In addition, this study provides important information with respect to the patterns of use of both legacy and novel PFAS in firefighting foams.

2.3. Materials and Methods

2.3.1. Incident Description

The tank fires at the Intercontinental Terminals Company (ITC) in Deer Park, TX in the greater Houston area (Figure 1) were discovered at around 10 am on March 17, 2019. The fire originated in an 80,000 barrel (12.7 million liter) aboveground storage tank that held naphtha. Firefighting efforts began shortly after the incident was reported; however, firefighters were unable to contain the fires and leaking naphtha. By March 18, 2019, seven adjacent storage tanks of similar size had caught fire. The fires were completely extinguished by the afternoon of March 20, 2019. On March 22, 2019 a portion of the barrier wall surrounding the tanks failed, releasing a mixture of spilled and AFFF chemicals into the Tucker Bayou that is located less than 500 meters from the site of the fires. The Tucker Bayou merges into the Buffalo Bayou, which in turn merges with the greater HSC/GB estuary. Recovery of the spillage produced about 33,000 barrels (5.2 million liters) of oil slick and foams mixed with water 62; however, the full extent of the contamination of the HSC/GB is unknown and it is likely that a wide range of PFAS dispersed into the water.

A number of chemically-diverse AFFFs were used in the ITC response [**Supplemental Table 1**, Dr. Michael Honeycutt (Texas Commission of Environmental Quality, TCEQ), personal communication] and included ANSULITE 3% (AFC3B), ANSULITE 3x3 AR-AFFF LV (A334-LV), ANSULITE 3x6 AR-AFFF (A364), ANSULITE LOW VISCOSITY 3X3 AR-AFFF Foam Concentrate, Dwight P. Williams Signature Series 1%x3%, THUNDERSTORM W813A 1X3 AR-AFFF, CHEMGUARD

ULTRAGUARD 3% AR-AFFF, and UNIVERSAL GOLD 1%/3% Alcohol. U.S. EPA and TCEQ staff were deployed to the area to monitor for gases (hydrogen sulfide, carbon monoxide and oxygen) and volatile organic compounds (naphtha, benzene, xylene and toluene). Air quality was the primary concern immediately following the fires. Water samples were also collected at regular intervals (daily and weekly) to measure metals and semi volatile organic chemicals starting on March 21, 2019 [63]. PFAS analysis was performed only for the water samples collected on March 21, 2019 [63].

2.3.2. Sample Collection

Surface water samples were collected from either open water (from a motorized boat) or from several shore-accessible locations as detailed in **Table 1**. Collection followed the general guidance on sampling as described in the EPA Method 537.1 [64]. Samples (n=52, 700-1,000 mL each) were collected over 8 field sampling trips (between March 21, 2019 and August 2, 2019) to the HSC/GB area. Because of the emergency nature of the ITC fire and intermittent "shelter in place" orders for some of the sampling sites, not every location had a sample collected on March 21, 22, and 29, 2019. The sampling locations and their relative distance from the ITC incident site are displayed in **Figure 1** and summarized in **Table 1**. Sampling dates and exact locations for each site are detailed in **Supplemental Table 3**. Samples were collected into one liter pre-washed high-density polyethylene (HDPE) bottles (cat. #1162D42, Thomas Scientific, Swedesboro, NJ) at depths of approximately 0.3 meters. To prevent contamination, clean nitrile gloves were used at every sampling site and bottles were double bagged for transport. Samples were stored on ice or at 4^{o}C until extraction following

recommendation by EPA Method 537.1. A deviation from the EPA method consisted of (i) collection of one sample per location and (ii) no addition of preservatives.

2.3.3. PFAS Reference Materials

Calibration standards and isotopically labeled compounds of perfluorinated carboxylic acids and sulfonates (**Supplemental Table 4**) were obtained from Wellington Laboratories (Guelph, Ontario).

2.3.4. Sample Preparation

Sample Extractions. The procedures for sample extraction were exactly as detailed in Waters Perfluorinated Compound Analysis manual [65]. For samples collected in March and April 2019, 50 mL aliquot of each water sample was used for extraction. For samples collected in June, July and August 2019, 250 mL aliquot of each water sample was used for extraction because we expected lower concentrations of PFAS months after the incident. Samples were decanted into a polypropylene centrifuge tube (cat. #28-106, Genesee Scientific, San Diego, CA) or HDPE bottles (cat. #414004-113, VWR) and extraction standards were added (see below and **Supplemental Table 5**). Samples were extracted with Oasis weak anion exchange (WAX) cartridges (cat. #186003519, Waters, Milford, MA) in a vacuum manifold exactly as detailed by [65]. To determine whether any analytes were lost during sample washes, we collected the 100% methanol wash from the samples and found no detectable PFAS (data not shown). Samples were also prepared without the 100% methanol wash and we observed significant interference from the sample matrix (data not shown). Therefore, the washing step with 100% methanol, before final elution with 0.1% NH_4OH, is a

necessary step to further remove salts and other interference matrices from complex environmental samples. Extracted samples were stored at -20°C until analysis.

Due to the unexpected nature of the incident, no pre-extraction standards were available during the first extraction, for these samples the pre-extraction standards were added directly prior to instrumental analysis. A list of the chemicals and solvents used in these experiments can be found in **Supplemental Table 5**.

2.3.5. Instrumental Analysis

Liquid chromatography (LC) tandem mass spectrometry (MSMS) data acquisition and quantification were performed using Agilent (Santa Clara, CA) 1260 Infinity II High Speed Pump coupled with a 6470 triple quadrupole MS (Agilent) with electron spray ionization (negative mode). LC conditions were adapted from the PFAS method of [66]. Briefly, the chromatographic separation was achieved with a C18 column (Agilent ZORBAX SB C-18, 2.1 x 50 mm, 1.8 μm). A flow rate was 0.4 ml/min, 20 μL injection volume and a binary mobile phase gradient consisted of mobile phases A (5 mM ammonium acetate in water) and B (5 mM ammonium acetate in 95% methanol). The gradient was as follows: 10% B held for 0.5 minutes, B increased to 30% by 2 minutes, B increased to 95% by 14 minutes and 100% B by 14.5 minutes. 100% B was then held for 2 minutes to elute strongly retained compounds then switched back to 10% B and held for 6 minutes to equilibrate the stationary phase. Acquisition method details are provided in **Supplemental Table 6**. MassHunter Acquisition Software (C.01, Agilent) was used for instrument control and data acquisition. MassHunter Quantitative Analysis Software (B.08, Agilent) was used for data processing and analysis. **Supplemental**

Figure 1A shows LC-MS chromatograms for the standards in a mixture of 27 PFAS that were used (see **Supplemental Table 4**).

The identification of compounds was based on 3 criteria. First, retention time had to match with tolerance of 0.1 min (average standard deviation of retention time was 0.04 min). Second, for MSMS transitions we followed the EPA Method 537.1 criteria that identify a single transition per compound from the reaction monitoring. Additional ions (see **Supplemental Table 6**) were used to verify all targets based on MSMS transitions detected in our laboratory using pure standards. Third, ratios of quantification and qualification ions had to be at a 20% tolerance. Compound quantification was based on the ratios between native compounds and isotopically labeled surrogates in the extraction standards, where available. Isotopically labeled fluorotelomer sulfonate (FTS) standards were not available in our laboratory at the time of the analysis. Therefore, the concentrations for FTS are relative and not absolute. However, the patterns through time are informative. Calibration curve mixtures and samples were in the same solvent matrix (96% MeOH) for LC-MSMS analysis.

2.3.6. Quality Assurance/Quality Control for Analysis

Blanks. For each batch of extracted samples (6-16 samples in each batch as shown in **Supplemental Table 3**), at least one procedural blank (ultrahigh purity water in the sample container) was also extracted following the same protocol as the field samples. Additionally, solvent blanks (96% methanol) were also run to track solvent and instrument background. Solvent blanks were run after every 5 field samples to monitor for background and carryover. All analytes in blank (procedural and solvent) samples

were below LOQ (data not shown). It should be noted that even after substantial washing, the procedural blanks contained various levels of PFBS. PFBS procedural blank concentrations were consistently below the limit of quantification (LOQ; see **Supplemental Table 3**), and PFBS signal (*i.e.*, peak area) in solvents blanks was consistently lower than 5% of the lowest calibration standard.

2.3.7. Calibration, Extraction, and Injection Standards

Calibration stock mixture was created by combining Wellington Laboratories' PFAC-MXC and individual compounds (**Supplemental Table 4, Calibration Mix Substances**). Calibration curve was created by serial dilution of the stock mixture (**Supplemental Table 4**). **Supplemental Figures 1D** and **1E** illustrate representative calibration curves for a number of perfluorinated and fluorotelomer standards, respectively. It should be noted that PFBS in the calibration curve (**Supplemental Figure 1D**) exhibited a response at a concentration of 0 ng/mL suggesting an internal contamination source such as the LC mobile phases used or pump seals and it means this compound cannot be accurately quantified. Representative data on the linearity of the calibration curves are in **Supplemental Table 7**.

Extraction standards (ES; MPFAC-C-ES) and injection standards (IS, MPFAC-C-IS) were from Wellington Laboratories (**Supplemental Table 4, External and Internal Standards**). ES were not available during the extraction of the first batch of samples (April 19, 2019 analysis date, **Supplemental Table 3**). This batch of samples was processed immediately after collection as recommended, not waiting for standards to arrive. Because of the unexpected nature of this disaster, extraction standards were

added to these samples before LC-MSMS analysis. The samples were quantified based on the ratio of the target response normalized to the mass labeled extraction standard. ES were spiked into each sample before extraction for all other samples at a 5 ng/mL final concentration (1 mL final elution volume). ES were also spiked into all calibration standards at a final concentration of 5 ng/mL. IS and calibration standards were spiked into all extracted samples prior to injection to the LC-MSMS at a final concentration of 5 ng/mL. IS were used to track potential instrument drift and assess relative recovery of the ES.

Continuing Calibration. To ensure sample analysis accuracy and consistency within sample batches, a full range calibration curve was run for each sample batch. Additionally, continuing calibration standards from mid and high concentration ranges were run after every 5 field samples throughout the analytical sequence.

LOD and LOQ. LOD was determined based on a serial dilution method for the standard mix. LOQ was determined based on a serial dilution of the standard mix and calculated concentration was >85% and <115% of accuracy. LOQ values for each analyte are listed in **Supplemental Table 3**. In the analyses conducted in April and May 2019, substantially higher LOQ values (**Supplemental Table 3**) were observed as compared to the later analysis dates. This difference may result in a biased comparison of PFAS occurrence among the sampling campaigns. To determine the variability contributed by sample extraction, one of the field samples (SCWS2 collected on April 24, 2019) was extracted twice and analyzed. For all analytes that were above LOQ, except PFBS and L-PFDoS, duplicates were within 20% (**Supplemental Table 8**). Overall method

precision for each analyte was determined by repeated injections of standards (n=3) over 12 hr period. Percent difference between repeat injections was below 20% for each analyte (**Supplemental Table 9**).

2.3.8. Temporal Analysis

Because a relatively small number of samples were available for individual PFAS at each sample location, formal time-series analysis could not be performed. However, two statistical analyses were performed to increase confidence in the visual observed trends. If a linear trend was observed ("peak" at first time point), then a linear trend test was performed to confirm that the trend was unlikely to be due to chance. If a "peak" was observed after the first time point, then the data were first differenced to find the change in concentrations between time points, then a change-point test was performed to confirm that change in the "slope" was unlikely to be due to chance. We used these analysis as corroborating evidenc, and did not require formal statistical significance ($p<0.05$), particularly for the open water locations, due to low sample sizes. Software used was RStudio version 1.2.1335 with R version 3.6.1, and the changepoint R package version 2.2.2 [67].

2.3.9. Spatial Analysis

Spatial interpolation is one of the most often used geographic techniques for spatial query, spatial data visualization, and spatial decision-making in geographic information system (GIS) mapping and environmental science [68]. In this longitudinal study, surface water samples were taken from the same locations every 6-12 weeks over a course of 6 months. The data on selected PFAS concentrations in these samples were interpolated

and visualized using ArcGIS software (v. 10.4, ESRI Inc., Redlands, CA). The total shape file for the Houston Ship Channel was taken from the Houston – Galveston Area Council GIS data set. The specific shape file used for the study was generated from subsections of the shape file for the entirety of the Houston Ship Channel. Sampling locations were spatially joined to the Houston Ship Channel using a Radial Base Function analysis, one of the most accurate spatial interpolation models [69]. Radial Basis Functions (RBF) are a series of exact interpolation techniques which create a smooth surface covering each measured data point. RBF is ideal for an area with a large number of data points with gently varying surfaces such as elevation [70]. The RBF analysis is part of the "Geospatial Analyst tool" in ArcGIS software.

Concentrations of PFOS and 6:2 FTS from the sampled sites were used as inputs for interpolating the estimated concentrations throughout the study area. The output of the interpolation was visualized using choropleth maps. These maps use themes to shade predetermined areas of maps that represent statistical data, in this case PFAS concentrations. The creation of each choropleth map was based on location inputs along the area of interest. Two different groups of longitudinal choropleth maps were created, one for PFOS and the other for 6:2 FTS. Both choropleth maps have 5 distinct categories of concentration based on quintiles in the data for the entire study. Categories based on both PFOS and 6:2 FTS concentration were displayed by color, with red being the highest concentration and white, the lowest. The RBF smoothing shades the areas of the Houston Ship Channel shape surrounding the sampling location with predicted concentration values. Finally, the choropleth maps were created for each sampling

period using a Lambert Conformal Conic projection suitable for the state of Texas. All spatial analyses were performed using ArcMap function in ArcGIS.

2.3.10. Hydrodynamic Modeling

To determine the possible paths taken by the water masses near the ITC site at the time of the incident and response, the Delft3D model suite [71] was used. The modeling suite is capable of simulating the water motion due to waves, tides and winds. A system of four nested grids was created, starting with one encompassing the entire Gulf of Mexico and ending with a smaller grid enveloping the HSC. The model grids used are shown in **Supplemental Figure 3**. Grid parameters are shown in **Supplemental Table 10**. Information from the larger grids (mainly time series of tidal elevations) was saved along the boundaries of the nested grid. Model input included information on waves, winds and tides; tides were run over all four grids, while winds were run only on the smallest domain (**Supplemental Figure 3D**). The model has been validated [72] for the case of hydrodynamics forced by cold front passage near Galveston Island.

Information on the grid configuration, nesting, forcing information and wind-wave calculation is as follows. For tides, we used information (in the form of tidal constituents) from the Inverse Tidal Model [73]. The constituents from March 15 – April 30, 2019 were applied at the boundaries of the Gulf of Mexico grid to represent tidal motion. Tidal elevations constructed from these constituents were then propagated across the Gulf of Mexico, successively feeding the smaller grids. This insured that the tides in shallow water were properly represented, as tidal constituents in shallow water can be inaccurate [74] and thus not suitable for directly forcing a shallow water model. Wind and wave

information was obtained from a buoy deployed by the National Data Buoy Center (Station 42035, located at 29.232°N, 94.413°W). Winds were input to the model every 6 hrs, and were assumed constant over the domain of Houston Ship Channel. The computational time step for all models was 1 min.

Simulations for waves in GB and HSC proved to be challenging because the lack of spatially-distributed wind measurements over the Gulf made it impossible to accurately model wind-wave generation to the edge of the GB domain boundary. While the wave conditions at Station 42035 can be used to initialize the model, these are conditions only at one point, and are likely different along the boundary due to variations in water depth. This lack of heterogeneity along the boundary was likely responsible for non-convergence of the wave model within the GB (and consequently the HSC) domains. Alternatively, we made use of wind-wave growth expressions to estimate the wave energy in Galveston Bay without the dedicated wave model. We first assumed that swell wave propagation from the offshore has little impact on the bay because it can only enter through the narrow inlet separating Galveston Island and Bolivar Peninsula. We then used the fetch-limited wave growth formula [75] to determine the wave height and period associated with an estimated fetch (length over which the wind can generate waves) of 37 km (the distance from the entrance to Galveston Bay to the edge of the HSC grid) for the highest wind speed in the data (10.7 m/s). This led to a wave height estimate of 1.05 m and a period of 4.56 s. To determine the likely impact of waves on the drogue motion, we assumed that the primary influence of waves on the drogue motion is through the Stokes drift (the mean net transport from waves). Using a simplified expression for this quantity for this maximum

wind-wave condition [76], we determined that the maximum Stokes drift velocity is 0.02 m/s, far smaller than the average tidal velocity and thus can be justifiably neglected.

2.4. Results

In the days and months following the fires at the International Terminals Company (ITC) in Houston, TX, surface water samples were collected from 7 shore-accessible and 5 open water locations in HSC/GB area as detailed in **Figure 1**. Samples (**Table 1**) were collected upstream (n=3), downstream (n=8), and in close proximity to the incident site (n=1) to determine the spatial distribution and the types of PFAS released at the point source of ITC industrial installation. There were 8 separate sampling campaigns conducted over the course of 6 months (March-August 2019) to determine temporal patterns of PFAS contamination in HSC/GB.

A total of 27 PFAS (see raw data in **Supplemental Table 3**) were analyzed in all collected samples (**Table 1**). **Supplemental Figure 1B-C** shows representative LC-MS chromatograms for samples collected from the open water at location SCWS2, which was closest to the ITC incident, in March (**Supplemental Figure 1B**) and June (**Supplemental Figure 1C**) 2019, respectively. A clear trend towards reduction in abundance of the detectable PFAS is evident from these data. Of 27 target PFAS, 15 were detected in amounts over the LOQ in at least one experimental water sample – PFOS, PFBS, PFHpA, PFNA, PFOA, PFHxS, 6:2 FTS, 8:2 FTS, perfluorohexanoic acid (PFHxA), perfluoropentanoic acid (PFPeA), perfluorobutanoic acid (PFBA), perfluoropentanesulfonic acid (L-PFPeS), perfluorodecanoic acid (PFDA),

perfluoroundecanoic acid (PFUdA), and perfluorododecanesulfonic acid (L-PFDoS). The remaining 12 species were below the limit of quantitation in every sample.

Temporal patterns in the concentrations of 6 PFAS that were most abundant across the samples collected at 5 open water locations (**Table 1**) are shown in **Figure 2**. In each sample, as expected, there is a clear spike of PFAS, especially 6:2 FTS and PFOS, immediately following the fires. 6:2 FTS peak concentrations reached 1,446 ng/L (sample SCWS1) on March 22nd which is significantly larger than the PFOS peak concentration of 247 ng/L (sample SCWS3). Other detected PFAS had peak concentrations below 50 ng/L. Concentrations were highest at close proximity to the site of the incident (sample location SCWS2) and immediately adjacent to the site (SCWS1). Sample SCWS3 was upstream from the incident site and had similar peak concentrations of 6:2 FTS and PFOS as sample SCWS5, which was the furthest downstream. Levels of these and other detected PFAS remained at comparable levels in April 2019, but declined considerably by June 2019 and remained low in July 2019. All "peaks" were identified by either linear trend or changepoint detection, with p-values ranging between 0.03 and 0.27 due to small sample sizes (n=4 per PFAS per location, **Supplemental Figure 2A**). Spatial patterns in PFAS concentrations measured using samples collected in this study were similar to those reported by the U.S. EPA in samples collected on March 21, 2019 (**Supplemental Table 2**).

Temporal patterns in the concentrations of 6 PFAS that were most abundant across the samples collected at 4 shore-accessible areas (**Table 1**) with the largest

number of sampling events are shown in **Figure 3**. Similar to the open water samples, 6:2 FTS and PFOS were most abundant and were also measured to have similar concentrations to the open water samples. All 4 areas shown were distal to the site of the incident and the levels of all detected PFAS spiked rapidly in the second or third sample taken. The Lynchburg Ferry sampling site was closest to the open water sample SCW5 and the concentrations of 6:2 FTS and PFOS peaked several weeks after the start of the incident. Peak levels of 6:2 FTS were 1,492 ng/L on March 29, 2019. Baytown Nature Center sampling location was further away and downstream from the Lynchburg Ferry location and the peak of PFAS was delayed until April; still, the concentrations of all PFAS reached similar peak levels to other samples. Morgan's Point and River Terrace Park sampling locations were farthest away from the incident site and concentrations of PFAS peaked in April. All "peaks" were identified by either linear trend or changepoint detection, with all p-values <0.05 (n=6 to 8 per PFAS per location, **Supplemental Figure 2B**).

Because clear spatial patterns in concentrations of PFAS were observed, we conducted data interpolation as detailed in Methods to estimate water concentrations across HSC/GB estuary based on sampled locations. For this analysis, we chose to construct the maps for March, April, and June 2019 by combining all data available to us for each of these months. To increase the number of observations, we also included data from US EPA that was available for one date in March 2019 (**Supplemental Table 2**). We chose to map 6:2 FTS and PFOS because these compounds were detected at the greatest concentrations. To enable interpretation of the spatial visualizations across the

temporal scale, data for each compound across all samples was divided into quintiles and plotted using red-white color scale (**Figure 4**). Both PFAS showed similar spatial patterns, with the greatest levels observed in March 2019 at, or near the incident site. Concentrations decreased by April 2019 at or near the incident site with the highest concentrations detected at distal sites downstream. By June 2019, concentrations of both compounds markedly decreased with some detectable levels around the incident site and at several distal locations.

It is noteworthy that we detected PFAS not only at the site of the incident and downstream, but also at several locations that were at a considerable distance upstream in the Houston Ship Channel (sampling locations SCWS3 and SCWS4), as well as in the North-most areas of the Galveston Bay (River Terrace Park location). To confirm that water movements in this part of the estuary can occur in both directions, hydrodynamic analysis was performed (**Figure 5**) using the Delft3D model as described in Methods. Importantly, the modeling exercise performed in this study was meant to address the question of why PFAS concentrations increased over time in locations that were upstream from the site of the incident. This modeling was not meant to address sediment transport or PFAS sorption, both important processes that can impact PFAS transport [77-78].

To illustrate the patterns of general water movements in the area of study, a numerical "drogue" – a parcel of water whose motion is tracked – was released at the Buffalo Bayou location closest to the location of the ITC starting March 17, 2019 at midnight, with one additional drogue released each day for seven consecutive days

(until midnight March 23, 2019). These dates were chosen to represent the time period that included active firefighting and the subsequent spill of the partially contained foam into the Tucker and Buffalo Bayous (see Methods and **Figure 1**). The simulated position of each of these seven drogues was tracked until April 30, 2019.

Two maps are shown, one that accounts for the water movement affected by tides (**Figure 5A**) and one that includes both tide and wind forces (**Figure 5B**). The dots on the map represent the cumulative path of seven daily drogues at a given point in time (60 min intervals) until April 30, 2019. The drogues move back and forth past the ITC incident site under the influence of the tides (**Supplemental Table 11**), and tides and winds (**Supplemental Table 12**). It is noteworthy that the drogues pass by all of the sampling locations. The density of the drogue positions is higher in the upper reaches of the HSC, upstream of the ITC, but there is also some motion toward GB. The trend towards clustering of the drogues in the upper reaches of the HSC is likely due to the relatively shallower water and slower flow velocities in this area. The trend toward GB may be attributed to longer-term tidal components present in the area influencing the water movement beyond the daily periodic trends. It is important to note that the model was simulating a trajectory of a drogue which represents a unit of water in the estuary and not the trajectory of a *contaminant*. The extent of the water mass transport is thus used as a surrogate for the possible extent of contaminant (*e.g.*, PFAS) transport where only advection of the material with the flow occurs. Phenomena that are not modeled may either increase (e.g., via diffusion, turbulent mixing) or decrease (e.g., via sorption or degradation) movement of contaminants.

2.5. Discussion

2.5.1. ITC Fire Response Resulted in a Release of PFAS into the Houston Ship Channel

While many of the known sites with routine use of AFFFs have been monitored for PFAS [79-80], less common is monitoring after specific large-scale releases. The present case study provides several important inferences regarding temporal and spatial distribution of PFAS after a major firefighting response. Two PFAS were detected in considerable amounts following the fires: PFOS and 6:2 FTS, both of which are known to be constituents or degradation products in AFFF [81]. Following a health advisory released by US EPA in 2002, the manufacturing of products containing PFOS and PFOA was discontinued in the U.S. However, many companies creating AFFF already had a supply of formulations containing PFOS in storage. These products became known as legacy AFFF. Legacy AFFF use is not banned by federal law in the U.S.; however, their use is limited to emergency situations. PFOS is also known to be the degradation product of C8 perfluorooctane sulfonamides [82]. While these are not common constituents of currently manufactured AFFFs, they were also historically used. Degradation of these C8 precursors may be contributing to the observed environmental concentrations of PFOS [57, 83].

AFFF release during the ITC fire occurred from March 17-22, 2019 [84]. The prior recorded release of AFFF in Houston occurred at the Ellington Field Joint Reserve Base in 2018. Water PFOS levels were reported at about 47 ng/L, 6-fold lower than the highest concentrations of PFOS detected after the ITC fires [85]. From the temporal analysis, we observed all PFAS decrease over 100-fold in the Houston area over the 6-

month sampling period. Similar temporal patterns have been reported at other known AFFF contamination sites [79-80, 86], with levels of PFAS decreasing precipitously within months of the known release.

A number of studies reported on surface water levels of diverse PFAS in the estuaries across the world that may have been impacted by continuous industrial discharges. For example, contamination of surface waters in the watershed of the River Rhine by PFAS was found to be dominated by PFBS and PFBA, with PFOS levels to be at around 10 ng/L [87]. A study of PFAS in the industrially polluted Vaal River in South Africa found that PFPeA was the highest (around 40 ng/L) among 15 substances evaluated [88]. In China, various studies reported that surface water PFAS are dominated by the PFOS, PFHxA, PFPeA and PFBA [89-90]. In the US, GenX and related perfluoroalkyl ether acids were detected in the Cape Fear River and in finished drinking water in North Carolina [91]. In our study of a water contamination event associated with a fire-fighting incident, we found 6:2 FTS to be at highest concentrations among 27 PFAS evaluated. This is likely because PFOS precursor-containing AFFFs are not frequently used, but AFFFs containing 6:2 FTS itself or its precursors could have been deployed in greater quantities. 6:2 FTS is a fluorotelomer which is known to be a constituent of some AFFFs, but is used primarily in many industrial applications as a replacement for PFOS [82, 92-93]. Upstream precursors, such as 6:2 fluorotelomer thioether amido sulfonate (6:2 FTSAS) and 6:2 fluorotelomer sulfonamidoalkyl betaine (6:2 FTAB), that are present in certain AFFFs formulations can transform to intermediates including 6:2 FTS [94-96]. 6:2 FTS is less persistent than PFOS and degrades to perflurohexanoic (PFHxA)

and perfluoroheptanoic (PFHpA) acids [97]. Indeed, we found that PFHxA followed closely the temporal patterns of 6:2 FTS (r^2=0.71, p<0.0001). 6:2 FTS can also generate even shorter-chain perfluoroalkyl carboxylates such as PFPeA and PFBA via environmental and engineered processes [98-99]. Elevation of these substances may also reflect the influence (*e.g.*, environmental degradation) of other fluorotelomer precursors not targeted in the present study. This may explain why these PFAS were also observed in elevated concentrations in the Houston area waterways after this incident.

2.5.2. PFAS Contaminants Distributed both Up- and Down-stream from the Site of the Incident

Interestingly, PFAS were also detected upstream from the ITC site, this behavior is not uncommon in tidal waterways [32]. Our analysis of the tidal movement of water in the HSC showed that water flowed upstream from the ITC incident site. As expected, in the weeks immediately following the fire, the highest levels of PFAS were observed in the HSC near the site; but after a month, these chemicals reached farther areas surrounding the GB before eventually diluting by summer. The water movement modeling undertaken in this study was meant to demonstrate the plausibility of both up- and down- stream transport of contaminated water from the site of the incident and AFFF discharge. The area of the incident is located inland, yet the tides, waves and wind make a major impact on water movement and mixing, as shown by our modeling simulations. These simulations, as well as spatial and temporal patterns in PFAS levels, support convincingly the notion that ITC was the point source for the PFAS detected both up-stream in the Buffalo Bayou and north of the Buffalo Bayou in the GB estuary.

While this water movement modeling was informative, it is not suitable for the purpose of PFAS fate and transport analysis in HSC/GB. Sorption behavior of PFAS is highly complex and could not be explained by a single soil or sediment property [78]. There are currently limited data on the sorption behavior of PFAS in marine or estuarine sediments and the properties controlling their sorption have not been well established [77]. Our study did not collect data on organic carbon, pH and sediment content in the surface water samples, properties that are known to have significant effect on PFAS sorption; therefore, additional studies with thorough characterization of the water and sediments are needed to better understand their role in PFAS transport and sorption.

2.5.3. Substantial Gaps Exist Due to Lack of Standards for Characterizing Risk from PFAS Releases

Our study is also highly informative for PFAS exposure characterization. Although no PFAS have federal, enforceable limits set for water contamination, many states sought to fill this gap by developing their own guidance levels. **Table 2** compares the PFAS surface water concentrations we observed with the range of available standards/guidance values as compiled by the Interstate Technology and Regulatory Council (ITRC) as of February 20, 2020 (see **Supplemental Table 13** for details).

Peak concentrations for five evaluated PFAS (PFOS, 6:2 FTS, PFHxS, PFOA, and PFHpA) exceeded the most stringent standards/guidance values for drinking water. Because the Houston Ship Channel is not known to be used as a source of drinking water, this comparison may be highly conservative on its own. However, because in the case of PFOS, the fish consumption-based standards are similar to or lower than the

drinking water-based standards, exceedance of drinking water standards may still indicate a potential concern, as well as highlighting the need for additional data on bioaccumulation potential for PFAS.

Fish consumption-based standards/guidance values are available for PFOS and PFOA. Based on our observations, we found that many samples were in exceedance of available standards (**Supplemental Figure 4**). Bioaccumulation factors appear to vary widely across PFAS [e.g., ~70 L/kg for PFOA but ~2400 L/kg for PFOS [100]], suggesting that extrapolation from water to fish concentrations is highly uncertain without PFAS-specific bioaccumulation data. For PFOS, in particular, the "background" water levels we detected in July-August 2019, which are above the most conservative surface water standards, would translate to 6 ~ 60 ng/g fish concentrations. While sampling of PFAS in fish in the Houston Ship Channel has not been reported, studies in other populated locations have reported levels in this range [101-102]. Although there are fish advisories warning against the consumption of all fish and crabs from the Houston Ship Channel waterways [103], it is still common to see anglers in this area, and these results suggest that PFAS should be included in risk assessments of consuming fish from the area [104].

Several of the locations we sampled were in public parks with shorelines accessible to swimming and/or wading. Thus, we used the drinking water standards to derive an "equivalently protective" standards under an alternative exposure scenario consisting of incidental ingestion while engaging in recreational swimming. As described in **Supplemental Table 13**, using US EPA Example Exposure Scenarios [105], the contaminant ingestion rate for a recreational swimmer would be about 260 times less

than that for drinking water. With this adjustment, none of the samples had PFAS concentrations above an "equivalent" recreational standard. While exposure to PFAS through this pathway is not likely to be of concern, the ITC fire did impact the lives of many Houston residents. The fire and firefighting response resulted in school closures for over 100,000 students [62].

Moreover, studies of firefighters using AFFFs show elevated serum concentrations of PFAS following exposure. Since firefighters use heavy inhalation protection it is believed exposure also occurs through ingestion and dermal routes [106].

2.5.4. Study Limitations and Future Directions

Several important limitations of this work need to be mentioned. First, the unpredicted nature of this disaster created challenges with data analysis. For instance, at the time of sampling in March 2019, the laboratory did not have ready access to the extraction standard to spike during the extraction process. Thus, in order to expedite the analysis of samples, it was decided to proceed without this step. We did add the extraction and injection standards prior to sample analysis. We acknowledge that the lack of extraction standards during sample preparation prevents absolute quantification of the compounds as extraction efficiency and matrix effect cannot be corrected. However, since the sample matrix (water) was identical across all samples, we believe that these data are still informative and provide valuable information for this and future events. For compounds that have both quantifying and qualifying ions, the ratios between the two were used to compare with pure standards to ensure robust compound identification. While it would have been possible to re-analyze the archived water

samples with the optimized analytical method (as opposed to immediate analysis within 1 week of collection as performed here), significant analyte interconversions for certain PFAS in aqueous samples stored at 4°C were observed within 7 days of storage [107]. The same study provides evidence that storage of water samples at −20°C precludes significant degradation of PFAS for up to 180 days [107].

Second, the analytical background levels of PFBS made it difficult to accurately quantify this compound; however, the remainder of PFAS followed a decreasing trend so one can reasonably assume that if PFBS were in the water samples, it would have followed a similar trend.

Third, the relative sparseness of the sampling locations is a general limitation in spatial interpolation. Large differences in values for co-located samples may not yield smooth interpolation; however, because we quantile ranked the data, these discrepancies were minimized. Overall, while spatial interpolation approaches are highly uncertain, these visualizations are very informative tools for science communication and decision support [108].

Fourth, this study was a targeted analysis of a limited number of PFAS. A wider coverage of known and putative PFAS and their degradation products is now possible using novel non-targeted analytical methods [109]. Inclusion of the methods into environmental sampling would likely further refine exposure estimates for these emerging persistent chemicals.

2.6. Conclusions

Our results show that the detected PFAS in the Houston Ship Channel over the course of a 6-months study period were likely from the firefighting response to the ITC fires. Although AFFF mixtures contain a proprietary blend of chemicals, we expected that their use in large quantities in the ITC incident would result in detectable concentrations of PFAS. Our finding of considerable temporal and spatial increases in levels of 6:2 FTS and PFOS suggests the usage of both fluorotelomer-based AFFFs [92] and of the legacy electrofluorination-based AFFFs [110]. While levels of most PFAS were below currently available actionable levels after considering the likely exposure pathways of recreational use, such comparison are severely limited by the absence of health-based water concentration benchmarks for comparison. Of particular concern is that concentrations of PFOS detected in this study exceeded standards based on fish consumption even after returning the "background" levels. At the same time, for most other PFAS, lack of data to estimate bioaccumulation precludes the ability to assess risks from this exposure pathway. Further studies are needed to examine other PFAS that may have been released from the ITC accident because of the diversity of the AFFF formulations that were used (**Supplemental Table 1**) and the unknown composition of those AFFFs. Additional analytical techniques that may provide high-resolution untargeted analysis of PFAS [109, 111], or estimate total perfluoroalkyl acid precursors via the total oxidizable precursor assay [112] may also be sensible paths towards establishing a more comprehensive characterization of environmental concentrations of, and human exposures to a wide variety of PFAS.

2.7. Acknowledgements

The authors thank Dr. Michael Honeycutt (TCEQ) for useful discussions and providing information for **Supplemental Table 1**. The authors also acknowledge extensive constructive comments from the reviewers that considerably improved this manuscript. This work was funded, in part, by grants P42 ES027704 and P30 ES029067 from the National Institute of Environmental Health Sciences. Noor Aly, Gaston Casillas and Sharmila Bhandari were supported, in part, by a training grant T32 ES026568 from the National Institute of Environmental Health Sciences.

2.8. Chapter II Figures and Tables

Figure 2.1: Map of sampling locations in the Houston Ship Channel and Galveston Bay near the site of the ITC fire

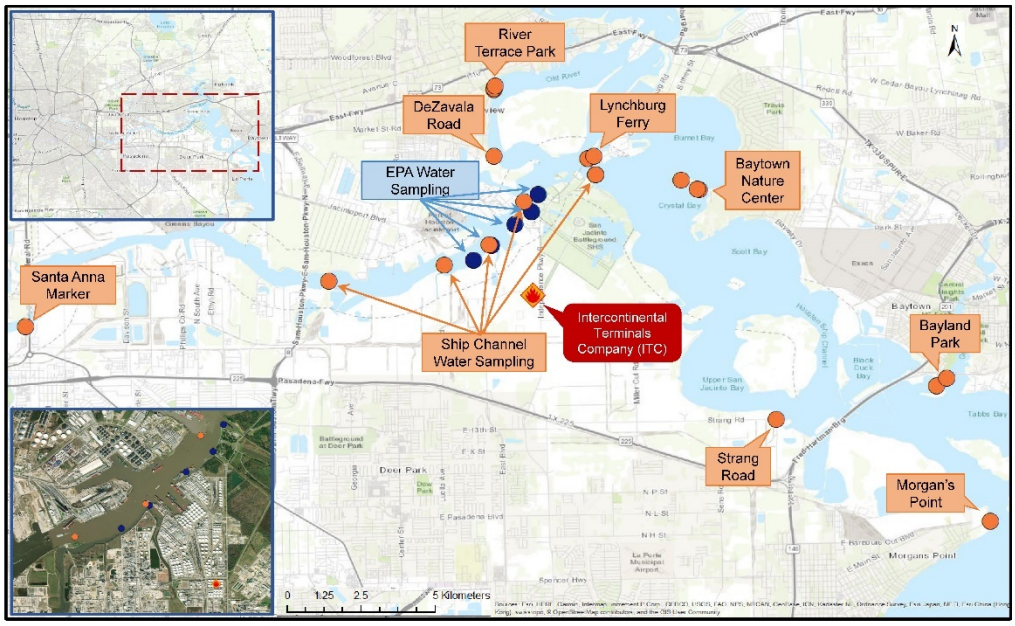

Area of detail magnified in the map is indicated in the inset (top left panel). A series of surface water samples (orange dots) were collected between March 21 and August 2, 2019 from the shore or open water. GPS coordinates for each sampling location are listed in **Table 1**. Locations of open water sampling performed by the U.S. EPA (March 21, 2019) are indicated by the blue dots; these data are included in **Supplemental Table 2**. The site of the incident (ITC, 29°43'45.8"N 95°05'23.8"W) is indicated and magnified in the inset (bottom left panel). Background map is from ESRI/OpenStreetMap. The lower left inset is from Google maps satellite layer.

Figure 2.2: Temporal (March-July 2019) patterns in water concentrations of 6:2 FTS, PFOS, PFHxS, PFHxA, PFHpA, and PFPeA at the HSC/GB open water sampling locations

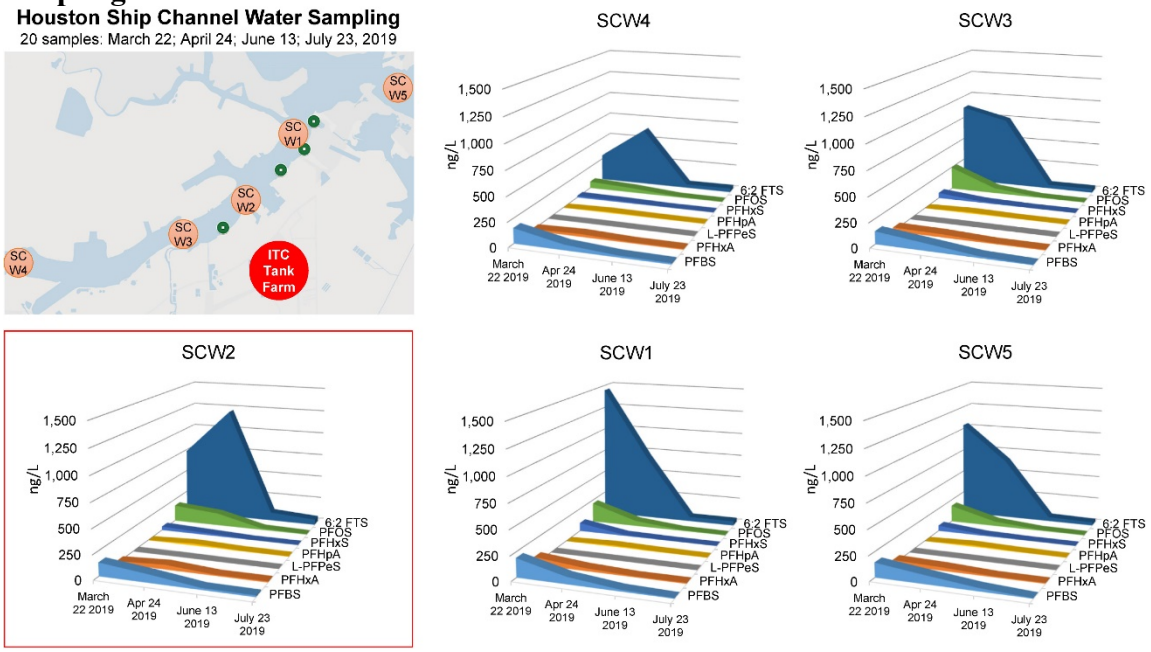

The site of the incident (ITC) is indicated (yellow-red diamond). Sampling locations are shown in the map inset, left (orange circles). Red box indicates the sampling location (SCW2) that was closest to the site of the incident. Raw data and sampling location coordinates are provided in **Supplemental Table 3**. Background map was from ESRI/OpenStreetMap.

Figure 2.3: Temporal (March-August 2019) patterns in water concentrations of 6:2 FTS, PFOS, PFHxS, PFHxA, PFHpA, and PFPeA at the HSC/GB shore-accessible sampling locations

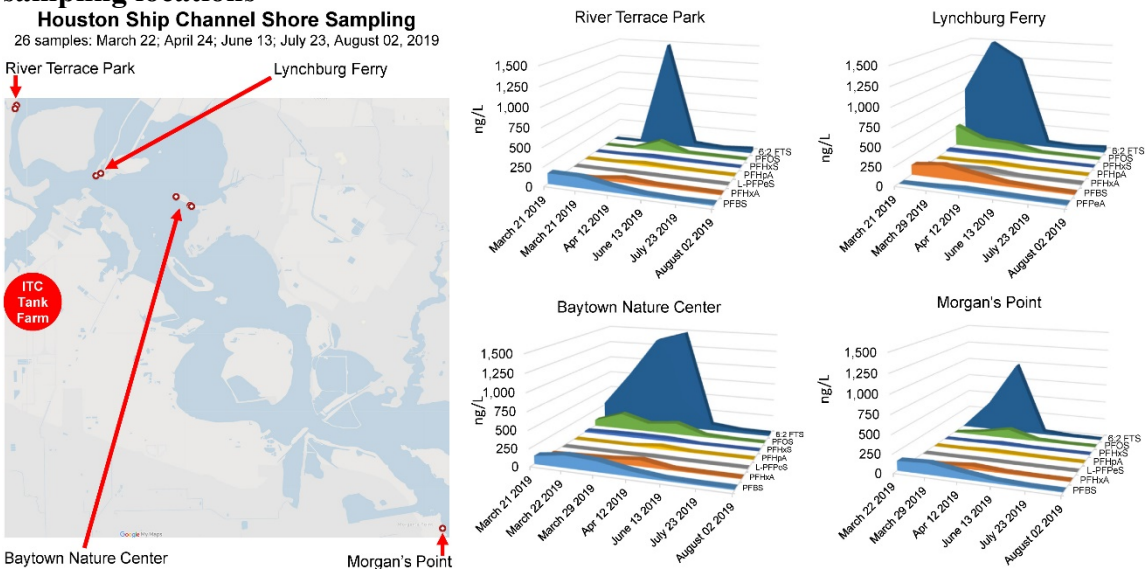

The site of the incident (ITC) is indicated (yellow-red diamond). Sampling locations are shown in the map inset, left (orange circles). Raw data and sampling location coordinates are provided in **Supplemental Table 3**. Background map was from ESRI/OpenStreetMap.

Figure 2.4: Interpolation of the spatial patterns in concentrations of PFOS (left panel) and 6:2 FTS (right panel) in HSC/GB for March, April and June 2019

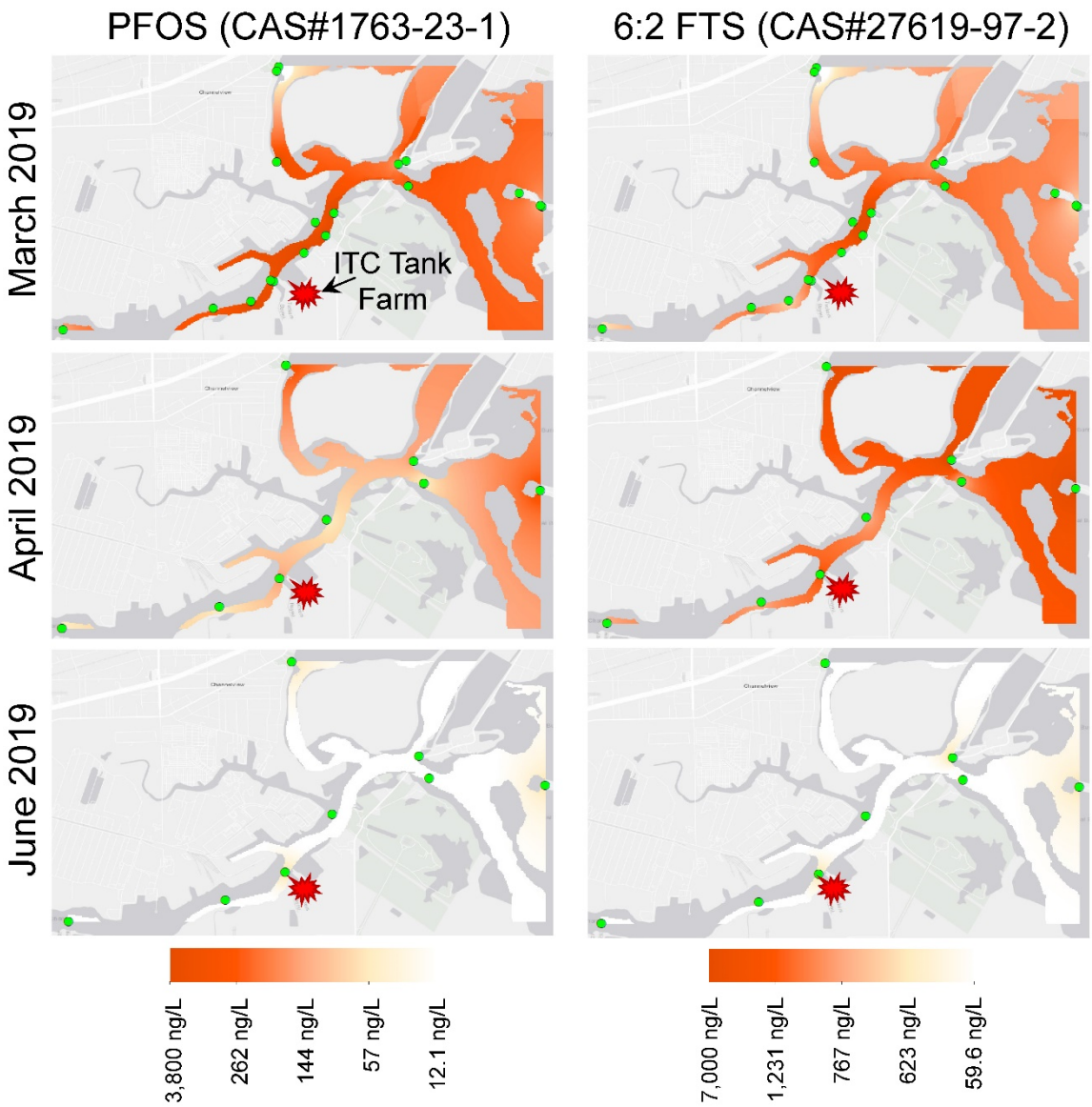

The site of the incident (ITC) is indicated by a red symbol. RBF maps (see Methods) are shown for the HSC/GB estuary where sampling locations are indicated by the green dots and the estimated concentrations of PFOS and 6:2 FTS are visualized as a color gradient (see the heatmap legend for each substance) based on quintiles in the data range, please refer to **Supplemental Tables 2-3** for raw data.

Figure 2.5: HSC/GB map showing the course of seven drogues at 60 min intervals

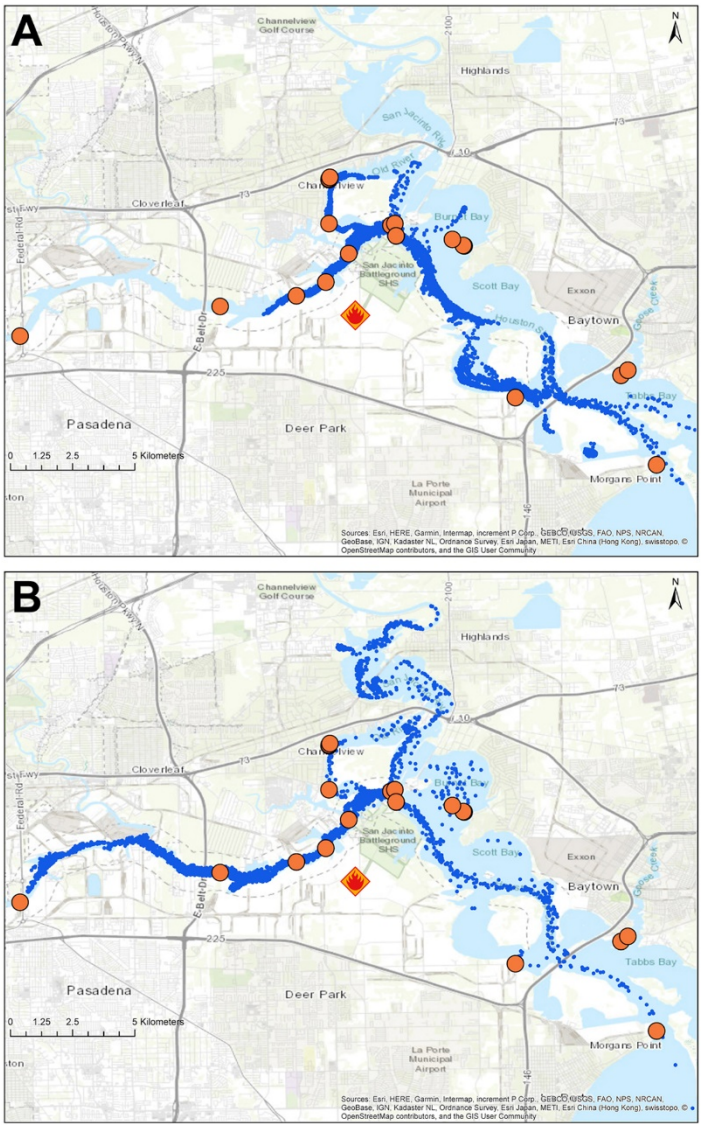

One drogue (blue dot) was released every day at midnight starting March 17th, 2019 and ending March 23rd, 2019. (A) The model that accounts for the water movement affected by tides based on the information in the Houston Ship Channel and Galveston Bay. (B) The model that includes both tide and wind forces. The location of the ITC incident is shown by the orange and red fire symbol. Orange circles show water sampling locations. The base maps are from ESRI/OpenMap.

Table 2.1: Study sampling locations in Houston Ship Channel/Galveston Bay.

Sample Location ID	Latitude	Longitude	Distance from ITC (km)
Open water (Ship Channel Water, SCW) samples			
SCWS4	29.735627	-95.14041	-4
SCWS3	29.739474	-95.11276	-1.2
SCWS2	29.74442	-95.10216	0
SCWS1	29.754676	-95.09387	1.4
SCWS5	29.761123	-95.07675	3.4
Shore-access samples			
Santa Anna Marker	29.7249	-95.2128	-12.4
Lynchburg Ferry	29.764953	-95.07861	3.2
Baytown Nature Center	29.759842	-95.05636	5.3
River Terrace Park	29.7817	-95.101	5.3
Strang Road	29.7027	-95.0336	12.1
Bayland Park	29.710724	-94.99537	15.4
Morgan's Point	29.678439	-94.9825	18.3

Please refer to Figure 1 for the detailed map of sampling locations. Geographical coordinates for each sampling site are listed in Supplemental Table 3.

Table 2.2: Comparison of ITC sample concentrations and available U.S. water standards/guidance values for PFAS.

	Median and range during sampling month(s)			U.S. Water Standards/Guidance Values (2015-2020)[a]		
PFAS	**Mar-19**	**Apr-19**	**June-August 2019**	**Fish Consumption**	**Drinking Water**	**Recreational[b]**
PFOS	113.9 (<LOQ-302.1)	96 (49.3-167)	5.9 (2.7-26.3)	11-Apr	6.2-667	≧1,700
6:2 FTS	732.9 (<LOQ-1492.4)	1095.7 (632.7-1653.6)	42.6 (6.1-91.2)	NA	100-200[c]	≧26,000
PFBS	141.6 (115.7-193.8)	74.8 (3.5-101.5)	16.4 (3.8-37.6)	NA	1,000-667,000	≧260,000
PFHxA	24.2 (<LOQ-78.4)	43.1 (29.4-87)	9.9 (5.1-18.5)	NA	93	≧24,000
PFHxS	21.5 (<LOQ-90.4)	21.3 (10.5-34)	1.8 (1-10.6)	NA	20-140	≧5,200
PFPeA	<LOQ (<LOQ-13.4)	26.5 (19.1-41.1)	13.1 (7.8-26.8)	NA	93	≧24,000
PFOA	<LOQ (<LOQ-13.7)	6.3 (4.8-8.7)	3 (1.7-7.2)	150-12,000	5.1-667	≧1,300
PFBA	<LOQ	17 (9.5-36.4)	7.1 (<LOQ-13.6)	NA	7,000-71,000	≧1,820,000
PFHpA	<LOQ	16.4 (8.1-37.2)	2.8 (1.6-11.3)	NA	20-560	≧5,200
PFNA	<LOQ	<LOQ	0.8 (0.3-2.3)	NA	9-290	≧2,300
PFDA	<LOQ	<LOQ	0.6 (<LOQ-3)	NA	20-370	≧5,200
PFDoA	<LOQ	<LOQ	<LOQ	NA	290[d]	≧75,000
L-PFDoS	<LOQ	1.6 (<LOQ-3.1)	<LOQ	NA	290[d]	≧75,000
PFTrDA	<LOQ	<LOQ	<LOQ	NA	290[d]	≧75,000
PFTeDA	<LOQ	<LOQ	<LOQ	NA	290[d]	≧75,000
8:2 FTS	<LOQ	<LOQ	<LOQ (<LOQ-5.9)	NA	200[c]	≧52,000

All concentrations are in ng/L. NA = Not available (neither U.S., nor international).

[a] Values compiled by Interstate Technology and Regulatory Council (ITRC) as of 20-Feb-2020 [https://pfas-1.itrcweb.org/fact-sheets/].

[b] Adjustment of drinking water values to scenario involving incidental ingestion during swimming/wading (see text).

[c] No U.S. values available; therefore we used international values compiled by ITRC.

[d] Limit is for the sum of PFDS, PFUnA, PFDoA, PFTrDA, PFTeDA

CHAPTER III

[2]3. ENVIRONMENTAL IMPACTS OF HURRICANE FLORENCE FLOODING IN EASTERN NORTH CAROLINA: TEMPORAL ANALYSIS OF CONTAMINANT DISTRIBUTION AND POTENTIAL HUMAN RISKS

3.1. Abstract

Background: Hurricane Florence made landfall in North Carolina in September 2018 causing extensive flooding. Several potential point sources of hazardous substances and Superfund sites sustained water damage and contaminants may have been released into the environment.

Objective: This study conducted temporal analysis of contaminant distribution and potential human health risks from Hurricane Florence-associated flooding.

Methods: Soil samples were collected from 12 sites across four counties in North Carolina in September 2018, January and May 2019. Chemical analyses were performed for organics by gas chromatography mass spectrometry. Metals were analyzed using inductively-coupled plasma mass spectrometry. Hazard index and cancer risk were calculated using EPA Regional Screening Level Soil Screening Levels for residential soils.

[2] *Reprinted with permission from "Environmental Impacts of Hurricane Florence Flooding in Eastern North Carolina: Temporal Analysis of Contaminant Distribution and Potential Human Health Risks" by Noor A. Aly, Gaston Casillas, Yu-Syuan Luo, Thomas J. McDonald, Terry L Wade, Rui Zhu, Galen Newman, Dillon Lloyd, Fred A Wright, Weihsueh A. Chiu, Ivan Rusyn, 2021. *Journal of Exposure Science and Environmental Epidemiology*, 31(5), 810-822, Copyright [2021] by Springer Nature.

Results: PAH and metals detected downstream from the coal ash storage pond that leaked were detected and were indicative of a pyrogenic source of contamination. PAH at these sites were of human health concern because cancer risk values exceeded 1×10^{-6} threshold. Other contaminants measured across sampling sites, or corresponding hazard index and cancer risk, did not exhibit spatial or temporal differences or were of concern.

Significance: This work shows the importance of rapid exposure assessment following natural disasters. It also establishes baseline levels of contaminants for future comparisons.

3.2. Introduction

Hurricanes and tropical storms are associated with inland flooding that has the ability to redistribute hazardous substances from manufacturing or storage facilities, thereby exposing communities and their residents to possible health risks [113-114]. Health impacts of floods have been widely studied [115-116]; however, the human and environmental health consequences of flooding depend on the geographic location and proximity to areas with high concentrations of chemicals. For example, in agricultural areas, flooding was associated with nutrient or pesticide runoff [117-118]; in urban areas, with bacterial or chemical contamination from water treatment and transportation facilities; and in industrial areas, with spills, emissions, or secondary disasters at the sites that process, manufacture, or store hazardous substances [119-120]. Recent example of a hurricane-associated flood that has been accompanied by the spread of contamination in water and soil is Hurricane Sandy that caused significant flooding in New Jersey and New York states in 2012. Arsenic, lead, polychlorinated biphenyls (PCB), and polycyclic aromatic

hydrocarbons (PAH) were detected in similar elevated concentrations in multiple locations following the hurricane, suggesting a common source [121]. The frequency and intensity of storms is increasing globally and it is expected that future events will be up to 20% wetter which will further increase the risks from extreme flooding [122-124]. Therefore, additional research is needed to improve our understanding of the connections among disaster-associated shifts in exposure to hazardous substances and health outcomes [125].

Another recent example of a catastrophic natural disaster that was associated with major flooding is Hurricane Florence, a slow-moving category 1 storm that made landfall on September 13th, 2018 near Wilmington, North Carolina. Hurricane Florence stalled upon landfall, it moved northward into West Virginia and dissipated only after about 5 days. This storm caused record flooding in eastern North Carolina, with some areas receiving over 100 cm (40 in) of precipitation in just five days. The high winds also caused significant damage to trees and power lines, leading to wide-spread and protracted power outages that may have prevented protective measures against spillage of hazardous substances. It is estimated that the wind and water damage caused by Florence totaled $24 billion, making this hurricane one of the most destructive to affect the United States [126]. The physical damage caused by Hurricane Florence was compounded by the concerns of the possible risk for long-term health effects from chemical contaminants that may have been released from a number of industrial and agricultural facilities in eastern North Carolina. One known area affected by Hurricane Florence included Sutton coal ash storage facility, which is located near the Cape Fear river in New Hanover County, North Carolina [127]. Coal-fired power plants generate large quantities of coal ash, residual material from

burning coal rich in pyrogenic PAH and enriched in some metals [128]. Typically, coal ash is mixed with water and placed in retaining ponds for storage [129]. When the Cape Fear river flooded during Hurricane Florence, the flood water caused a leak of one of Sutton coal ash ponds, spilling the contaminants into the Cape Fear river and downstream into the surrounding areas.

To address concerns about potential chemical contamination as the result of Florence-associated flooding in eastern North Carolina [130-132], this study conducted analysis of contaminant distribution, potential point sources, and associated human health risks. We hypothesized that leakage from the coal ash pond in New Hanover County could result in observable increased levels of hazardous PAH and heavy metals. Because of the lack of historical data on the contaminants of concern in these areas, we conducted temporal analysis by sampling immediately after the storm (in September 2018) and at two 4-month intervals thereafter (January and May 2019). The sampling strategy included collection of soil specimens downstream of two coal ash storage sites, as well as in other areas of agricultural use or where small-scale manufacturing sites were located. In total, soil samples were collected from 12 sites across four counties in eastern North Carolina. A broad spectrum of chemical contaminants of concern, including PAH, metals, pesticides, PCB and other industrial chemicals was evaluated and hazard index and cancer risk for residential soil exposure was calculated for each site/time.

3.3. Materials and Methods

3.3.1. Chemical and Reagents

All chemicals and reagents were ACS reagent grade or equivalent unless otherwise

specified. The following chemicals were used as general analytical materials. Deionized (DI) water, nitric acid (HNO_3, Baker Analyzed, #02-003-469, ThermoFisher Scientific, Waltham, MA), hydrochloric acid (HCl, Baker Analyzed, #02-003-046, ThermoFisher Scientific), hydrogen peroxide (H_2O_2 30%, #H1009, Sigma Aldrich, St. Louis, MO), potassium persulfate ($K_2S_2O_8$, #379824, Sigma Aldrich), sodium chloride (NaCl, #S9888, Sigma Aldrich), hydroxylamine sulfate ($H_8N_2O_6S$, #379913 Sigma Aldrich), potassium permanganate ($KMnO_4$, #223468, Sigma Aldrich), hydroxylamine hydrochloride ($HONH_2 \cdot HCl$, #431362 Sigma Aldrich), Hydromatrix^{TM} (#198003, Varian, Palo Alto, CA), methylene chloride (CH_2Cl_2, #300-4, Burdick and Jackson, Muskegon, MI), hexane (#GC60394-4, Burdick and Jackson), acetone (#010-4, Burdick and Jackson), methanol (#230-4, Burdick and Jackson), pentane (#158941, Sigma Aldrich), hexane (#32293, Sigma Aldrich), nitrogen gas, anhydrous sodium sulfate (Na_2SO_4, #3375-07, J.T. Baker, Phillipsburg, NJ), glass microfibre filters (#1821-021, Whatman, Maidstone, UK), alumina oxide (#21,447-6, Sigma Aldrich), copper (#1720-05, J.T. Baker), white quartz sand (#S-9887, Sigma Aldrich), and silica gel (#3401-05, J.T. Baker).

The following chemicals were used as internal standards: 2,4,5,6-tetrachloro-m-xylene (TCMX, US-RCB-031, ThermoFisher Scientific), fluorene-d_{10} (#442848, Sigma Aldrich), pyrene-d_{10} (#490695, Sigma Aldrich), benzo(a)pyrene-d_{12} (#451797, Sigma Aldrich), PCB Standard Mix (#48246, Sigma Aldrich), Trace Metals Standard I (#C809J26, Thomas Scientific, Swedesboro, NJ).

The following chemicals were used as quantitation standards and/or surrogate standards: 4,4-dibromooctafluorobiphenyl (#101990, Sigma Aldrich), TCMX,

phenanthrene-d_{10} (#364622, Sigma Aldrich), chrysene-d_{12} (#364614, Sigma Aldrich), naphthalene-d_8 (#176044, Sigma Aldrich), acenaphthene-d_{10} (#442432, Sigma Aldrich), perylene-d_{12} (#48081, Sigma Aldrich), PCB 103 (C-103N, AccuStandard, New Haven, CT), and PCB 198 (C-198N, AccuStandard, New Haven, CT).

3.3.2. Study Area and Sampling Strategy

A total of 55 soil samples were collected across four separate locations (**Figure 1** and **Supplemental Table 1**) in eastern North Carolina in September 2018, January 2019, and May 2019. Sampling dates, times and exact locations are detailed in **Supplemental Table 2**. Because of the limited access to some of the sampling sites on subsequent visits, replicate samples are not available at every location for January and May 2019 sampling dates. Surface-level soil samples were collected using plastic and metal shovels into 8-ounce amber sampling jars (#05-719-69, Thermo Scientific) according to US EPA Soil Sampling protocols [133]. To prevent sample cross-contamination, clean nitrile gloves were used at every sampling site. Samples were stored on ice following their collection and during shipping. Upon receipt at the laboratory, samples were stored at -80^{o}C until further processing.

3.3.3. Sample Processing

Prior to digestion (for metal analysis) or extraction (for organic chemical analysis), samples were freeze-dried using model 75040 Freeze Drier 8 (Labconco, Kansas City, MO). All sample analysis results are reported based on the sample dry weight recorded after this procedure. Quality assurance procedures from the NOAA National Status and Trends Program [134], the US EPA Environmental Monitoring and Assessment Program-

Near Coastal [135] and the U.S. Fish and Wildlife Service for trace contaminant analysis [136] were followed.

3.3.4. Organic Compound Analysis

Freeze-dried soil samples were weighed and placed in automated Accelerated Solvent Extractor (ASE, Dionex™ Model 200, Sunnyvale, CA) together with Hydromatrix™ to remove any residual water and analyzed for pesticides, PCB and PAH following methods detailed elsewhere [137]. Experimental samples and associated quality control samples (i.e., blank, matrix spike, duplicate and standard reference material) were spiked with the appropriate surrogate standards [d_{10}-naphthalene,d_{10}-acenaphthene,d_{10}-phenanthrene, and d_{12}-chrysene, d_{26}-nC_{12}, d_{42}-nC_{20}, d_{50}-nC_{24}, d_{62}-nC_{30}, PCB congeners 103 and 198 and 4,4-dibromooctafluorobiphenyl (DBOFB)] before extraction [138]. Following the ASE extraction, the sample extracts were purified using partially deactivated silica/alumina column chromatography to eliminate interfering materials and treated with acid washed granulated copper to eliminate potential interference from elemental sulfur.

PAH, PCB and pesticide analyses were performed by gas chromatography-mass spectrometry (GC-MS) using 6890N GC System/5975C inert Mass Selective Detector (Agilent Technologies) in the selective ion mode after the addition of the appropriate internal standards (d_{10}-fluorene, d_{12}-benzo(a)pyrene, d_{10}-pyrene, and TCMX) to evaluate the efficiency of the analytical methods [138]. The sample extracts were injected in the splitless mode into a 30 m × 0.25 mm i.d. (0.25 μm film thickness) DB-5MS fused silica capillary column (J&W Scientific, Folsom, CA) at an initial temperature of 60ºC, held for

3 min, and temperature was then programmed at 12°C min^{-1} to 300°C with a hold of 6 min at the final temperature for PAH analytes. For PCB, the initial temperature was set at 75°C, held for 3 min, and then ramped to 150, 260, and 300°C at 0, 0, and 20°C/min, respectively, with a final hold of 1 min and a total run time of 66 min. Aliphatic hydrocarbons were analyzed by GC-flame ionization detection (FID), after the addition of d_{38}-nC_{16} as internal standard, using a DB-5MS fused silica capillary column and an oven-temperature program starting at 40°C, held for 2 min and ramped up to 320°C at a rate of 6°C per min and a final hold of 15 min. The GC-MS and GC-FID were calibrated by injections of PCB standard mix (#48246, Sigma Aldrich) at five concentrations (1, 10, 50, 100 and 200 ng/mL). Identification of target analytes was based on the retention time of their respective peaks (aliphatic hydrocarbons) or the respective quantitation ions and a series of confirmation ions (PAH, PCB and pesticides). Lower limit of quantitation (LLOQ, see **Supplemental Tables 3** and **4** for information) was established using the lowest calibration level adjusted for the sample weight and final sample extract volume.

3.3.5. Metal Analysis

Freeze-dried soil samples (1g each) were digested with 10 ml of a 1:1 HNO_3:DI water by heating at 95°C for 10 min. After cooling the sample to ambient temperature, 5 ml of concentrated HNO_3 was added and the sample was heated at 95°C for an additional 30 min. After cooling to ambient temperature, 3 ml of 30% H_2O_2 was added and the sample was momentarily returned to the 95°C. Additional H_20_2 is added in 1 mL increments until effervescence is completed; the sample was then heated until the volume is reduced to 5 ml. The cooled sample was filtered and brought up to a final volume of

100 ml with DI water. Instrumental analysis was performed using a NexION 300D inductively coupled plasma mass spectrometer (ICP-MS, PerkinElmer, Waltham, MA). The LLOQ was established by the measured concentration signal being 10 times the standard deviation of the blank, for the analyses of trace metals the LLOQ was in the range of 0.002–50 µg/g (see **Supplemental Table 5** for LLOQs for each analyte). The ICP-MS was optimized and calibrated each day of operation using one analytical blank (methylene chloride) and trace metals standard I (#C809J26, Thomas Scientific, Swedesboro, NJ) using the average of three replicate integrations. The linearity of the initial calibration was deemed sufficiently linear if $r^2 \geq 0.995$. The ongoing validity of the calibration was determined by the subsequent verifications performed every ten samples.

Mercury (Hg) determinations in soil samples were made after an acid-permanganate digestion of the dry-powdered samples followed by stannous chloride reduction to Hg metal and detection by cold vapor atomic absorption spectroscopy using a flow injection mercury system (Model FIMS-400, PerkinElmer). Specifically, 200 mg of each freeze-dried soil sample was digested with 4 ml of a concentrated H_2SO_4/HNO_3 (2.5:1.5 v/v) mixture by heating at 95ºC for 30 min. After cooling the mixture to ambient temperature, 10 ml of DI water, 10 ml of $KMnO_4$ (5 g in 100 mL of DI water) solution, and 5 ml of $K_2S_2O_8$ (5 g in 100 mL of DI water) solution was added and the sample was heated at 95ºC for 30 min. Sample was chilled to ambient temperature and 5 ml of a $NaCl/H_8N_2O_6S$ (12 g of each in 100 mL of DI water) solution was added to reduce excess permanganate and the sample was diluted to 40 ml with DI water. The instrument was calibrated by injections of a mercury standard (#C809J26, Thomas Scientific) at five

different concentrations (1, 10, 50, 100 and 200 ng/mL). The calibration was deemed sufficiently linear if $r^2 \geq 0.995$. Calibration verification standard and analytical blank samples were analyzed at the start and after every 10 samples and at the end of each analytical run.

3.3.6. Analytical Quality Control (QC)

For every batch of 20 samples or less, a procedure blank (prepared using all reagents and procedures for digestion but not containing the sample matrix), and standard reference materials (for organic compounds we used SRM 1944 - New York/New Jersey Waterway Sediment and SRM 2779 - Gulf of Mexico Crude Oil, National Institute of Standards and Technology, Gaithersburg, MD; for metals we used SRM-SAND-B, High Purity Standards, North Charleston, SC and SRM-MESS-4, National Research Council of Canada, Ottawa, Canada) were run to evaluate the overall accuracy and precision of the procedures used for sample preparation and analysis. Duplicates were included to estimate sample homogeneity and analytical variability. A laboratory blank spike (procedure blank fortified with appropriate trace elements and carried through digestion procedure) and a matrix spiked (fortified sample that is carried through digestion procedure and analyzed to identify any matrix dependent interferences) samples were run with each batch to identify potential digestion interferences and to evaluate the accuracy and performance of analysis. See **Supplemental Tables 6** and **7** for QC data.

3.3.7. Cook's Distance Outlier Test

Cook's distance measure [139] was computed to determine the locations that had outlier concentrations for the individual metals. Cook's distance *D* is a measure of an

observations' influence on a linear regression. Instances with a large influence may be outliers, and the measure is often computed for data sets to identify influential points that may not be good predictors for a fit of a linear model. *D* is calculated by removing the i_{th} data point from the model, recalculating the regression, and summing a scaled version of the squared estimated responses before and after the observation has been removed using formula [1]:

$$D_i = \frac{\sum_{j=1}^{n}\left(\hat{y}_j - \hat{y}_{j(i)}\right)^2}{p\hat{\sigma}^2} \quad [1].$$

The $\hat{y}_j$ denotes the predicted response for observation *j* when using the full dataset, and $\hat{y}_{j(i)}$ the same fitted value when observation *i* has been removed, *p* the total number of predictors in the regression model (*p*=2 for our setting, including intercept), sample size *n*, and $\hat{\sigma}^2$ the estimated error variance from the model. We deemed observation/outliers as influential with D_i>1.0. See **Supplemental Table 8** for the results of this analysis.

Determining Pyrogenic Index and PAH Source Apportionment

A pyrogenic index (PI) was calculated for all samples from concentrations of the 16 EPA priority PAHs and a series of alkylated PAHs in order to determine the likely source of the PAH in each sample [140]. A PI is calculated by taking the sum of concentrations of three- to six-ring PAHs and dividing it by the sum of concentrations of a series of alkylated PAHs using formula [2]:

$$PI = \frac{\Sigma(3-6 \text{ ring priority PAHs})}{\Sigma(Alkylated\ PAHs)} \quad [2]$$

A value greater than one suggests that PAHs are more likely to be from a combustion

source while values lower than one suggests that PAHs are more likely to be from a petroleum source.

Ratios of certain PAH in environmental samples are used as indicators to determine potential sources of PAHs [141]. In this study, we calculated the ratios using data on fluoranthene, pyrene, benzo(a)anthracene, chrysene, anthracene, phenanthrene, indeno(1,2,3)pyrene, and benzo(g,h,i)pyrene. The values for PI and selected ratios used for PAH source apportionment are listed in **Supplemental Table 9**.

3.3.8. Hazard Index and Cancer Risk Calculations

We characterized non-cancer and cancer risk values (see **Supplemental Tables 10** and **11** for the calculated values) for each sample using U.S. EPA Regional Screening Level Soil Screening Levels (SSL) for soils [142]. Non-cancer risk at each location was expressed as a hazard index (HI) and was calculated by summing the individual Hazard Quotients (HQ) for each chemical, ratios between the measured soil concentration C_k for compound k (converted to mg/kg) and the corresponding non-cancer $SSL_{nc,k}$ to determine HI using formula [3]:

$$HI = \sum_{k=1}^{n} \frac{C_k}{SSL_{nc,k}} \quad [3]$$

The calculation of HI was based on the individual PAH non-cancer $SSL_{nc,k}$ corresponding to a hazard quotient of 1. Several chemicals did not have SSLs, so they were not included in the calculation. Cancer risk for exposure to pesticides, polychlorinated biphenyls and other industrial chemicals at all locations except were calculated similarly, using cancer $SSL_{c,k}$ instead. For cancer risk of PAH, we converted each PAH concentration to

benzo[a]pyrene (BaP)-equivalents using the Toxic Equivalency Factors (TEFs) from [143], $C_{BaPeq,k} = C_k\ TEF_k$, and then calculated the cancer risk using the cancer $SSL_{c,BaP}$ for BaP (**Supplemental Table 11**) following formula [144]:

$$\text{Cancer Risk} = 10^{-6} \sum_{k=1}^{n} C_{BaPeq,k}/SSL_{c,BaP}\ ^{144}$$

This calculation is based on the individual PAH cancer $SSL_{nc,k}$ corresponding to a cancer risk of 1×10^{-6} [145-146].

3.3.9. Enrichment Factor Calculation for Metals

In order to perform a comparative analysis of presence of coal combustion-enriched metals among soil samples in this study and to the data from a previous publication [147], we calculated an enrichment factor (EF). An enrichment factor is the ratio of the concentration of each metal between a test location and a reference location and was calculated using formula [5]

$$EF_m = \frac{C_i}{\frac{1}{n}\sum_{i=1}^{n} C_{BL}} \text{ [5]}$$

Where EF_m is the enrichment factor for m^{th} metal, C_i is concentration of that metal in sample i, and C_{BL} is concentration of that metal in samples from Bladen county. In this study we performed these calculations using concentrations of metals in samples downstream from the reported leaked coal ash facility (New Hanover 1 and 4). As a reference, we used an average of concentrations of each test metal from all locations in Bladen County. See **Supplemental Table 12** for the product of these calculations.

3.4. Results

Soil samples were collected from a total of 28 locations in four counties in eastern North Carolina (**Figure 1**) in the days and months following Hurricane Florence. A total of 55 samples (**Supplemental Tables 1-2**) were collected for either organic compounds or metal in locations that included New Hanover County, an industrial area which received high flooding (n=16 samples), Robeson and Bladen Counties, rural areas which received low to moderate flooding (n=30), and Wayne County, an industrial area which received low flooding (n=9). To determine the effects of this major flooding event, three separate sampling campaigns were conducted over the course of 9 months (September 2018-May 2019) to establish a post-disaster "baseline" condition for comparison with contaminant levels immediately after the flooding event. Analyses were performed for a total of 92 PAH, 23 metals, 28 pesticides, 5 industrial chemicals, and 157 PCB (see raw data in **Supplemental Tables 3-5**).

Many of the examined hazardous substances were present in detectable levels (above LLOQ) across most samples (**Figure 2**). Among 16 PAH which have been designated as high priority pollutants by the EPA due to their potential toxicity in humans and organisms and their prevalence and persistence in the environment PAH [148], each of them was found in at least 50% of the samples (**Figure 2A**). Fluoranthene, pyrene, benz(a)anthracene, and anthracene were found in all samples. The concentrations of PAH detected varied greatly, over several orders of magnitude. For example, concentrations of fluoranthene in soils varied from 1,487 ng/g in New Hanover county to 0.37 ng/g in Bladen

county. Dibenzo(a,h)anthracene, which had the lowest detectable concentration of these PAH at 0.12 ng/g in Robeson county, was detected at 125 ng/g in New Hanover county.

Among 23 metals which were analyzed in these samples, iron, aluminum and magnesium, all naturally abundant in the Earth's crust [149], were detected in 100% of samples (**Figure 2B**). Concentrations of metals also ranged widely among samples, those naturally abundant in the Earth's crust, such as iron, were detected in concentrations between 3,014-14,070 μg/g. Metals which have much lower natural abundances, such as arsenic, were detected in concentrations between 1.04-4.05 μg/g. Other metals, including selenium, antimony, and barium, which are known to be found in coal ash ponds and may have potential adverse human health effects [128, 147], were found in at least 50% of samples.

Among other organic pollutants that were detected, there were 33 pesticides, industrial chemicals and PCB (**Figure 2C**). For example, a degradation product of the organochlorine pesticide DDT, 4,4'-DDE was detected in at least 80% of analyzed samples. The concentrations of pesticides ranged from below limits of quantitation to a maximum of 61 ng/g for endosulfan II. The median concentration of pesticides was 0.6 ng/g. Industrial chemicals were detected in 15-20% of samples and had concentrations up to a maximum of 2.9 ng/g for hexachlorobenzene. Industrial chemicals had a median concentration of 0.6 ng/g. PCB were detected in 5-35% of samples and had concentrations ranged up to a maximum of 8.7 ng/g for PCB 138/164/163.

Both spatial and temporal trends in PAH levels in soil samples are shown in **Figure 3A**. The heatmap shows that the distribution of PAH among sample locations and dates varied widely, the highest concentrations were detected in New Hanover county, mainly

in location NH1 that was closest to Sutton lake. The lowest concentrations of PAH were detected in Robeson county. Next, we characterized PAH ratios in all samples to determine possible sources of contamination (**Figure 3B**). Based on three characteristic ratios, most of the samples contained PAH derived from coal and/or biomass combustion except for two samples, one in Wayne and one in Robeson counties, which were likely containing PAH from a petrogenic source. In addition, a pyrogenic index (PI) was calculated [150] as the ratio of EPA priority 3-6 ring PAH to the total of alkylated PAH homologues for each sample (**Figure 3C**). Presence of petroleum products and/or crudes is indicated by the PI in the range of 0.01−0.05, none of the samples in this study had PI<0.05. Petroleum product burn residue and soot samples have PI in the range of 1.5 to 2.0, while even higher PI indicate the likely pyrogenic source. We found that most samples had PI>1 except for three from Bladen County, two in Robeson County, and one in Wayne County. In addition, we calculated PAH-based non-cancer hazard index (HI, **Figure 3D**) and cancer risk (**Figure 3E**) from exposure to residential soils at each sampling location. All locations had HI<<1 indicating no potential human health hazard from PAH levels detected in these samples. However, most samples in New Hanover county, and one sample each from Bladen and Wayne counties had a cancer risk values $>1\times10^{-6}$ in at least one time point. Most of these samples were from the period immediately following Hurricane Florence, and NH1 location had elevated cancer risk over one order of magnitude of the regional screening level. All samples from Robeson county were below the 1×10^{-6} threshold.

Regarding the data from the analysis of metals, we first calculated distributions of each analyte in relationship to the abundance of the aluminum and iron, two major elements that are known to vary widely in the Earth's crust, that are used for geochemical correlations that can better identify metal contamination in soils [149]. We used Cook's distance outlier test on the correlation analyses of each metal with aluminum (**Supplemental Figure 1**) or iron (**Supplemental Figure 2**) to determine which metals and samples may exhibit elevated concentrations of metals. We found that the samples with outlier metal concentrations were almost exclusively from New Hanover county. Next, to determine the potential for the metal contaminants in these samples to be from the coal ash, we calculated the enrichment of metals in these New Hanover county samples as compared to the rural areas in Bladen county with no known coal ash contaminations (**Figure 4A**). As a reference of a coal ash-contaminated sediment, we also show the enrichment factors for the same metals from the recent study of Sutton Coal Ash Pond sediments [147] location that is upstream from the sampling sites examined herein. We found that strontium, barium, manganese, cobalt and nickel in New Hanover county samples 1 and 4 had enrichment factors similar to those in samples from Sutton Coal Ash Pond [147]. **Figure 4B** shows a distribution of concentrations, normalized to aluminum (see **Supplemental Table 13**), for several metals in the samples collected in this study or those for soils from East or West North Carolina and the US [151]. In the NH1 sample collected in September 2018 (marked in red on **Figure 4B**), concentrations of antimony, barium and strontium, metals known to be found in coal ash and contaminated soil/sediments, were detected in highest absolute amounts, as compared to other samples in this study. These

concentrations were also on the high end as compared to the data for soils from East or West North Carolina and the US [151].

We also analyzed samples from September 2018 and January 2019 for other organic compounds such as pesticides, industrial chemicals and PCB (**Supplemental Table 4**). We found that most of these compounds were below the limit of quantitation. Among the analytes that were quantifiable (**Figure 5A**), we found a number of chlorinated pesticides and PCB; most of these were found in samples from Robeson and New Hanover counties. No discernable temporal trends or spatial patterns were found for these analytes. Hazard quotients were also calculated for each individual chemical and **Figure 5B** shows the cumulative hazard index for each sample. Even though pesticides contributed the most to hazard index in all samples with the most significant being 4,4'-DDD, all HI were <<1. Similarly, cumulative cancer risk for these chemicals was calculated for each individual location (**Figure 5C**). Similarly, pesticides contributed the most to the overall cancer risk with aldrin and dieldrin with the greatest contribution; the cancer risk values at each location were $<1\times10^{-6}$.

3.5. Discussion

Hurricane Florence was the top-10 wettest tropical cyclone on record in the United States and produced record-setting rainfall amounts for both North and South Carolina [152]. Natural disasters in general, and flood events in particular, are known to involve mobilization of contaminants (major and minor elements, organic substances such as PAH, PCB, etc.) in the environment and may lead to human exposure [125]. Still, the major

challenges in disaster research response (DR2) and studies of the potential human exposure pathways from events like Hurricane Florence are (i) state of preparedness and ability to rapidly deploy for sample collection, (ii) informed selection of the sampling locations, and (iii) ability to make comparative analyses to the pre-disaster conditions to judge the effect of the disaster.

With respect to the degree of the overall preparedness of environmental scientists to participate in DR2, a number of scientific questions about the environmental health impacts of disasters and the effectiveness of response and recovery strategies are now considered through major government-academia coordination efforts [16, 153]. Both national, regional and local capacity in DR2 is now established for researchers through training in field study design, environmental sample collection, and safety procedures associated with deployments into the areas where restrictions on public access are just being removed and dangers may still exist [154]. Indeed, such prior training and availability of sampling supplies to rapidly deploy to North Carolina allowed our research group to conduct environmental sampling immediately after the rain subsided. These samples represent the most direct evidence of the environmental conditions in the areas impacted by flooding.

Selection of sampling locations in a large area effected by the Hurricane Florence-associated flooding was based on input from local non-governmental organizations and media reports [130-132]. Specifically, it was determined that coal ash was one of the concerns from the Hurricane Florence floodwaters, because it is a hazardous waste by-product of coal-fired electric power plants. Coal ash contains high levels of metals, PAH and other hazardous substances [129, 155-156]. Indeed, concerns over the release of these hazardous

substances with coal ash from a number of storage sites flooded by the Hurricane Florence-associated precipitation were documented in North Carolina [157]. Other potential environmental chemical exposure vectors included flooding of the farms, transportation infrastructure, and municipal water treatment facilities. To account for the vast area impacted by the flooding and to select representative locations for various types of contaminants (**Figure 1**), we chose areas with a known coal ash spill (New Hanover county), with a coal ash facility that did not leak (Wayne county), as well as agricultural use areas with some small-scale manufacturing facilities and previous reports to the toxic release inventory (Robeson and Bladen counties). Overall, none of these areas had information on the broad range of environmental contaminants; therefore, sampling after the disaster was deemed to be the most sensible strategy to determine whether the event resulted in toxic releases of concern to human health.

The most notable finding of our study is the observation that except for the areas impacted by the known coal ash spill from Sutton lake in New Hanover county, few other sampled locations demonstrated evidence for re-distribution of the hazardous contaminants in the environment because of Hurricane Florence. These data are important for two reasons. First, because they provide actionable information to alleviate community concerns about flood waters potentially carrying hazardous substances from the sites of storage to the areas where exposures to the general population may occur. Indeed, not only we reported the levels of PAH, metals and other chemicals, we also showed that based on these data, both non-cancer hazard and cancer risks from exposures through residential soils in most of the areas tested were negligible. Second, these data provide important

reference information for comparison in future studies. Eastern North Carolina is prone to flooding associated with tropical cyclones (e.g., hurricanes Fran in 1996 and Matthew in 2016) and it is likely that an event similar to the Hurricane Florence may occur soon. Comparative analysis of pre- and post-disaster exposure pathways is among the biggest challenges in DR2 [137, 158].

At the same time, the "positive" findings also constitute a number of public health-informative outcomes. Specifically, we showed that the coal ash-associated PAH and metals were found downstream from the pond breach site for the Sutton lake facility. One previous study showed that levels of coal ash-associated metals in the Cape Fear river close to Sutton lake were lower than those in the coal ash pond sediment, but still elevated [147]. Indeed, we provide evidence that coal ash spill may have reached further downstream (**Figure 6A**) because we observed temporal and spatial trends in strontium, barium and antimony, strongest at NH1 site closest to Sutton lake, indicative of the higher concentrations in September 2018, immediately after the spill. The PAH data at this location, however, showed elevated levels at all three sampling time periods and it is difficult to conclude that at this sampling site, which is in the industrial area, that the levels of PAH are from the coal ash spill as opposed to representative of the historical contamination because of other pyrogenic sources. Still, lack of finding of the elevated levels of both metals and PAH at the areas around several capped coal ash ponds in Wayne county (**Figure 6B**) indicate that that area did not suffer from an unmonitored coal ash spill and that the primary areas of concern, as indicated by the high cancer risk from PAH, was in New Hanover county.

Overall, this study presents a comprehensive new dataset that includes both temporal and spatial data on a broad range of hazardous substances of human health relevance. We present evidence for the lack of human health concern in most of the studies areas in eastern North Carolina that were impacted by extensive flooding during Hurricane Florence. At the same time, we show that the reported coal ash spill in New Hanover county was likely associated with a release of a number of metals and PAH that were detected at elevated levels more than 10 kilometers downstream. This and previous coal ash spills that were largely unmonitored have resulted in mobilization of a number of soluble hazardous substances through the floodwaters. Because of the possible widespread transport of contaminated waters and elevated levels of hazardous substances in the soils, additional detailed and longitudinal exposure assessment studies are needed in the areas closest to the sites of unmonitored coal ash spills, especially those that may be affected by natural disasters.

3.6. Acknowledgements

The authors wish to thank Dr. Elena Craft (Environmental Defense Fund) for assistance with sampling logistics. This work was funded, in part, by grants P42 ES027704, P30 ES029067, and T32 ES026568 from the National Institute of Environmental Health Sciences. The use of specific commercial products in this work does not constitute endorsement by the funding agency.

3.7. Compliance with ethical standards

Conflict of interest: The authors declare no competing interests.

3.8. Chapter III Figures and Tables

Figure 3.1: Map of south-eastern North Carolina depicting sampling locations and precipitation amounts caused by Hurricane Florence

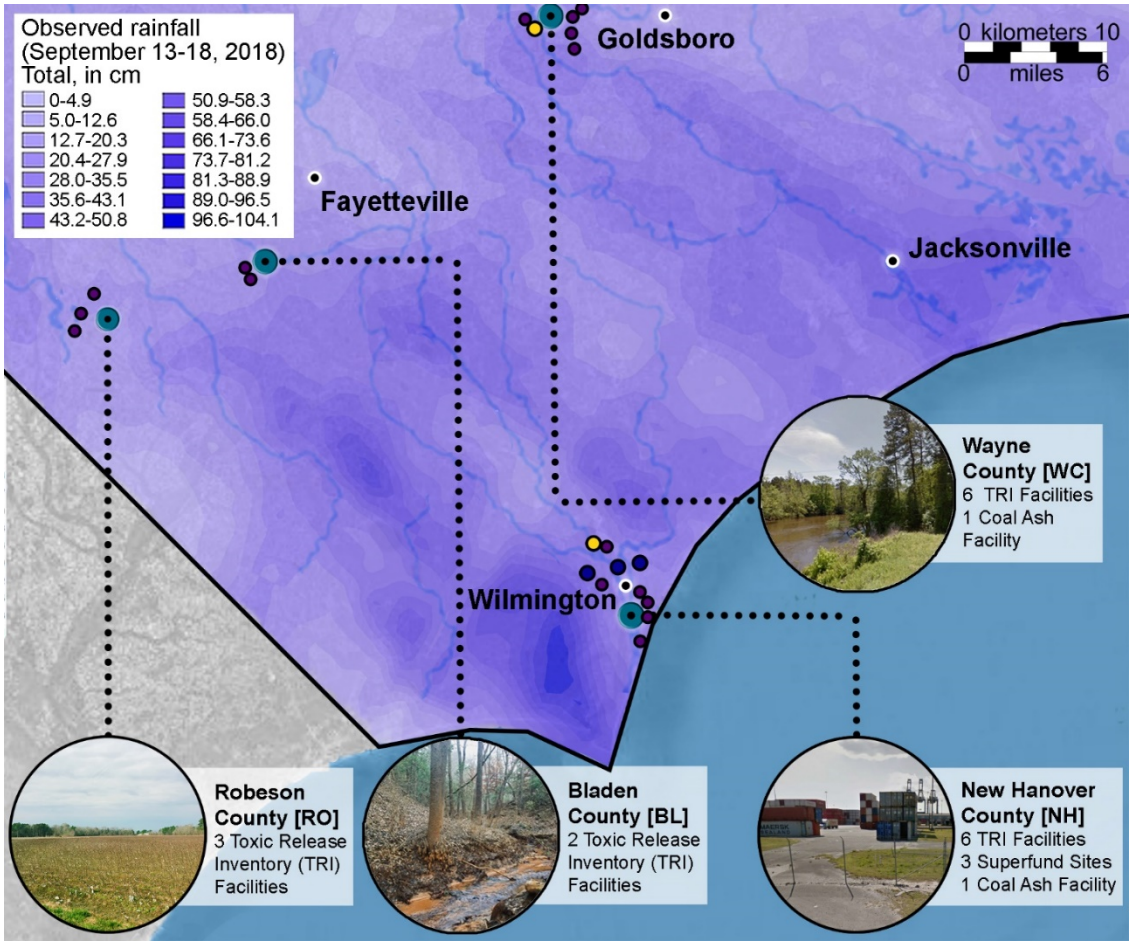

Toxic Release Inventory facilities (purple dots), Superfund sites (dark blue dots) and coal ash facilities (yellow dots) are also indicated. Soil samples were collected between September 2018 and May 2019 See **Supplemental Table 2** for dates, locations and the number of samples collected. GPS coordinates for sampling locations, Toxics Release Inventory and Superfund sites, and coal ash facilities are listed in **Supplemental Table 14**. Background map was from ESRI/OpenStreetMap.

Figure 3.2: Summary of the hazardous contaminants from various evaluated chemical classes

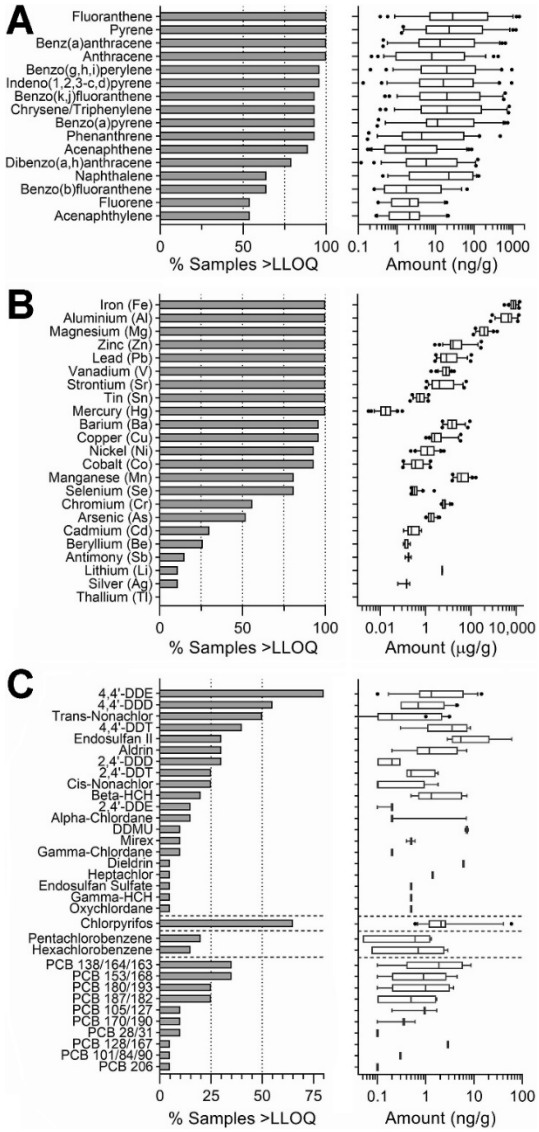

Left panels show percentage of soil samples which contained quantifiable amounts of **(A)** 16 EPA priority PAHs, **(B)** metals, or **(C)** pesticides, industrial chemicals and PCBs. Right panels show their respective ranges of concentrations. All raw data are available in **Supplemental Tables 3-5**.

Figure 3.3: Data on PAH in soil samples

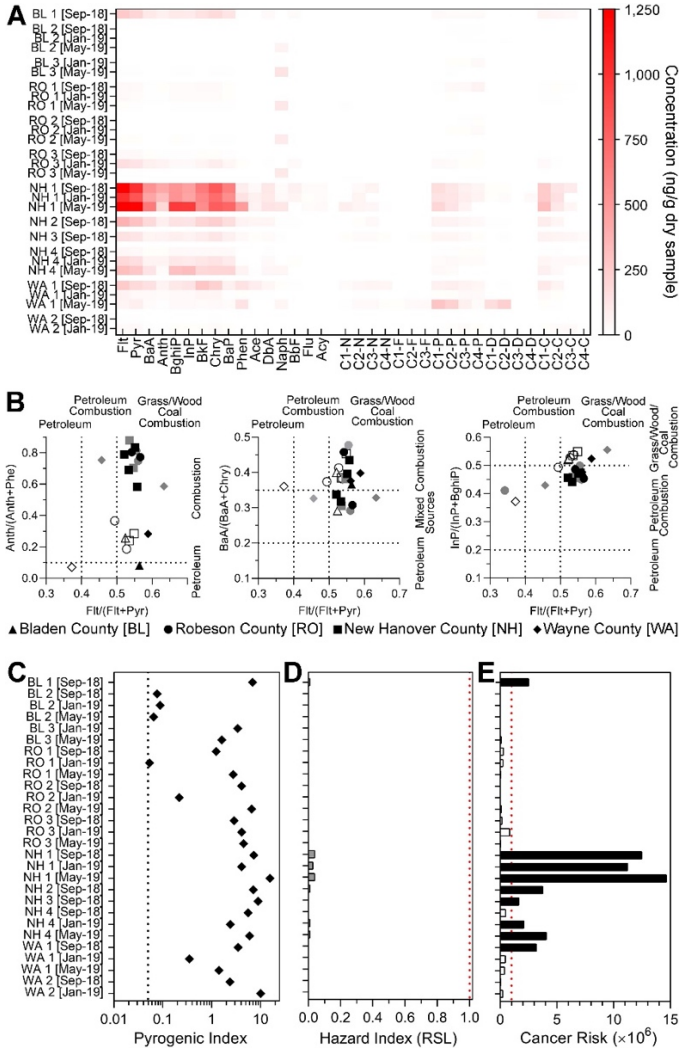

(A) A heatmap displays a range of concentrations of the 16 EPA priority PAH and a series of alkylated PAH used to calculate pyrogenic index at each soil sample. **(B)** Scatter plots showing the ratios (as depicted in the axis legends) for select PAH across all tested samples. Symbol shapes are representative of the sampling locations (see legend); symbol shading is indicative of the time when each sample was collected (black is for samples collected in September 2018, gray is for samples collected in January 2019 and white is for samples collected in May 2019). **(C)** The pyrogenic index (PI) was calculated for each sample as indicated in methods. The vertical dotted line indicates an upper value for PI from petroleum products or crude oil [150]. Also shown are screening-level risk characterization values for non-cancer **(D)** and cancer **(E)** risks, based on EPA Soil Screening Levels. Vertical dashed lines denote screening levels of potential concern, based on a non-cancer Hazard Index=1 and a cancer risk of 10^{-6}. All raw data for PAH is available in **Supplemental Table 11.**

Figure 3.4: Data on metal in soil samples

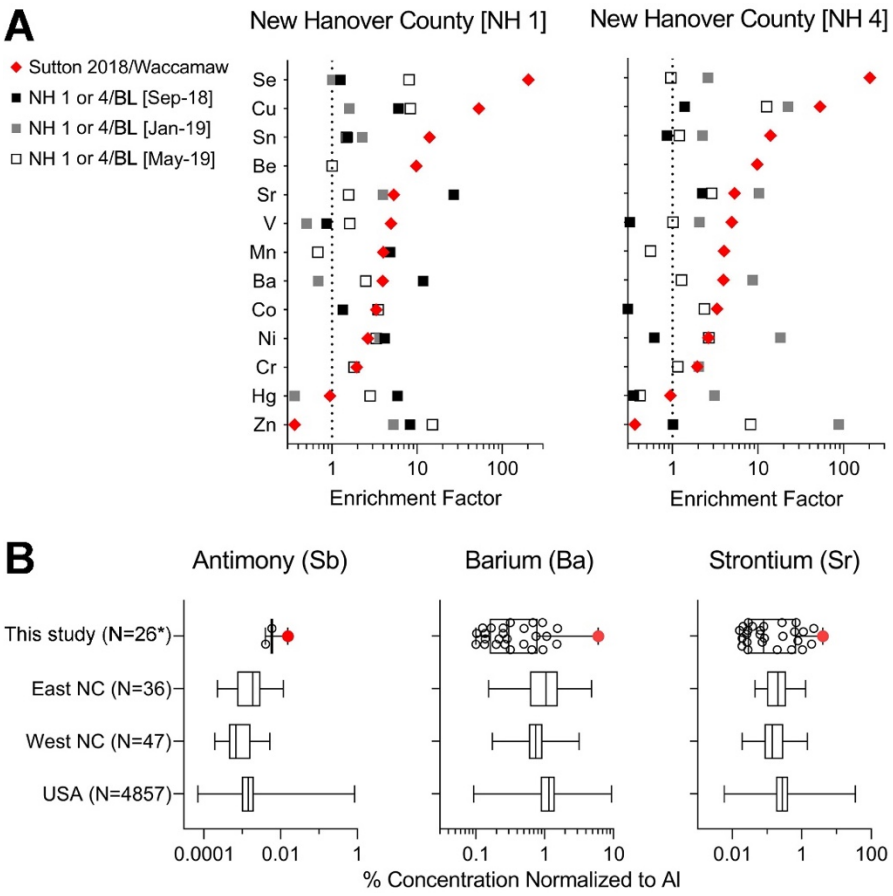

(A) Distribution and enrichment of trace metals in sediment of Sutton coal ash pond (red diamonds, from [147]) and soils (squares) from New Hanover county sites 1 and 4. Square symbol shading is indicative of the time when each sample was collected (black is for samples collected in September 2018, gray is for samples collected in January 2019 and white is for samples collected in May 2019). Sutton 2018 data was normalized to lake Waccamaw data and NH1 or 4 sample data were normalized to the average of the values for all samples from Bladen (BL) county for the corresponding time period. **(B)** Box and whiskers plots show the range of concentrations for antimony (Sb), barium (Ba) and strontium (Sr), normalized to aluminum, for samples from this study, or data from USGS [151] for North Carolina and the entire United States. Box is interquartile range, vertical line is the median, whiskers are min-max values. Dots in the plots for this study show individual sampling locations, the red dot indicates location NH1-September 2018. The numbers in parenthesis indicate the number of samples included into each box and whiskers plot. The asterisk indicates that one of the samples from this study (NH4-January 2019) was excluded from the metal analyses because the concentration of iron in this sample was an outlier (based on Cook's distance) as compared to aluminum and other metals. All raw and normalized data for metals is available in **Supplemental Tables 5** and **13.**

Figure 3.5: Data on pesticides, industrial chemicals and PCB in soil samples

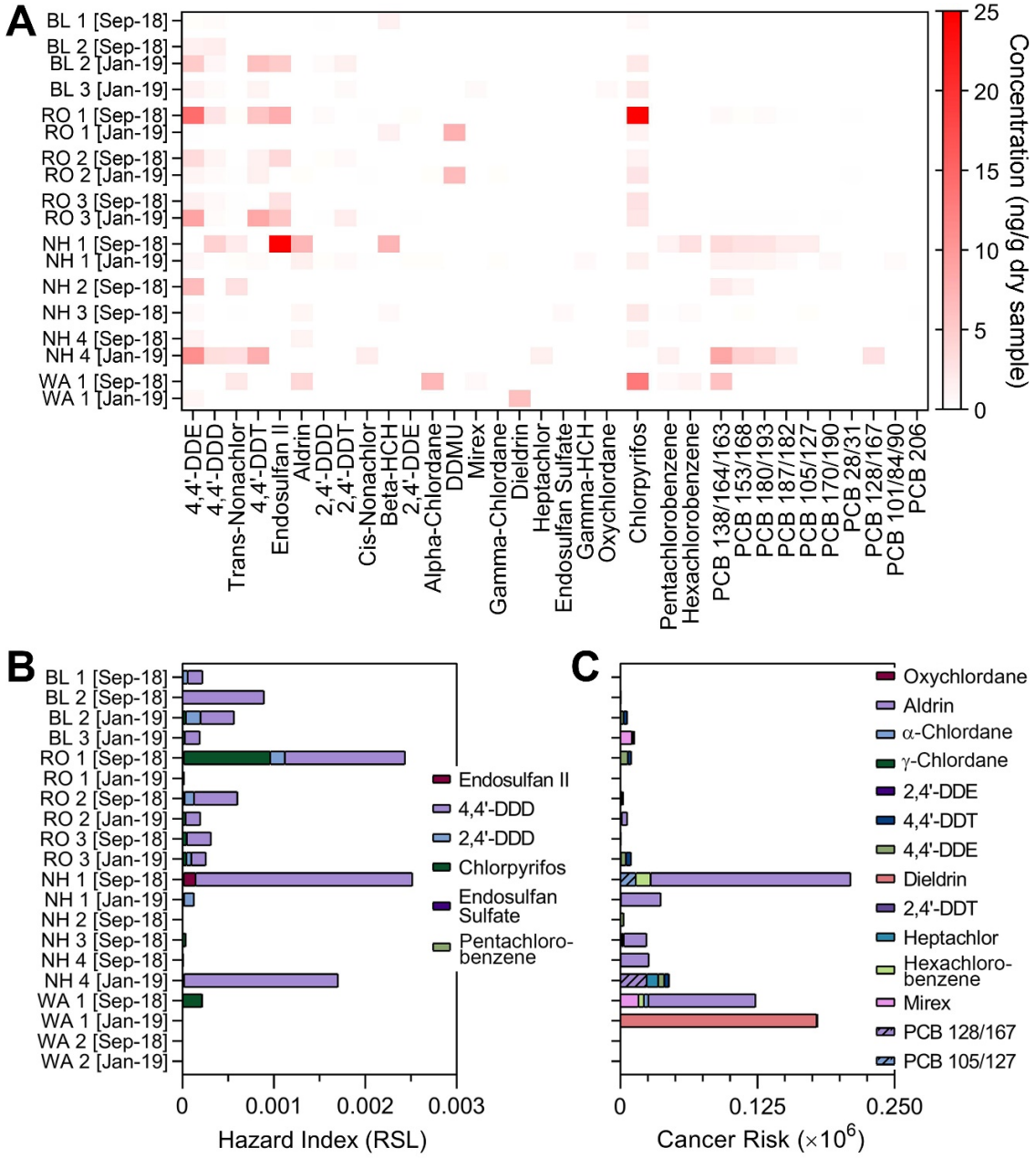

(A) A heatmap displays a range of concentrations of the detectable chemicals in each soil sample. Also shown are screening-level risk characterization values for non-cancer **(B)** and cancer **(C)** risks, based on EPA Soil Screening Levels. Stacked bar graphs contain individual compound-derived hazard quotients as indicated in the color legend next to each graph. All raw data for the chemicals displayed in this figure are available in **Supplemental Table 4.** Data for May 2019 were not collected because the levels of these chemicals in previous two sampling periods were unremarkable.

Figure 3.6. Map of two sampled coal ash pond locations and surrounding areas in south-eastern North Carolina

Sampling locations (blue inverted water drops) are indicated with the location ID (see **Supplemental Table 2** for detailed sample location information). **(A)** Locations in New Hanover county are shown. Sutton lake coal ash pond is outlined in red. **(B)** Locations in Wayne county are shown. Retired coal ash ponds near Quaker Neck lake are outlined in red. Background maps were from ESRI/OpenStreetMap.

CHAPTER IV

[3]4. UTILIZING ION MOBILITY SPECTROMETRY - MASS SPECTROMETRY FOR THE CHARACTERIZATION AND DETECTION OF PERSISTENT ORGANIC POLLUTANTS AND THEIR METABOLITES

4.1. Abstract

Persistent organic pollutants (POPs) are xenobiotic chemicals of global concern due to their long-range transport capabilities, persistence, ability to bioaccumulate, and potential to have negative effects on human health and the environment. Common POPs cover a range of diverse chemical classes. Identifying POPs in both the environment and human body is therefore essential for assessing potential health risks. Currently, platforms coupling chromatography approaches with mass spectrometry (MS) are the most common analytical methods employed to evaluate both parent POPs and their respective metabolites and/or degradants in samples ranging from drinking water to biofluids. Unfortunately, different types of analyses are commonly needed to assess both parent and metabolite/degradant POPs from various classes which presents a number of technical and logistical challenges when rapid analyses are needed, and sample volumes are limited. To address these challenges, we characterized 64 compounds including parent per- and polyfluoroalkyl substances (PFAS), pesticides, polychlorinated

[3] *Reprinted with permission from "Utilizing Ion Mobility Spectrometry-Mass Spectrometry for the Characterization and Detection of Persistent Organic Pollutants and their Metabolites" by Noor A. Aly, James N. Dodds, Yu-Syuan Luo, Fabian A. Grimm, MaKayla Foster, Ivan Rusyn, Erin S. Baker, 2021. Analytical and Bioanalytical Chemistry, Copyright [2021] by Springer Nature.

biphenyls (PCBs), industrial chemicals, and pharmaceuticals and personal care products (PPCPs) using ion mobility spectrometry coupled with MS (IMS-MS), and their metabolites and/or degradants. Different ionization sources including electrospray ionization (ESI) and atmospheric pressure photoionization (APPI) were employed to determine optimal ionization for each chemical. Collectively, this study advances the field of exposure assessment by structurally characterizing the 64 important environmental pollutants, assessing their best ionization sources, and evaluating their rapid screening potential with IMS-MS.

4.2. Introduction

Xenobiotics are of great concern to humans and the environment due to their wide use in agriculture, industrial processes, and ubiquitous presence in consumer products. Many xenobiotics are considered POPs and have been shown to pose carcinogenic, mutagenic or reproductive/developmental hazards [159]. The Stockholm Convention on POPs is an international treaty designed to protect human health and the environment. Through this treaty a number of chemicals were recognized as of great concern, including per- and polyfluoroalkyl substances (PFAS), pesticides, polychlorinated biphenyls (PCBs), industrial chemicals, and industrial chemical byproducts [160]. In 2001, the Stockholm Convention listed twelve substances (Table 1). In 2017, an additional sixteen POPs were added to the list, and currently three more chemicals are under review. To date, the original twelve listed substances have either been phased out completely or their use restricted; however, many are persistent and still detected in the soil, water and blood [161].

There are also a large number of POPs not yet identified including emerging chemicals, and pharmaceuticals and personal care products (PPCPs) [162]. These unknown POPs and other POPs formed by metabolism and degradation further complicates exposure studies. Metabolism of xenobiotics through various enzymes including cytochrome P450 oxidases, UDP-glucuronosyltransferases (SULT) and glutathione S-transferases (GULT) is extremely common [163]. POPs are also commonly degraded by bacteria, or through photochemical and other processes, forming intermediates and metabolites that are often more toxic and stable than the parent compounds [164]. Thus, the ability to identify not only parent POPs, but also their metabolites and degradants is essential to fully characterizing exposure and understanding potential adverse effects on human health and the environment [165-166].

Due to the chemical diversity of parent POPs and their metabolites and degradants, to date multiple time-consuming sample extractions and analytical methods are commonly employed [167]. For example, traditional methods use a solid phase or liquid-liquid extraction to isolate and concentrate the molecules of interest. Then, a number of analytical approaches often coupling gas, liquid or supercritical fluid chromatography (GC, LC or SFC) with mass spectrometry (MS) are used to accurately identify and quantify the molecules in the environmental and human samples [168]. While current methods for sample preparation (e.g. extraction and derivatization) and analytical measurements of POPs and their metabolites/degradants provide high selectivity and throughput, the increasing number of POPs and the structural differences in their metabolites and degradation products makes it difficult to rapidly screen for the broad

range of chemicals in cases of complex or unknown exposures. Other separation and coupled separation techniques are thus of great interest for the exposure assessment studies. For example, ion mobility spectrometry coupled with MS (IMS-MS) has shown promise to screen diverse POPs including PFAS and PCBs and their subsequent products without extensive sample preparation [168-169], however, extensive analyses on their metabolites and degradant products has not been performed. IMS is a rapid separation technique, occurring on a millisecond time frame and allowing gas-phase structural analyses [170]. By coupling IMS with MS, both structure and m/z information can be obtained for the molecules of interest, and high sensitivity small molecule measurement have been reported for IMS-MS analyses in various matrices including a limit of detection of 100 pg/mL in serum [169-172]. Additionally, since IMS-MS occurs post-ionization, various ionization sources can be used and it can be implemented after GC or LC separations when multidimensional characterization is desired.

In this study, we utilized IMS-MS to characterize 27 chemicals listed by the Stockholm Convention and 37 POPs from a range of other chemical classes of concern, including PAHs, PCBs, industrial products and byproducts PPCPs, PFAS, pesticides and their corresponding metabolites and degradation products. These chemicals were selected since many are included in the Agency for Toxic Substances and Disease Registry (ATSDR) or International Agency for Research on Cancer (IARC) monographs. The selected PPCPs as well as their sulfate and glucuronide metabolites are frequently detected in wastewater, and we also tried to include metabolites and degradation products of all parent chemicals. In the IMS-MS evaluations, all chemicals were assessed for their

preferred ionization method and isomer separations to determine if simultaneous rapid screening of both parents and metabolites was possible in the same analysis or if multiple evaluations must be performed [173]. This study, therefore used electrospray ionization (ESI) and atmospheric pressure photoionization (APPI) sources to assess both the parent and metabolites/degradants of the specific POPs noted in **Table 1**. Since these two sources provide complementary chemical assessments (e.g., ESI works well for polar molecules while APPI is commonly utilized for nonpolar molecules), evaluating the different chemicals with both is important. The results for simultaneous evaluations of the parent and metabolites/degradants in solvents and complex mixtures such as aqueous film-forming foams (AFFFs) showcase capabilities and challenges for performing rapid assessments of each molecule type with IMS-MS.

Table 1: The POPs and their metabolites/degradants used in this study (grouped by chemical classifications, Stockholm Convention annex, and ionization method).

4.3. Materials and Methods

4.3.1. Sample Preparation

Chemical standards for all molecules except the PCBs were obtained from US EPA (Dr. Ann Richard) or were purchased from Sigma-Aldrich (St. Louis, MO), Santa Cruz Biotechnology (Dallas, TX) and Toronto Research Chemicals (Ontario, CA) (**Supplemental Table 1**). All purchased chemical standards were >97% pure according the manufactures. The PCB standards were synthesized as detailed in Grimm et. al [174]. High purity solvents (≥99.9%) including water, methanol, acetone, acetic acid and toluene

were purchased from Sigma-Aldrich. PCBs and PAHs were dissolved in toluene and diluted to a final concentration of 5 μM in 50:50 methanol: acetone. The remaining standards were diluted in 80:20:0.1 methanol:water:acetic acid to a final concentration of 1 to10 μM (**Supplemental Table 1**). AFFF samples were acquired from Chemguard (Marinett, WI), FireStopper International (Varhaug, Norway), and Angus Fire (Angier, NC) and diluted 100-fold in deionized water.

4.3.2. IMS-MS Analyses

An Agilent 6560 IMS-QTOF MS (Agilent Technologies, Santa Clara) was utilized for all nitrogen gas drift tube IMS (^{DT}IMS) measurements in this work and all individual standards were directly injected in triplicate into the APPI and ESI sources and evaluated in both positive and negative ionization mode. Furthermore, blanks were injected between each standard to make sure no carryover occurred during the runs. PFAS standards and AFFF solutions were run in triplicate with only ESI in negative ionization mode due to their know preference for this analysis type [109]. For the IMS analyses, the ions were passed through the inlet glass capillary, focused by a high-pressure ion funnel, and accumulated in an ion funnel trap [175]. Ions were then pulsed into the 78.24 cm long IMS drift tube filled with ~3.95 torr of nitrogen gas, where they travelled under the influence of a weak electric field (10–20 V/cm). Ions exiting the drift tube were refocused by a rear ion funnel prior to Quadrupole Time-of-flight (QTOF) MS detection and their drift time was recorded. For each detected feature, collision cross section (CCS) values were calculated using a single electric field voltage [30]. Drift times and CCS values for each tested substance are listed in

Supplemental Table 1. The detailed instrumental settings follow those previously published in an interlaboratory examination and a drift tube IMS CCS analyses and can be found in **Supplemental Document 1** [30]. Prior to each experimental analysis the instrument was tuned and a mass calibration was performed using Agilent Tune Mix (G2421A/ G2432A, Agilent).

4.3.3. LC-IMS-MS Instrumental Analysis

For the AFFF analyses [176], 20 µL of each sample was injected on a ZORBAX SB C-18 column (2.1 x 50 mm, 1.8 µM; Agilent) using a 1260 Infinity II system (Agilent). LC conditions were as detailed by [109] with mobile phase A consisting of 5 mM ammonium acetate in 95% water and mobile phase B made up of 5 mM ammonium acetate in 95% methanol. The initial chromatographic condition was maintained at 90% A and 10% B for 0.5 min. The gradient was ramped such that there was 30% B by 2 min, 95% B by 14 min, and 100% B by 14.5 min. The 100% B condition was held for 2 min, resulting in a total run time of 16.5 min. Following each run, the amount of B was returned to 10% for 6 min to equilibrate the column prior to the next injection. A flow rate of 0.4 ml/min was used through the entire gradient. Blank samples were performed before and after each AFFF analysis run to ensure that no carryover existed between samples. Blank subtraction was also utilized to make sure contaminates were not included in the evaluations. IMS-MS analyses were performed using with ESI in negative mode.

4.3.4. Data Analysis

The Agilent IM-MS Browser software was utilized for all single field CCS calculations. Agilent Mass Profiler software was utilized to assess the drift times for the observed ions and calculate the CCS values. Relative standard deviations (RSDs) of <1% were observed for all triplicate CCS measurements.

4.4 Results and Discussion

In this study, 64 chemicals were studied with 18 parent POPs from various chemical classes including industrial chemicals, PAH, PCB, pesticides, PFAS and pharmaceuticals, and 46 of their metabolites or degradation products (**Table 1**). Many of the assessed chemicals are recognized as chemicals of concern by the Stockholm Convention. For example, chemicals categorized in **Table 1** as Annex A are those where production must be eliminated, Annex B must be restricted, and Annex C currently have measures being taken to reduce their unintentional release [177]. While some chemicals analyzed in this study have not been listed by the Stockholm Convention, they are also considered POPs and may have adverse human health effects. For example, chemicals in the treaty such as PCBs, pesticides and PFAS were of great interest in our study due to their known toxic effects. Pesticides that were analyzed in our study included aldrin, dieldrin, heptachlor, hexachlorobenzene and endosulfan. These organochlorine pesticides have classic POP qualities and exposure is associated with adverse health effects such as endocrine disruption or carcinogenicity. Studying PCBs is also important as their persistence in the environment corresponds to their degree of chlorination with half-lives

varying from 10 days to one and a half years with potential endocrine disruptors and have genotoxic properties. In our study PCB 3 and its isomeric metabolites were evaluated as the structure of these chemicals can have varying effects on their metabolism and elimination. Finally, PFAS were studied as this category of chemicals has gained worldwide attention due to their potential hazardous human health effects and ecological environments [178]. In 2009, perfluorooctanoic acid (PFOA) and perfluorooctane sulfonate (PFOS) were added to the Stockholm Convention and their use was banned or severely restricted [160]. PFAS as a class have a variety of applications including chemical industry, consumer products and production of AFFFs because of their unique properties such as thermal stability, hydrophobicity and surface activity [179]. Because these characteristics allow manufacturing goods to have beneficial properties such as stain and water resistance, >5000 PFAS are thought to have been produced [82, 180]. Because of their chemical properties, PFAS have long-distance transport potential, bioaccumulate, and toxic effects such as immunotoxicity, genotoxicity, reproductive toxicity, neurotoxicity, and carcinogenicity. This makes PFAS in general of great concern and especially since some PFAS can be metabolized or degraded. Therefore, exposure to PFAS can be from a direct source such as drinking water or air inhalation, or indirect source such as the uptake of transformation products [44].

4.4.1 Investigation of a preferred ionization method for POP parent and metabolites/degradants

Analysis of the 64 chemicals with IMS-MS was performed using both an ESI and APPI source. The ESI studies were performed in both positive (ESI[+]) and negative (ESI[-]) ion modes to study the protonated and deprotonated ions, while APPI was only performed in positive mode (APPI[+]) to assess protonation and positive radical formation. While the APPI negative ion mode was initially evaluated for deprotonated ions, it was not used in this study due to its lower sensitivity when compared to the ESI[-] analyses [181]. In our analysis of the 18 parent POPs and 46 metabolites and degradation products, we detected a total of 108 different ions; some ionized in both the APPI and ESI sources for both polarity modes. Thus, a total of 108 CCS values are reported in **Supplemental Table 1**. In comparison of the ionization modes, most chemicals (n=42) were detected in ESI[-] mode, followed by APPI[+] (n=29) and then ESI[+] (n=21), with 6 chemicals found in all modes (**Figure 1A**). ESI[-] also had the greatest number of unique identifications with 30, illustrating its potential as the most comprehensive ion source for these molecules. Since it is established ESI works best for polar molecules, while APPI is optimal for nonpolar compounds [182], our findings also reflect that most of our parent POPs studied were nonpolar and more commonly observed with APPI[+], while their metabolites/degradants were polar and observed in ESI. A majority of the molecules detected with APPI could also be detected using the ESI source, except for PAH, PCB, TCE/PCE and some pesticides. The different ionization modes and compound classes were then assessed to see if linear correlations in CCS versus *m/z* plots occurred (**Figures**

1B and **1C**). While we noticed that the chemicals greatly overlapped in CCS for the different ionization modes (**Figure 1B**), in **Figure 1C** the PFAS separated from all other POPs with a much lower slope due to their high degree of fluorination. In addition, *m/z*-specific areas such as those for the PAHs were also noted to be smaller than the other classes allowing their distinction. To further illustrate known metabolic and degradation pathways, specific examples for the different classes are given below.

4.4.2. PCB parents and metabolites

PCBs were commonly used industrial chemicals in adhesives, electrical equipment and oil based paints [183] from the 1920s until their production in the United States was banned in 1979. Despite their discontinued production, PCBs can be detected worldwide, including in Arctic regions [184]. Furthermore, exposure to PCBs has known adverse human health effects, with recent findings suggesting some metabolites also have toxic properties [185]. Specifically, some hydroxyl PCB have higher estrogenic activity than their parents, act as disruptors of thyroid homeostasis, and have neurotoxic potential. Additionally, hydroxyl PCB are transferrable from mothers to fetus via placenta [186] and some can inhibit glucuronidation and sulfation reactions, hindering their elimination [185]. The specific PCBs analyzed in this study were PCB 3 and PCB 11, because these lower chlorinated PCBs have gained attention in recent years due to their detectability in air samples [187]. Furthermore, these PCBs are likely to undergo cytochrome P450 enzyme-catalyzed where they can hydroxylate, and form sulfate metabolites [185] (**Figure 2A**).

In our study, the parent PCBs and their methoxy metabolites were only detected using the APPI source due to their nonpolar structures. Because the parent PCBs and methoxy metabolites do not have functional groups that are easily protonated or deprotonated, they predominantly form radicals with APPI. However, the hydroxyl and sulfate metabolites were preferentially detected using ESI[-] because of the addition of polar functional groups which easily deprotonate. Relative abundances of sulfate PCB ions detected by ESI were considerably higher than all other PCB ions detected in all modes. Abundances of hydroxylated ions detected by ESI were comparable to PCB 3 and the methoxy metabolite detected by APPI (**Figure 2B**). Furthermore, isomeric separation was also observed between 3'-PCB 3 sulfate and 4'-PCB 3 sulfate (**Figure 2B**). However, while 2'-OH-PCB 3 could be distinguished from 3'-OH-PCB 3 and 4'-OH-PCB 3; 3'-OH-PCB 3 and 4'-OH-PCB 3 could not be separated (**Figure 2B**). These findings are noteworthy because OH-PCB have varying adverse effects. For instance, it has been reported that 4'-OH-PCB 3 is a carcinogen, while 3'-OH-PCB 3 and 2'-OH-PCB 3 are not [188]. Hydroxylated and sulfated PCB also bind to thyroid hormones with varying affinities [189]. Although some isomers are indistinguishable with this technique, the ability to separate some of these molecules with IMS is still useful for screening samples and deciding when it is necessary for additional front-end separation techniques such as LC or SPE. Additionally, both APPI and ESI sources have a similar response to the PCB ions detected with each mode except the sulfate ions which have much higher relative abundances due to their higher ionizability (**Figure 2C**).

4.4.3. PPCPs, industrial chemicals and their metabolites

This study also analyzed common wastewater pollutants and their metabolites. The increasing occurrence of POPs in wastewater has received attention in recent years because of potential adverse human health and ecosystem effects [190]. The pollutants of concern in wastewater include PPCPs and industrial chemicals. These have been documented to have endocrine disrupting effects and possible carcinogenicity to humans and can lead to disruptions in the ecosystems, as well as have possible concern to human health through the food chain [191]. Here we assessed common wastewater pollutants including bisphenol A (BPA) (**Figure 3**), paracetamol/acetaminophen (**Figure 4**), propofol, mycophenolic acid, morphine and estrone as many have been documented as endocrine disruptors in fish [192-193]. Furthermore, these chemicals are metabolized with SULT and GULT, and sulfate and mono ß-D-glucuronide conjugates are formed **(Figure 3A, Figure 4A)** [194]. As expected, when analyzed individually, the parent, sulfate and glucuronide versions of these molecules were readily separated based on *m/z* and IMS drift time, but the additional IMS dimension gives further confidence for identifying these compounds from other components in biological and environmental samples. BPA parent and metabolites were all detected in ESI[-] and separated based on *m/z* and drift time **(Figure 3B).** The high polarity of the sulfate metabolite showed higher ionization than both BPA and the glucuronide metabolite. However, despite the low abundance of BPA, it could still be identified in the sample. While the APPI source could only ionize the BPA glucuronide metabolite, the relative abundance was very similar to what was observed using the ESI source **(Figure 3C).** In the example of paracetamol and its sulfate and

glucuronide metabolites, they were all detected using both ESI[+] and ESI[-] and readily separated based on *m/z* and IMS drift time (**Figure 4B**). Although the sample contained each standard in equimolar concentrations, different relative abundances were observed based on ionization type. ESI[+] had higher ionization of paracetamol glucuronide as an $[M+Na]^+$ ion but low ionization of paracetamol sulfate $[M+Na]^+$, while the opposite was observed for the deprotonated ions using ESI[-]. Also, paracetamol sulfate was not observed as an $[M+H]^+$ ion in ESI[+], while paracetamol glucuronide was. The parent paracetamol had similar ionization response in both positive and negative ESI modes, and while detected with APPI, the response was slightly lower (**Figure 4C**). Furthermore, in ESI[+], two conformers were observed for the $[M+H]^+$ adduct of paracetamol. These two peaks may be either due to structural flexibility of paracetamol or differences in its protonation sites (protomers) as both situations have been observed for other small molecules. Importantly, this signature provides added identification confidence for paracetamol in complex mixtures. [195-196] When examining the metabolites for paracetamol, the sodiated glucuronide conjugate exhibited a lower drift time than its protonated form illustrating compaction due to the Na^+ binding both the parent atoms and conjugate together. However, this did not occur in the sulfated conjugate and it is expected that the Na^+ only bound to the sulfate oxygens.

Since it was observed that a majority of the common wastewater pollutants and their metabolite standards ionized best with the ESI source, these chemicals were further evaluated with ESI for rapid screening capabilities. In wastewater samples, the commonly found pollutants include bisphenol A, paracetamol, propofol and mycophenolic acid and

their metabolites with concentrations ranging from detection limits of 0.05-50 ng/L to levels as high as 43,000 µg/L [173, 197]. To evaluate the ionization differences and IMS separations of these chemicals with IMS-MS, we combined all of the standards in an equimolar mixture to form our own "wastewater" sample. Similar to when the chemicals were analyzed individually, we were able to detect all parent chemicals except for bisphenol A in ESI[+] and propofol in ESI[-] (**Figure 5A**). Ion abundances of all chemicals detected in both positive and negative ESI modes from the equimolar solutions are also illustrated, indicated detection but some ionization differences (**Figure 5B**). As expected, the sulfate and glucoronide conjugates had significantly higher abundances in ESI[-] than all the parent chemical, while several of the sodiated parent chemicals ionized best in ESI[+].

4.4.4. Analysis of pesticides and their metabolites or degradation products

The original Stockholm Convention listed 12 chemicals which were primarily polyhalogenated organic compounds with high lipid solubility, this feature allows them to bioaccumulate in fatty tissue of animals and have great stability and resist hydrolysis and photolytic degradation in the environment [164]. Included in these polyhalogenated organic compounds are the organochlorine pesticides aldrin, dieldrin, hexachlorobenzene, and endosulfan. These chemicals and their degradation products **(Figure 6A)** were also assessed with IMS-MS since aldrin and endosulfan can degrade through oxidative pathways mediated by microbial or enzymatic processes and hexachlorobenze degrades through dechlorination processes. These chemicals were detected primarily using APPI[+]

as most do not have functional groups. However, the molecules with sulfate were also detected using ESI and interestingly no significant difference in detected abundances for protonated and deprotonated chemicals was observed, however, sodiated ions had comparatively low abundances (**Figure 6B**).

4.4.5. PFAS and their degradation products in AFFFs

PFAS precursors are abundant in the environment and have been detected in many human samples [198]. Their transformation products often have longer half-lives and can be more toxic than their precursors. Therefore, the analysis of both PFAS precursors and degradation products are necessary to assess possible human health effects. Limited studies have been conducted on the environmental occurrence and transformation of PFAS [199-200]. However, it is known that fluorotelomers 6:2 FTAB and 6:2 FTS, and PFOS and PFOA degrade to shorter chain PFAS including PFHpA, PFHxA, PFHxS, PFPeA, PFBS and PFBA as shown in **Figure 7A** [198]. Degradation of PFAS has been observed in microorganism-mediated processes, activated sludge plants and aerobic sediment [95]. Additionally, remediation methods such as atmospheric pressure plasma jet treatment have elucidated possible degradation pathways of PFOS and PFOA [201].

Using ESI[-], PFAS were identified by either their $[M-H]^-$ and/or $[M-H-CO_2]^-$ ions and separated based on their *m/z* and IMS drift time values (**Figure 7B**). Since the PFAS of interest for this study were preferentially ionizable by ESI[-], this was the only source utilized for their evaluations [109]. Furthermore, abundance measurements showed that the longer chain PFAS such as PFOS, PFHxS, PFOA, PFHpA and PFBS had similar

responses, but the short chain PFAS including PFHxA, PFPeA and PFBA had lower relative abundances (**Figure 7C**). Next, the AFFFs Firestopper, Tridol and Chemguard were assessed because these complex mixtures are commonly deployed in massive amounts during fire incidents and are thus released into the environment [202]. Understanding the environmental presence of PFAS from these products can assist in exposure assessment and bioremediation efforts [176] (**Figure 7D**). In our studies, we specifically looked for 6:2 FTAB since it is a known ingredient of AFFFs and can degrade using a pathway showed in **Figure 7A**. Interestingly, in the AFFF analyses, 6:2 FTAB was only detected in Firestopper while it was observed at low levels in Tridol and absent from Chemguard. Firestopper also had high amounts of 6:2 FTS, the subsequent degradation product of 6:2 FTAB and the only short chain PFAS detected was PFHxA illustrating a majority of the components stayed as 6:2 FTAB and 6:2 FTS. In Tridol, both 6:2 FTAB and 6:2 FTS were detected as well as the short chain degradation products PFHxA and PFHxA. Since Tridol did not contain any of its expected precursors for PFHxA either full degradation occurred, or an additional pathway may exist that is currently unknown. In Chemguard, 6:2 FTAB was not detected but its degradation product 6:2 FTS was detected. PFOA and its subsequent degradation product PFHpA were also observed in this AFFF. In Chemguard, PFHpA showed isomeric separation of branched and linear PFHpA in the drift time distributions, were the branched occurs at a shorter drift time [109]. Interestingly, our standard from **Figure 7B** only showed the linear form and only the branched form was detected in Tridol. The short-chain PFHxA was also detected in Chemguard which may have occurred by the degradation of either 6:2 FTS or PFOA. IMS-

MS analyses of the AAAFs was very impactful in this case as it helped highlight isomeric forms for the PFHpA that may be different in toxicity.

4.5 Conclusion

POPs remain a major issue for human and environmental health and their large-scale production, diversity, complexity, and wide distribution worldwide require new analytical methods to perform rapid and confident exposure assessments. IMS-MS shows great promise for these studies due to its rapid, multi-dimensional characteristics enabling screening capabilities of POPs and their metabolites and/or degradation products. To demonstrate the utility of IMS-MS for environmental exposure assessment, in this study we analyzed a wide range (n=64) of POPs and their metabolites/degradation products, including PCB, PAH, PFAS, industrial chemicals, pesticides and PPCP. For assessment of the PCB, PAH and some pesticides, APPI[+] was necessary for their detection due to the nonpolar chemistry of each. However, analyses of the PCB and PAH metabolites preferred ESI[-]. For other common POPs such as PPCP and some industrial byproducts found in wastewater, ESI[+] or [-] may be sufficient for analysis of both parent and metabolite/degradant products and was noted to have higher sensitivity than APPI, providing better rapid chemical screenings at lower concentrations. Additionally, in the analysis of PFAS and their degradants in AFFF solutions, ESI[-] was the optimal analysis mechanism. In all of the studies IMS-MS illustrated separation capabilities for the isomeric species such as hydroxyl and sulfate PCB, and linear and branched PFAS, although, some limitations in separation of isomeric species, such as the separation of 3'-

OH-PCB 3 and 4'-OH-PCB did occur. While additional separation techniques such as LC may be needed in some cases for the positive identification of molecule such as the PCB metabolites, IMS-MS illustrated a potential screening capability for the POPs and the metabolites and degradants in wastewater and AFFFs without having to perform derivatization and excessive sample cleanup needed by many current techniques.

4.6. Acknowledgement

This work was funded, in part, by grants from the National Institutes of Health (P30 ES025128, P42 ES027704 and P42 ES031009) and a cooperative agreement with the United States Environmental Protection Agency (STAR RD 84003201). The views expressed in this manuscript do not reflect those of the funding agencies. The use of specific commercial products in this work does not constitute endorsement by the authors or the funding agencies.

4.7 Declarations

The authors declare that they have no known competing financial interests or personal relationships that could have appeared to influence the work reported in this paper.

4.8 Chapter IV Figures and Tables

Figure 4.1: Summary of Identified Chemicals

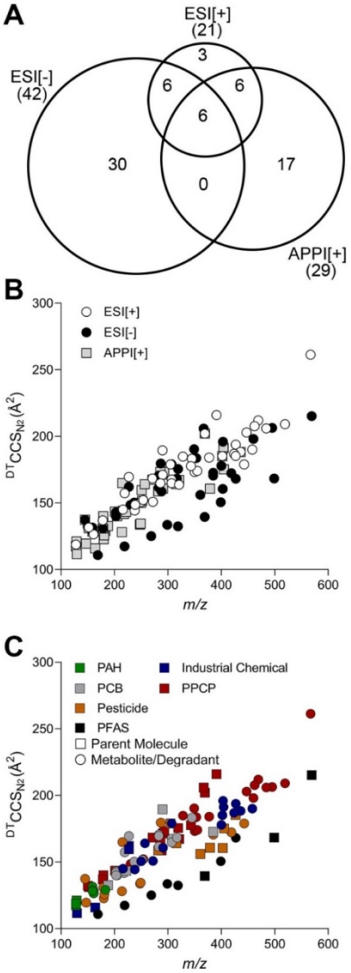

A) Number of chemicals detected using each ionization method. **B)** CCS values were calculated for each ion observed and are plotted again *m/z* values for each ionization mode. ESI[+] (white), ESI[-](black), and APPI[+] (gray). **C)** The observed CCS and *m/z* values are also graphed for all parent POPs (squares) and metabolites/degradants (circles) for each chemical class with industrial chemicals (blue), PAH (green), PCB (gray), pesticides (orange), pharmaceuticals (red), polyphenols (purple) and PFAS (black). Additionally, information for each data point can be found in Supplemental Table 1.

Figure 4.2: PCB3 Metabolism and IMS-MS Characterization

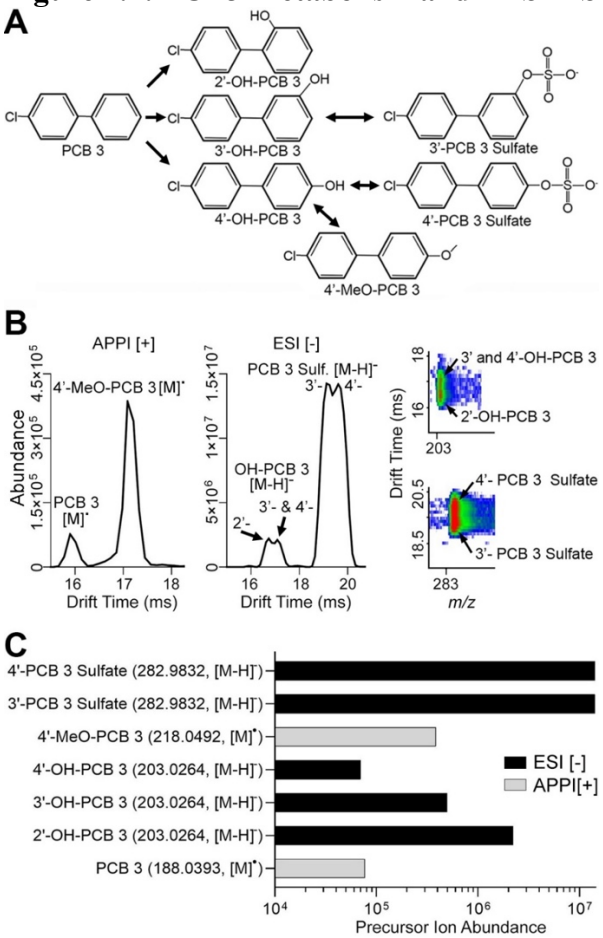

A) Enzymatic metabolism pathway of PCB 3 [185] where metabolites are hydroxyl (OH), methoxy (MeO) and sulfate conjugates of parent PCB. **B)** IMS drift time separations of parent PCB and MeO metabolites in APPI[+] and hydroxyl and sulfate metabolites in ESI[-]. The nested IMS and MS spectra of the hydroxyl and sulfate isomers illustrate the same m/z values but multiple peaks in the drift time. **C)** Comparison of PCB ion abundances using ESI and APPI sources.

Figure 4.3: Bisphenol A Metabolism and IMS-MS Characterization

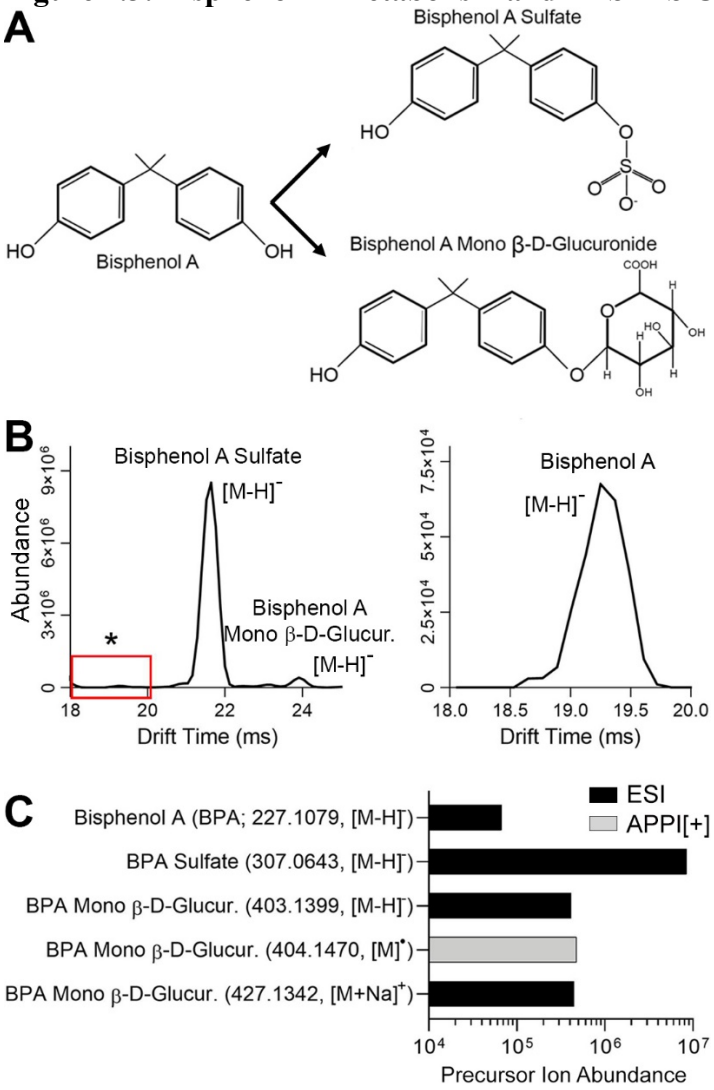

A) Metabolism of bisphenol A by SULT and GULT, where metabolites occur due to sulfate and mono ß-D-glucuronide conjugates of bisphenol A. **B)** IMS drift time separation of bisphenol A and the sulfate and mono ß-D-glucuronide metabolites. Due to ion suppression by bisphenol A sulfate, the abundance of bisphenol A is shown in the insert **C).** Comparison of BPA ion abundances using ESI and APPI sources.

Figure 4.4: Paracetamol Metabolism and IMS-MS Characterization

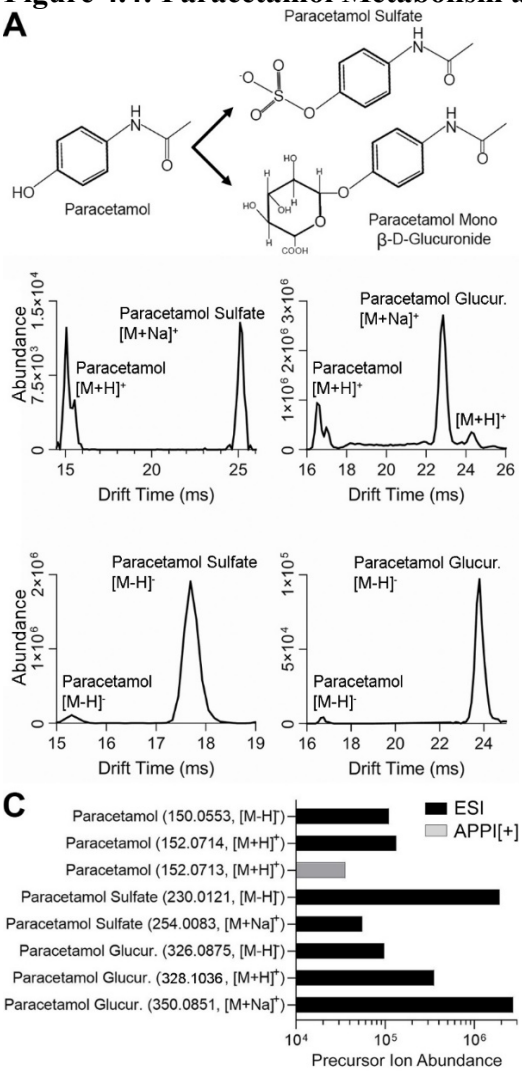

A) Metabolism of paracetamol by SULT and GULT, where metabolites occur due to sulfate and mono ß-D-glucuronide conjugates of paracetamol. **B)** IMS drift time distributions of paracetamol and the sulfate and mono ß-D-glucuronide metabolites where the top two panels show $[M+H]^+$ and $[M+Na]^+$ ions and the bottom two panels show the $[M-H]^-$ ions. **C)** The comparison of ion abundances illustrates all compounds were detected with ESI, while only one was detected with APPI.

Figure 4.5: Common Wastewater Pollutants IMS-MS Characterization

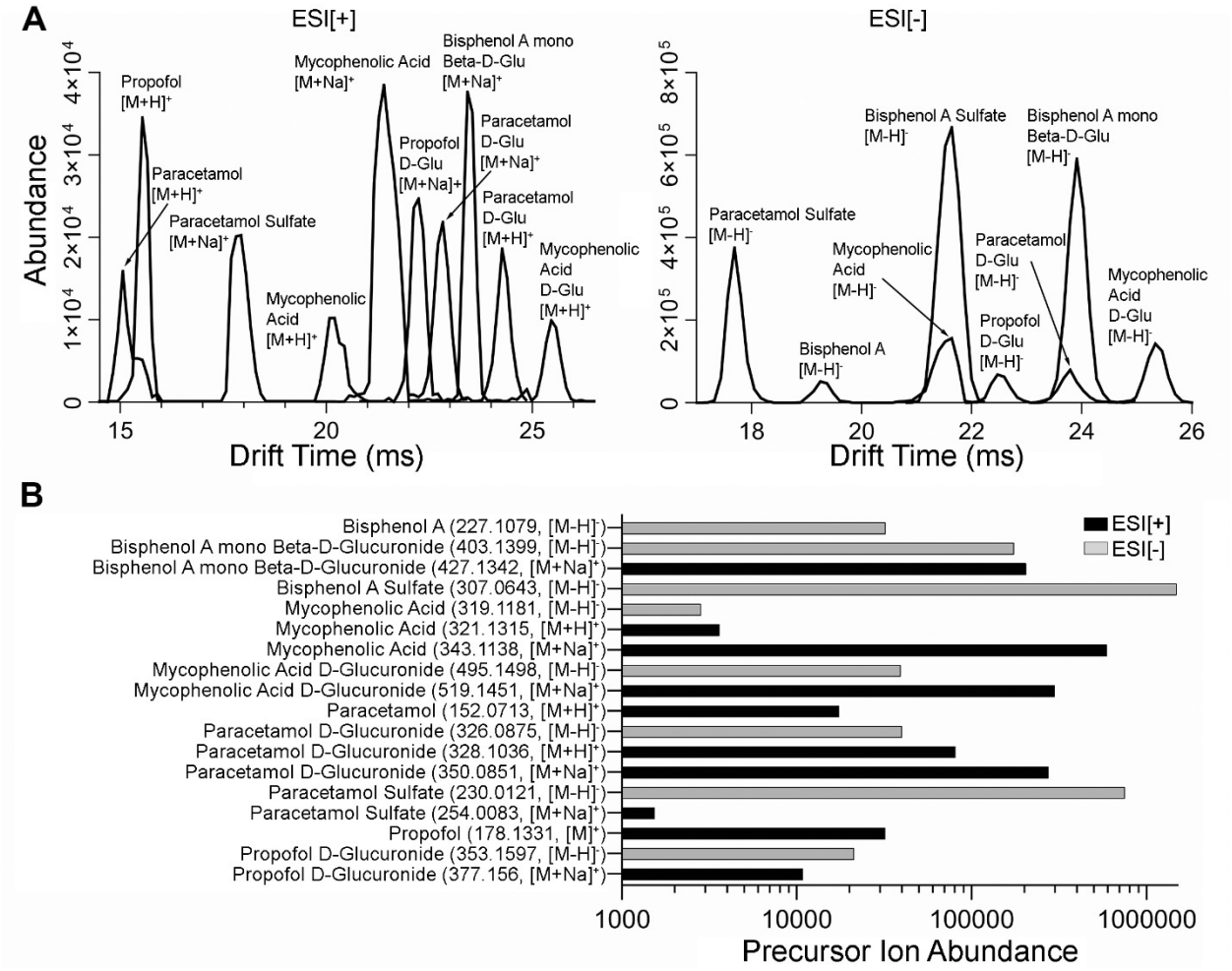

A) IMS drift time distributions of commonly found chemicals in wastewater including propofol, paracetamol, mycophenolic acid and bisphenol A and their sulfate and glucuronide metabolites. The right panel shows ($[M+H]^+$ and $[M+Na]^+$ ions observed in ESI[+] and the left panel illustrates $[M-H]^-$ ions observed in ESI[-]. **B)** The comparison of ion abundances illustrates both ESI[+] and ESI[-] are needed to detect all chemicals but only one mode is possible a majority of chemicals can still be analyzed.

Figure 4.6: Pesticide Degradation and IMS-MS Detection

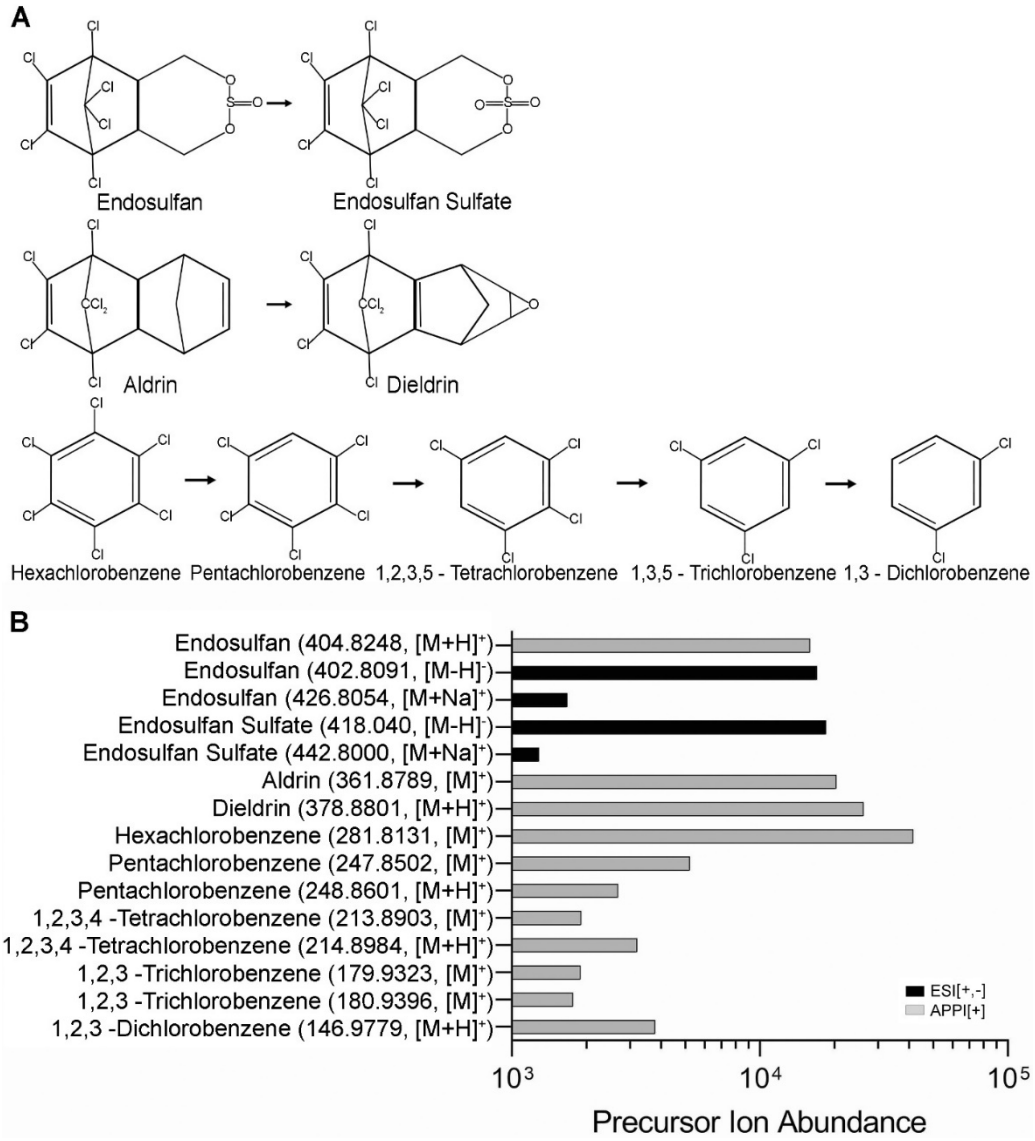

A) Oxidation and dechlorination degradation of endosulfan, aldrin and hexachlorobenzene are common in the environment. **B)** A comparison of ion abundances using ESI and APPI sources illustrate most compounds are only detected with APPI, but those with sulfates are only detected with ESI.

Figure 4.7: PFAS Degradation Pathways, IMS-MS Characterization and AFFF Solutions

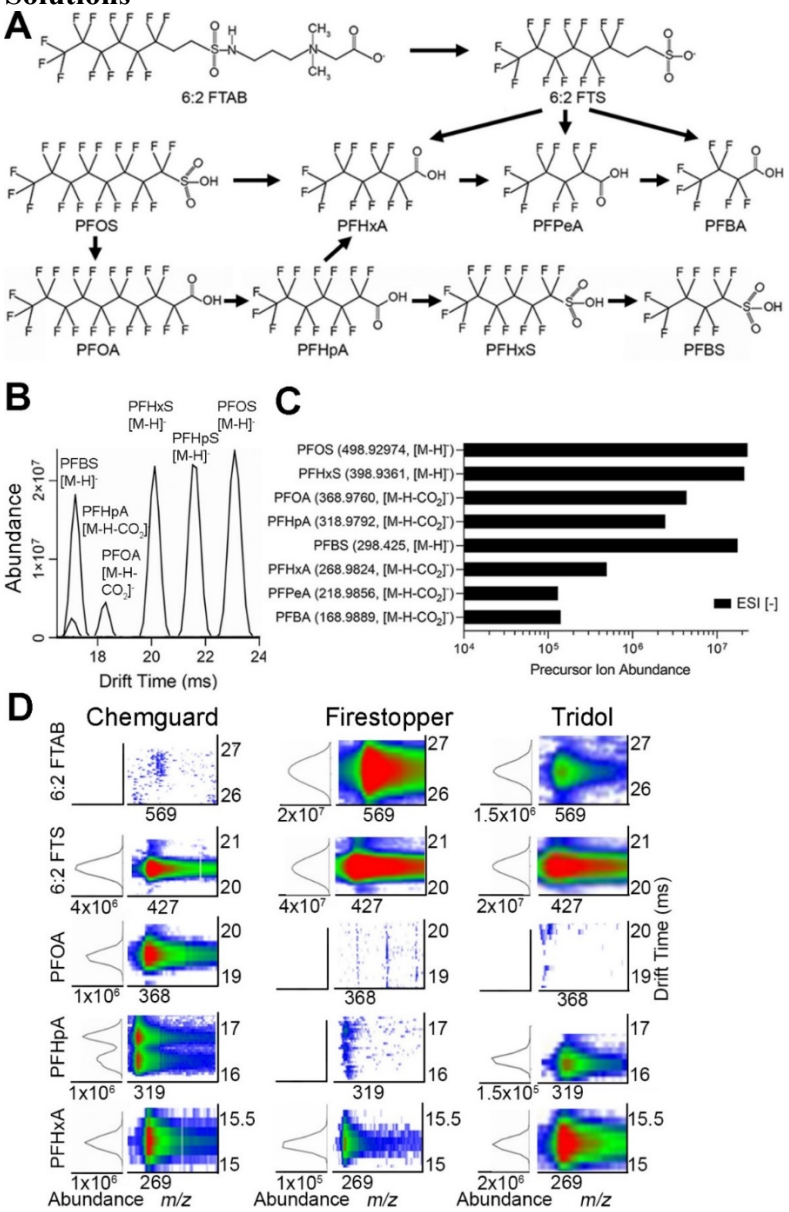

A) The degradation pathways which occur under aerobic conditions for common PFAS in AFFFs [198]. **B)** IMS drift time separation of PFAS and **C)** comparison of ion abundances of PFAS using ESI[-]. **D)** Nested IMS and MS spectra of the observed PFAS and possible degradation products in three AFFFs.

Table 4.1: List of Studied Chemicals

	Name[a]	Ionization	SC Annex	Classification
1	Bisphenol A	ESI[-]	N/A	Industrial Chemical
	Bisphenol A mono β-D-Glucuronide	APPI[+]and ESI[+,-]		
	Bisphenol A Sulfate	ESI[-]		
2	PCE	APPI[+]	N/A	Industrial Chemical
	TCVG	APPI[+] and ESI[+,-]		
	TCVC			
	NAC-TCVC			
3	TCE	APPI[+]	N/A	Industrial Chemical
	DCVG	APPI[+] and ESI[+,-]		
	DCVC			
	NAC-DCVC			
4	Naphthalene	APPI[+]	N/A	PAH
	2,3-Dihydroxynaphthalene	ESI[-]		
	1,5-Dihydroxynaphthalene			
	1,2-Dihydroxynaphthalene			
5	PCB 3	APPI[+]	A	PCB
	4'-MeO-PCB 3		A	PCB
	4'-OH-PCB3	ESI[-]		
	3'-OH-PCB3			
	2'-OH-PCB3			
	2-PCB3 Sulfate			
	3'-PCB3 Sulfate			
	4'-PCB3 Sulfate			
6	PCB 11	APPI[+]	A	PCB
	4-MeO-PCB 11			
	4-OH-PCB 11	ESI[-]		
	4'-PCB 11 Sulfate			
7	4-OH-PCB 52	ESI[-]	A	PCB
	4-PCB 52 Sulfate			
8	4,4'-DDMU	APPI[+] and ESI[+]	B	Pesticide
	p,p'-DDE	APPI[+]		
9	Aldrin	APPI[+] and ESI[+]	A	Pesticide
	Dieldrin	APPI[+]		

	Name[a]	Ionization	SC Annex	Classification
10	Endosulfan Endosulfan Sulfate	APPI[+] ESI[+,-]	A	Pesticide
11	Hexachlorobenzene Pentachlorobenzene 1,2,3,4-Tetrachlorobenzene 1,2,4-Trichlorobenzene 1,4-Dichlorobenzene	APPI[+]	C	Pesticide
12	PFOS PFOA	ESI[-]	A	PFAS
	6:2 FTAB 6:2 FTS PFHxS PFHpA PFBS PFHxA PFPeA PFBA	ESI[-]	N/A	
13	Estrone Estrone 3-β-D-Glucuronide Estrone 3-Sulfate	APPI[+] and ESI[+] ESI[+,-]	N/A	PPCP
14	Paracetamol Paracetamol β-D-Glucuronide Paracetamol Sulfate	APPI[+] and ESI[+,-] ESI[+,-]	N/A	PPCP
15	Propofol Propofol-D-Glucuronide	APPI[+] and ESI[+] ESI[+,-]	N/A	PPCP
16	Mycophenolic Acid Mycophenolic Acid-D-Glucuronide	APPI[+] and ESI[+,-] ESI[+,-]	N/A	PPCP
17	Morphine Morphine 6-β-D-Glucuronide	ESI[+,-]	N/A	PPCP
18	Curcumin Curcumin β-D-Glucuronide	APPI[+] and ESI[+,-] ESI[+,-]	N/A	PPCP

a. Abbreviated chemical names are shown in Table 1 and full names and additional information is included in Supplemental Table 1.

CHAPTER V

5. CONCLUSIONS

5.1 Summary

Natural and anthropogenic disasters may result in widespread contamination and have potential adverse effects on the environment and human health. The need for high-throughput, high sensitivity and broad-spectrum exposure assessments following these events is vital for the understanding of these potential effects and their application to risk assessment. Traditional exposure assessments performed with GC-MS and LC-MS may be comprehensive but often lack range and throughput is limited. Current limitations in these aspects are a critical gap in terms of disaster research, particularly where exposures can be complex and response time is important. The overarching goals of these collective studies were to compare and develop methods for rapid exposure assessment of complex environmental samples in disaster research with the use of traditional and novel methods. We do this by first showing how traditional exposure assessment methods are used to determine spatial and temporal effects of contamination following environmental disasters in two case studies. We also use the resulting data to determine potential human health hazard and cancer risk. Second, we aimed to utilize the use of the novel analytical method of IMS-MS by characterizing and identifying common persistent organic pollutants along with their metabolites and degradation products, including those which might contain isomeric species.

In our first specific aim we analyzed the spatial and temporal trends of PFAS following the response to large-scale fires at Intercontinental Terminal Company (ITC)

in Houston Texas in March 2019. Nearly 5 million liters of class B firefighting foams were used to extinguish the fires, and these foams are known to contain per- and polyfluoroalkyl substances (PFAS), a class of compounds widely used as surfactants. These PFAS are persistent organic pollutants that have been reported in waterways and drinking water systems across the United States. These substances are of interest to both regulatory agencies and the general public because of their persistence in the environment and association with adverse health effects. Much of this material flowed into the Houston Ship Channel and Galveston Bay (HSC/GB) and concerns were raised about the levels of PFAS in these water bodies, which have commercial and recreational uses.

To evaluate the impact of the ITC incident response on PFAS levels in HSC/ GB, we collected 52 surface water samples from 12 locations over a 6-month period after the incident. Samples were analyzed using liquid chromatography mass spectrometry to evaluate 27 PFAS, including perfluorocarboxylic acids, perfluorosulfonates and fluorotelomers. We showed that the detected PFAS in the Houston Ship Channel over the course of the study period were likely from the firefighting response to the ITC fires. Our finding of considerable temporal and spatial increases in levels of 6:2 FTS and PFOS suggests the usage of both fluorotelomer-based AFFFs[92] and of the legacy electrofluorination-based AFFFs [Moe, 2012 #16192. While levels of most PFAS were below currently available actionable levels after considering the likely exposure pathways of recreational use, particular concern is that concentrations of PFOS detected

in this study exceeded standards based on fish consumption even after returning to "background" levels.

In our second specific aim, we conducted a temporal analysis of contaminant distribution caused by flooding from Hurricane Florence and determined potential human health risks. Hurricane Florence made landfall in North Carolina in September 2018, causing extensive flooding. Several potential point sources of hazardous substances and Superfund sites sustained water damage, and contaminants may have been released into the environment. To conduct a temporal analysis of contaminant distribution and determine potential human health risks from Hurricane Florence associated flooding we collected soil samples from 12 sites across four counties in North Carolina in September 2018, January and May 2019. Chemical analyses were performed for organics by gas chromatography-mass spectrometry. Metals were analyzed using inductively coupled plasma mass spectrometry. Hazard index and cancer risk were calculated using EPA Regional Screening Level Soil Screening Levels for residential soils.

In summary, we found evidence for the lack of human health concern in most of the studied areas in eastern North Carolina that were impacted by extensive flooding during Hurricane Florence. At the same time, we show that the reported coal ash spill in New Hanover county was likely associated with release of a number of hazardous contaminants that were detected at elevated levels greater than 10 kilometers downstream. We calculate that this coal ash spill had resulted in mobilization of a number of soluble hazardous substances through the flood waters.

In our third specific aim, we utilize ion mobility spectrometry-mass spectrometry for the characterization and detection of persistent organic pollutants (POPs) and their metabolites. POPs are xenobiotic chemicals of global concern due to their long-range transport capabilities, persistence, ability to bioaccumulate, and potential to have negative effects on human health and the environment. Identifying POPs in both the environment and human body is therefore essential for assessing potential health risks. Currently, platforms coupling chromatography approaches with mass spectrometry (MS) are the most common analytical methods employed to evaluate both parent POPs and their respective metabolites and/or degradants in samples ranging from drinking water to biofluids. Unfortunately, different types of analyses are commonly needed to assess both parent and metabolite/degradant POPs from various classes. These numerous analyses thus present a number of technical and logistical challenges when rapid evaluations are needed, and sample volumes are limited.

To address these challenges, we characterized 64 compounds including parent per- and polyfluoroalkyl substances (PFAS), pesticides, polychlorinated biphenyls (PCBs), industrial chemicals, and pharmaceutical and personal care products (PPCPs), in addition to their metabolites and/or degradants, using ion mobility spectrometry coupled with MS (IMS-MS). Different ionization sources including electrospray ionization (ESI) and atmospheric pressure photoionization (APPI) were employed to determine optimal ionization for each chemical.

In summary, we show for assessment of the PCB, PAH and pesticides, APPI [+] was necessary for their detection due to the nonpolar chemistry of each. However,

analyses of the PCB and PAH metabolites preferred ESI[-]. For other common POPs such as PCPP and some industrial byproducts found in wastewater, ESI[+] or [-] may be sufficient for analysis of both parent and metabolite/degradant products and was noted to have higher sensitivity than APPI, providing better rapid chemical screenings at lower concentrations. Additionally, in the analysis of PFAS and their degradants in AFFF solutions, ESI[-] was the optimal analysis mechanism. In all of the studies, IMS-MS illustrated separation capabilities for the isomeric species such as hydroxyl and sulfate PCB, and linear and branched PFAS, although, some limitations in separation of isomeric species, such as the separation of 3'-OH-PCB 3 and 4'-OH-PCB did occur. While additional separation techniques such as LC may be needed in some cases for the positive identification of molecules such as the PCB metabolites, IMS-MS illustrated a potential screening capability for the POPs and the metabolites and degradants in wastewater and AFFFs without having to perform time-consuming derivatization and excessive sample cleanup steps needed by many current techniques. This study is an important step in enabling rapid assessment of composition for complex environmental samples and has shown IMS-MS has promise to increase throughput of environmental exposure assessments.

Collectively, in this dissertation we compare and develop methods for rapid exposure assessment of complex environmental samples in disaster research with the use of traditional and novel methods. Several critical problems have been addressed in this project to understand how traditional methods are used and how novel methods can be improved to be used in future exposure assessments. We demonstrate that IMS-MS can

be used for environmental sample screening and will aid in the critical need for increased throughput and response time in disaster research.

5.2. The Significance of the Study

Health research has been conducted following numerous environmental disasters including the attacks on the World Trade Center, Hurricane Katrina and the Deepwater Horizon Oil Spill. However, a number of difficulties and limitations arose in these studies. Much of the research conducted is convenience-based sampling using non-systematic collection of health information. Data collection frequently takes place many months after the event and baseline information is often missing and longitudinal health data are unavailable. Exposure data are often not measured, thereby limiting the ability to detect potential associations between reported health effects and specific exposures. Community input into research topics and protocol design is not typically solicited by researchers and as a result may not address the health issues important to those most affected. The resources, processes, and information necessary for conducting timely disaster research remain largely inaccessible to public health responders and the academic community.

The studies in this work aim to show methods for disaster research response performed on a rapid time scale, covering large sampling areas and over a significant period of time [203]. The overall objectives of specific aims one and two were to address previous limitations in disaster research response where spatial and temporal components are often missing and response time is slow. We are able to show how

traditional methods can be used to determine spatial and temporal patterns following disaster events. In the study following PFAS we observe significant patterns, concentrations decrease over time, and we are able to observe their distribution in a large area. In the study following Hurricane Florence, we observe few spatial and temporal patterns in most sample locations, suggesting the flooding from the storm caused little redistribution of contaminants. However, one sample location did exhibit temporal patterns where concentrations of contaminants decreased then increased, suggesting the flooding may have diluted existing contamination and as industry resumed, contaminants were again released. We also found that contaminants we detected in this location may have been coal-ash associated, suggesting that the flooding could be associated with contaminant redistribution. Through these studies we were able to find baseline concentrations of environmental pollutants by continuous sampling and monitoring in the months following the event. These data are frequently missing from exposure assessments in these scenarios. In future studies in these areas this information can be used to assess exposure following a disaster event. Further, we quantify risk and hazard of exposures and effectively communicate this information to stakeholders and effected populations. Study results about the ITC fire response from the Texas A&M Superfund center were discussed in a public forum setting and were reported in over 20 news outlets across the country. The studies in this dissertation collectively show how traditional targeted methods of analysis can be applied in disaster research on a rapid time scale and over a wide spatial area and effectively determine possible hazard and risk.

In specific aim three we address the limitations of targeted analysis. In disaster scenarios, contamination may be widespread and unknown, driving a need for a rapid high-throughput screening protocol. We successfully show how the analytical technology IMS-MS is a feasible tool for screening of a wide range of environmental pollutants. Not only can IMS-MS identify parent molecules, but it can also detect and identify their metabolites and degradation products. These chemicals are often found in biological and environmental samples, by understanding the chemical metabolism and degradation we can provide further information about exposure. Another significant observation in this study was the separation and identification of isomeric species. Some isomeric species may exhibit varying degrees of toxicity and hazard so the full characterization we are able to provide with IMS-MS is significant in understanding the extent of possible exposure and adverse health outcomes.

5.3. Limitations

Despite the fact the results from the studies in this dissertation have showcased the successful use of traditional methods to conduct exposure assessments and perform risk assessments following disaster events, several challenges and limitations do exist. First, the unpredicted nature of disaster events highlights the importance of having the infrastructure of trained personnel to rapidly deploy for sample collection. Sample analysis also needs to be conducted in an efficient and timely manner. For instance, at the time of sampling the Houston Ship Channel and Galveston Bay in March 2019, the laboratory did not have ready access to the extraction standard to spike during the extraction process. Thus, to expedite the analysis of samples, it was decided to proceed

without this step. We did add the extraction and injection standards prior to sample analysis. We acknowledge that the lack of extraction standards during sample preparation prevents absolute quantification of the compounds as extraction efficiency and matrix effect cannot be corrected. However, since the sample matrix (water) was identical across all samples, we believe that these data are still nonetheless informative and provide valuable information for this and future events. For compounds that have both quantifying and qualifying ions, the ratios between the two were used to compare with pure standards to ensure robust compound identification. While it would have been possible to re-analyze the archived water samples with the optimized analytical method (as opposed to immediate analysis within 1 week of collection as performed here), significant analyte interconversions for certain PFAS in aqueous samples stored at 4 ºC were observed within 7 days of storage [107]. The same study provides evidence that storage of water samples at -20 ºC precludes significant degradation of PFAS for up to 180 days[107]. Since water samples were not stored at -20 ºC we assumed significant analyte conversions would have occurred and analysis would be inclonclusive.

Another variable in disaster research is access to sampling locations throughout the sampling period. In both the ITC and Hurricane Florence studies, subsequent sampling trips had restricted access. The trainees conducting the sampling had to use their discretion to determine if collecting a sample would be safe or feasible. Although some locations could not have multiple samples collected, enough samples in the overall study areas could be collected to determine trends.

The relative sparseness of the sampling locations is a general limitation for disaster research to conduct proper spatial interpolation. Moreover, large differences in values for co-located samples may not yield smooth interpolation. In the ITC study, because we quantile ranked the data, these discrepancies were minimized. Overall, while spatial interpolation approaches are highly uncertain, these visualizations are very informative tools, especially for public communication and decision support[108]. Since the samples for the Hurricane Florence study were limited and far apart a spatial analysis could not be conducted. Further, since only three time points were sampled in the Hurricane Florence study, it is challenging to draw strong conclusions regarding temporal trends or determine whether a causal relationship exists between flooding and the presence of contaminants. Thus, the need for more comprehensive baseline monitoring remains key to understanding the impact of natural disasters on release and/or redistribution of contaminants.

The final limitation in the ITC and Hurricane Florence studies is that both used targeted analysis of a limited number of PFAS, organic contaminants and metals. It is possible that these samples contained numerous other chemicals that may have potential human and environmental health implications.

Generally, new technologies can help with advancing science and opening the doors to new applications, but this comes at the price of few trained professionals who have the capacity to operate, maintain, and repair the analytical tools. In the case of specific aim three, the IMS-MS had significant technical difficulties during the study.

The instrument downtime created challenges in acquiring adequate data and extra quality control measures had to be taken to ensure the data was trustworthy.

The study conducted in specific aim three highlights commonly observed pollutants, however, it is by no means comprehensive. Many more metabolites and degradation products exist than the ones analyzed. There are also many more chemicals which may be detected in the environment.

The limitations above guide us for future studies in exposure assessments following disaster events. In the next section, we will discuss the potential future directions that would advance the fields of exposure assessment, regulatory science and human health risk assessment.

5.4. Future Directions

The studies in this work highlight where advances can still be made to improve exposure assessment in the field of disaster research. A significant missing piece of this work is the inclusion of real-world environmental samples analyzed through IMS-MS. Although previous studies of complex mixtures have been performed with IMS-MS, the majority are limited to targeted studies[169, 204]. To integrate IMS-MS in exposure sciences, a database of CCS values of environmental chemicals will need to exist. We are currently developing such a database with chemicals from the Environmental Protection Agency (EPA) ToxCast program. When a complex sample with unknown composition is acquired, it can be analyzed utilizing the IMS-MS, with the added advantage of minimal sample cleanup and preparation in order not to dilute or lose any possible contaminants. Based on the study performed in this dissertation regarding persistent organic pollutants,

the ESI[-] source should be used since it showed the highest overall sensitivity and detection capacity. Then, samples should be analyzed utilizing ESI[+] and APPI [+] to broaden the scope of detected features by including polar compounds. Each sample should be run in triplicate to avoid any false identifications. Given that the run-time of IMS-MS analysis is performed on a sixty-second time frame, these analyses should be feasible for rapid screening applications such as disaster response. The IMS-MS analysis will result in full mass spectra with CCS and *m/z* values of all detectable chemicals in the samples. These values may then be cross-referenced to the database to identify chemicals. Once individual chemicals are identified, to further understand exposure and risk, samples will need to be prepared for a targeted study using a traditional analytical tool such as GC/LC-MS. This will allow us to quantify contaminant concentrations and determine whether adverse human health effects may be associated with exposure. The water samples from the study following PFAS in the Houston Ship Channel have been analyzed using IMS-MS as well. Only 27 specific PFAS species were searched for in our initial study utilizing LC-MS, however, we are aware that many thousands of PFAS species exist and thought IMS-MS could be used to further characterize the samples. In a study performed by Valdiviezo et al, untargeted analysis was conducted using LC-IMS-MS on the same water samples from specific aim one. Data generated from the untargeted analyses were highly concordant with the results of the traditional analyses, and provided information on almost three times as many additional compounds that contributed to more than half of total PFAS detected in the surface waters in HSC/GB[205]. This study highlighted how untargeted analyses may serve as a beneficial tool for rapid

exposure characterization following an emergency response prior to using targeted methods for quantification of environmental contaminants.

Another limiting aspect of IMS-MS is that it is a qualitative analysis, while this can be useful for rapid screening of samples, it is not sufficient for quantifying exposures to perform hazard and risk assessments. Additional analyses are still necessary if this information is deemed necessary. Future studies need to be performed to understand matrix effects and detection limits of IMS-MS which may increase our ability to quantify concentrations of analytes of interest. Studies utilizing Rapidfire SPE cartridges may also be of interest. Cartridges have the potential to improve the efficiency of IMS-MS and decrease response time by reducing sample preparation and clean-up, a time-consuming aspect of disaster research.

Overall, IMS-MS displays promise as a screening tool for complex environmental samples. This analytical method can identify a broad range of chemicals on a rapid time scale, these qualities are attractive in disaster research as it can provide a more comprehensive understanding of exposure and improve response time. With these additional studies, IMS-MS can be part of a paradigm shift in disaster research and untargeted analyses.

6. REFERENCES

1. Patel, S. S.; Lovko, V. J.; Lockey, R. F., Red Tide: Overview and Clinical Manifestations. *J Allergy Clin Immunol Pract* **2020,** *8* (4), 1219-1223.

2. Conner, W. H.; Day, J. W.; Baumann, R. H.; Randall, J. M., Influence of hurricanes on coastal ecosystems along the northern Gulf of Mexico. *Wetlands Ecology and Management* **1989,** *1*, 45-56.

3. Garcia, Y.; Castellanos, M. C.; Pausas, J. G., Fires can benefit plants by disrupting antagonistic interactions. *Oecologia* **2016,** *182* (4), 1165-1173.

4. Climate and weather related disasters surge five-fold over 50 years, but early warnings save lives - WMO report. https://news.un.org/en/story/2021/09/1098662.

5. NOAA National Climate Report 2020. https://www.ncdc.noaa.gov/sotc/national/202013.

6. Institute of Medicine (US) Roundtable on Environmental Health Sciences, R., and Medicine, *Environmental Public Health Impacts of Disasters: Hurricane Katrina*. National Academies Press (US): Washington D.C., 2007.

7. Manuel, J., In Katrina's Wake. *Environ Health Perspectives* **2006**.

8. Waddell, S. L.; Jayaweera, D. T.; Mirsaeidi, M.; Beier, J. C.; Kumar, N., Perspectives on the Health Effects of Hurricanes: A Review and Challenges. *Environmental Research and Public Health* **2021**.

9. Rath, B.; Young, E. A.; Harris, A.; Perrin, K.; Bronfin, D. R.; Ratard, R.; Vandyke, R.; Goldshore, M.; Magnus, M., Adverse respiratory symptoms and environmental exposures among children and adolescents following Hurricane Katrina. *Public Health Rep* **2011,** *126* (6), 853-60.

10. Antipova, A.; Curtis, A., The post-disaster negative health legacy: pregnancy outcomes in Louisiana after Hurricane Andrew. *Disasters* **2015,** *39* (4), 665-86.

11. Lowers, H. A.; Meeker, G. P.; Lioy, P. J.; Lippmann, M., Summary of the development of a signature for detection of residual dust from collapse of the World Trade Center buildings. *J Expo Sci Environ Epidemiol* **2009,** *19* (3), 325-35.

12. Lippmann, M.; Cohen, M. D.; Chen, L. C., Health effects of World Trade Center (WTC) Dust: An unprecedented disaster's inadequate risk management. *Critical reviews in toxicology* **2015,** *45* (6), 492-530.

13. Lichtveld, M.; Sherchan, S.; Gam, K. B.; Kwok, R. K.; Mundorf, C.; Shankar, A.; Soares, L., The Deepwater Horizon Oil Spill Through the Lens of Human Health and the Ecosystem. *Curr Environ Health Rep* **2016,** *3* (4), 370-378.

14. EPA Summary of the Comprehensive Environmental Response, Compensation, and Liability Act (Superfund). https://www.epa.gov/laws-regulations/summary-comprehensive-environmental-response-compensation-and-liability-act.

15. NIEHS Disaster Research (DR2) Program. https://www.niehs.nih.gov/research/programs/disaster/about/index.cfm.

16. Horney, J. A.; Rios, J.; Cantu, A.; Ramsey, S.; Montemayor, L.; Raun, L.; Miller, A., Improving Hurricane Harvey Disaster Research Response Through Academic-Practice Partnerships. *Am J Public Health* **2019,** *109* (9), 1198-1201.

17. Wild, C. P., Complementing the genome with an "exposome": the outstanding challenge of environmental exposure measurement in molecular epidemiology. *Cancer epidemiology, biomarkers & prevention : a publication of the American Association for Cancer Research, cosponsored by the American Society of Preventive Oncology* **2005,** *14* (8), 1847-50.

18. Wallace, M. A. G.; Pleil, J. D.; Oliver, K. D.; Whitaker, D. A.; Mentese, S.; Fent, K. W.; Horn, G. P., Targeted GC-MS analysis of firefighters' exhaled breath: Exploring biomarker response at the individual level. *J Occup Environ Hyg* **2019,** *16* (5), 355-366.

19. Laszlo, C. F.; Paz Montoya, J.; Shamseddin, M.; De Martino, F.; Beguin, A.; Nellen, R.; Bruce, S. J.; Moniatte, M.; Henry, H.; Brisken, C., A high resolution LC-MS targeted method for the concomitant analysis of 11 contraceptive progestins and 4 steroids. *J Pharm Biomed Anal* **2019,** *175*, 112756.

20. Graves, E. E.; Jelks, K. A.; Foley, J. E.; Filigenzi, M. S.; Poppenga, R. H.; Ernest, H. B.; Melnicoe, R.; Tell, L. A., Analysis of insecticide exposure in California hummingbirds using liquid chromatography-mass spectrometry. *Environ Sci Pollut Res Int* **2019,** *26* (15), 15458-15466.

21. Pannkuk, E. L.; Laiakis, E. C.; Authier, S.; Wong, K.; Fornace, A. J., Jr., Targeted Metabolomics of Nonhuman Primate Serum after Exposure to Ionizing Radiation: Potential Tools for High-throughput Biodosimetry. *RSC Adv* **2016,** *6* (56), 51192-51202.

22. Landmesser, A.; Scherer, G.; Pluym, N.; Niessner, R.; Scherer, M., A novel quantification method for sulfur-containing biomarkers of formaldehyde and acetaldehyde exposure in human urine and plasma samples. *Anal Bioanal Chem* **2020,** *412* (27), 7535-7546.

23. National Academies of Sciences Engineering and Medicine, *Using 21st Century Science to Improve Risk-Related Evaluations*. The National Academies Press: Washington, DC, 2017.

24. Andra, S. S.; Austin, C.; Patel, D.; Dolios, G.; Awawda, M.; Arora, M., Trends in the application of high-resolution mass spectrometry for human biomonitoring: An analytical primer to studying the environmental chemical space of the human exposome. *Environ Int* **2017,** *100*, 32-61.

25. Soltow, Q. A.; Strobel, F. H.; Mansfield, K. G.; Wachtman, L.; Park, Y.; Jones, D. P., High-performance metabolic profiling with dual chromatography-Fourier-transform mass spectrometry (DC-FTMS) for study of the exposome. *Metabolomics : Official journal of the Metabolomic Society* **2013,** *9* (1 Suppl), S132-S143.

26. Jamin, E. L.; Bonvallot, N.; Tremblay-Franco, M.; Cravedi, J. P.; Chevrier, C.; Cordier, S.; Debrauwer, L., Untargeted profiling of pesticide metabolites by LC-HRMS: an exposomics tool for human exposure evaluation. *Anal Bioanal Chem* **2014,** *406* (4), 1149-61.

27. Diaz, R.; Ibanez, M.; Sancho, J. V.; Hernandez, F., Target and non-target screening strategies for organic contaminants, residues and illicit substances in food, environmental and human biological samples by UHPLC-QTOF-MS. *Anal Methods-Uk* **2012,** *4* (1), 196-209.

28. Fan, R. J.; Zhang, F.; Wang, H. Y.; Zhang, L.; Zhang, J.; Zhang, Y.; Yu, C. T.; Guo, Y. L., Reliable screening of pesticide residues in maternal and umbilical cord sera by gas chromatography-quadrupole time of flight mass spectrometry. *Sci China Chem* **2014,** *57* (5), 669-677.

29. Yi, L.; Dong, N.; Yun, Y.; Deng, B.; Ren, D.; Liu, S.; Liang, Y., Chemometric methods in data processing of mass spectrometry-based metabolomics: A review. *Anal Chim Acta* **2016,** *914*, 17-34.

30. Stow, S. M.; Causon, T. J.; Zheng, X.; Kurulugama, R. T.; Mairinger, T.; May, J. C.; Rennie, E. E.; Baker, E. S.; Smith, R. D.; McLean, J. A.; Hann, S.; Fjeldsted, J. C., An Interlaboratory Evaluation of Drift Tube Ion Mobility-Mass Spectrometry Collision Cross Section Measurements. *Anal Chem* **2017,** *89* (17), 9048-9055.

31. Nichols, C. M.; Dodds, J. N.; Rose, B. S.; Picache, J. A.; Morris, C. B.; Codreanu, S. G.; May, J. C.; Sherrod, S. D.; McLean, J. A., Untargeted Molecular Discovery in Primary Metabolism: Collision Cross Section as a Molecular Descriptor in Ion Mobility-Mass Spectrometry. *Anal Chem* **2018,** *90* (24), 14484-14492.

32. Munoz, G.; Desrosiers, M.; Duy, S. V.; Labadie, P.; Budzinski, H.; Liu, J.; Sauvé, S., Environmental Occurrence of Perfluoroalkyl Acids and Novel Fluorotelomer

Surfactants in the Freshwater Fish Catostomus commersonii and Sediments Following Firefighting Foam Deployment at the Lac-Mégantic Railway Accident. *Environmental Science and Technology* **2017,** *51* (3), 1231-1240.

33. NIEHS Perfluoroalkyl and Polyfluoroalkyl Substances (PFAS). https://www.niehs.nih.gov/health/topics/agents/pfc/index.cfm (accessed October 01, 2019).

34. ATSDR, Toxicological Profile for Perfluoroalkyls. U.S. Department of Health and Human Services, Ed. Agency for Toxic Substances and Disease Registry: Atlanta, GA, 2018.

35. Boone, J. S.; Vigo, C.; Boone, T.; Byrne, C.; Ferrario, J.; Benson, R.; Donohue, J.; Simmons, J. E.; Kolpin, D. W.; Furlong, E. T.; Glassmeyer, S. T., Per- and polyfluoroalkyl substances in source and treated drinking waters of the United States. *Sci Total Environ* **2019,** *653*, 359-369.

36. Poothong, S.; Papadopoulou, E.; Padilla-Sanchez, J. A.; Thomsen, C.; Haug, L. S., Multiple pathways of human exposure to poly- and perfluoroalkyl substances (PFASs): From external exposure to human blood. *Environ Int* **2020,** *134*, 105244.

37. U.S. EPA Basic Information on PFAS. https://www.epa.gov/pfas/basic-information-pfas.

38. NHANES National Health and Nutrition Examination Survey 2011-2012 Data Documentation, Codebook, and Frequencies Polyfluoroalkyl Chemicals. https://wwwn.cdc.gov/Nchs/Nhanes/2011-2012/PFC_G.htm (accessed February 01, 2020).

39. Lewis, R. C.; Johns, L. E.; Meeker, J. D., Serum Biomarkers of Exposure to Perfluoroalkyl Substances in Relation to Serum Testosterone and Measures of Thyroid Function among Adults and Adolescents from NHANES 2011-2012. *Int J Environ Res Public Health* **2015,** *12* (6), 6098-114.

40. Patlewicz, G.; Richard, A. M.; Williams, A. J.; Grulke, C. M.; Sams, R.; Lambert, J.; Noyes, P. D.; DeVito, M. J.; Hines, R. N.; Strynar, M.; Guiseppi-Elie, A.; Thomas, R. S., A Chemical Category-Based Prioritization Approach for Selecting 75 Per- and Polyfluoroalkyl Substances (PFAS) for Tiered Toxicity and Toxicokinetic Testing. *Environ Health Perspect* **2019,** *127* (1), 14501.

41. Nicole, W., PFOA and cancer in a highly exposed community: new findings from the C8 science panel. *Environ Health Perspect* **2013,** *121* (11-12), A340.

42. NTP, *Immunotoxicity Associated with Exposure to Perfluorooctanoic Acid or Perfluorooctane Sulfonate*. National Toxicology Program: Research Triangle Park, NC, 2016.

43. Pelch, K. E.; Reade, A.; Wolffe, T. A. M.; Kwiatkowski, C. F., PFAS health effects database: Protocol for a systematic evidence map. *Environ Int* **2019,** *130*, 104851.

44. Sunderland, E. M.; Hu, X. C.; Dassuncao, C.; Tokranov, A. K.; Wagner, C. C.; Allen, J. G., A review of the pathways of human exposure to poly- and perfluoroalkyl substances (PFASs) and present understanding of health effects. *J Expo Sci Environ Epidemiol* **2019,** *29* (2), 131-147.

45. McCord, J.; Newton, S.; Strynar, M., Validation of quantitative measurements and semi-quantitative estimates of emerging perfluoroethercarboxylic acids (PFECAs) and hexfluoroprolyene oxide acids (HFPOAs). *J Chromatogr A* **2018,** *1551*, 52-58.

46. U.S. EPA, Health Effects Support Document for Perfluorooctanoic Acid (PFOA). Office of Water, U.S. Environmental Protection Agency: Washington, DC, 2016.

47. Ritscher, A.; Wang, Z.; Scheringer, M.; Boucher, J. M.; Ahrens, L.; Berger, U.; Bintein, S.; Bopp, S. K.; Borg, D.; Buser, A. M.; Cousins, I.; DeWitt, J.; Fletcher, T.; Green, C.; Herzke, D.; Higgins, C.; Huang, J.; Hung, H.; Knepper, T.; Lau, C. S.; Leinala, E.; Lindstrom, A. B.; Liu, J.; Miller, M.; Ohno, K.; Perkola, N.; Shi, Y.; Smastuen Haug, L.; Trier, X.; Valsecchi, S.; van der Jagt, K.; Vierke, L., Zurich Statement on Future Actions on Per- and Polyfluoroalkyl Substances (PFASs). *Environ Health Perspect* **2018,** *126* (8), 84502.

48. Martin, J. Update on Southern New Hampshire PFAS Investigation. https://www4.des.state.nh.us/nh-pfas-investigation/?p=1126 (accessed January 15, 2020).

49. U.S. EPA Third Unregulated Contaminant Monitoring Rule. https://www.epa.gov/dwucmr/third-unregulated-contaminant-monitoring-rule (accessed 1/28/2020).

50. Johnsen-Harris, B.; Chetwynd, J. House passes sweeping PFAS protections: 2025 ban on military use, Superfund cleanup and clean water safeguards. https://environmentamerica.org/news/ame/house-passes-sweeping-pfas-protections-2025-ban-military-use-superfund-cleanup-and-clean (accessed October 01, 2019).

51. Xu, W.; Wang, X.; Cai, Z., Analytical chemistry of the persistent organic pollutants identified in the Stockholm Convention: A review. *Anal Chim Acta* **2013,** *790*, 1-13.

52. Pan, Y.; Zhang, H.; Cui, Q.; Sheng, N.; Yeung, L. W. Y.; Sun, Y.; Guo, Y.; Dai, J., Worldwide Distribution of Novel Perfluoroether Carboxylic and Sulfonic Acids in Surface Water. *Environmental science & technology* **2018,** *52* (14), 7621-7629.

53. Hayes, J.; Faber, S.; Andrews, D.; Lothspelch, A. PFAS Nation: Toxic Discharges Suspected From Almost 500 Industrial Facilities Across U.S. https://www.ewg.org/news-and-analysis/2019/06/pfas-nation-toxic-discharges-suspected-almost-500-industrial-facilities (accessed October 14, 2019).

54. Spratlen, M. J.; Perera, F. P.; Lederman, S. A.; Robinson, M.; Kannan, K.; Herbstman, J.; Trasande, L., The Association Between Perfluoroalkyl Substances and Lipids in Cord Blood. *J Clin Endocrinol Metab* **2020,** *105* (1).

55. Spratlen, M. J.; Perera, F. P.; Lederman, S. A.; Robinson, M.; Kannan, K.; Trasande, L.; Herbstman, J., Cord blood perfluoroalkyl substances in mothers exposed to the World Trade Center disaster during pregnancy. *Environ Pollut* **2019,** *246*, 482-490.

56. ITRC History and Use of Per- and Polyfluoroalkyl Substances (PFAS). https://pfas-1.itrcweb.org/wp-content/uploads/2017/11/pfas_fact_sheet_history_and_use__11_13_17.pdf (accessed 1/28/2020).

57. Barzen-Hanson, K. A.; Roberts, S. C.; Choyke, S.; Oetjen, K.; McAlees, A.; Riddell, N.; McCrindle, R.; Ferguson, P. L.; Higgins, C. P.; Field, J. A., Discovery of 40 Classes of Per- and Polyfluoroalkyl Substances in Historical Aqueous Film-Forming Foams (AFFFs) and AFFF-Impacted Groundwater. *Environmental science & technology* **2017,** *51* (4), 2047-2057.

58. Place, B. J.; Field, J. A., Identification of novel fluorochemicals in aqueous film-forming foams used by the US military. *Environmental science & technology* **2012,** *46* (13), 7120-7.

59. Awad, E.; Zhang, X.; Bhavsar, S. P.; Petro, S.; Crozier, P. W.; Reiner, E. J.; Fletcher, R.; Tittlemier, S. A.; Braekevelt, E., Long-term environmental fate of perfluorinated compounds after accidental release at Toronto airport. *Environmental science & technology* **2011,** *45* (19), 8081-9.

60. Mejia-Avendano, S.; Munoz, G.; Vo Duy, S.; Desrosiers, M.; Benoi, T. P.; Sauve, S.; Liu, J., Novel Fluoroalkylated Surfactants in Soils Following Firefighting Foam Deployment During the Lac-Megantic Railway Accident. *Environmental science & technology* **2017,** *51* (15), 8313-8323.

61. Thomas, A. ITC Fire Response Causes Toxic Contamination of Houston Ship Channel. https://www.sierraclub.org/press-releases/2019/09/itc-fire-response-causes-toxic-contamination-houston-ship-channel (accessed January 28, 2020).

62. Ortiz, A.; Schneider, A. Harris County Prepares To Sue ITC Over Fire At Deer Park Facility. https://www.houstonpublicmedia.org/articles/news/2019/03/26/326600/harris-county-to-sue-itc-over-fire-at-deer-park-facility/ (accessed February 01, 2020).

63. U.S. EPA ITC Fire Response. https://epa.maps.arcgis.com/apps/Cascade/index.html?appid=f5eca85b79484cd69ea3a68cec886797.

64. Shoemaker, J.; Tettenhorst, D. *Method 537.1: Determination of Selected Per- and Polyfluorinated Alkyl Substances in Drinking Water by Solid Phase Extraction and Liquid Chromatography/Tandem Mass Spectrometry (LC/MS/MS).* Washington, DC, 2018.

65. Silcock, P.; Karrman, A.; van Bavel, B. Advancing Perfluorinated Compound Analysis Using Simultaneous Matrix Monitoring. https://www.waters.com/webassets/cms/library/docs/720003162en.pdf (accessed September 17, 2019).

66. Anumol, T.; Yang, D. D.; Sosienski, T.; Batoon, P. Analysis of per/polyfluoroalkyl substances (PFASs) in drinking water using the Agilent Ultivo triple quadrupole LC/MS. https://www.agilent.com/cs/library/applications/5991-8969EN_PFAS_Application.pdf (accessed October 17, 2019).

67. Killick, R.; Eckley, I. A., changepoint: An R Package for Changepoint Analysis. *J Stat Softw* **2014,** *58* (3), 1-19.

68. Fotheringham, A. S.; Wegener, M., *Spatial models and GIS: New and Potential Models*. CRC Press: Boca Raton, FL, 1999.

69. Meng, Q.; Liu, Z.; Borders, B. E., Assessment of regression kriging for spatial interpolation – comparisons of seven GIS interpolation methods. *Cartogr Georg Inf Sc* **2013,** *40* (1), 28-39.

70. ArcGIS How Radial Basis Functions Work. https://pro.arcgis.com/en/pro-app/help/analysis/geostatistical-analyst/how-radial-basis-functions-work.htm#GUID-3F6EE7BD-30DE-494E-9007-B1519953A6CE (accessed February 01, 2020).

71. Lesser, G. R.; Roelvink, J. A.; Ven Kester, J. A. T. M.; Stelling, G. S., Development and validation of a three-dimensional morphological model. *Coastal Engineering* **2004,** *51* (8-9), 883-915.

72. Kim, J. Y.; Kaihatu, J. M.; Chang, K. A.; Feagin, R. A.; Huff, T., Estimation of wind wave induced erosion rates in wetlands on Galveston Island based on UAV

photogrammetry. In *Fall Meeting of the American Geophysical Society*, San Francisco, CA, 2019.

73. Egbert, G. D.; Erofeeva, S. Y., Efficient Inverse Modeling of Barotropic Ocean Tides. *Journal of Atmospheric and Oceanic Technology* **2002,** *19.2*, 183-204.

74. Le Provost, C., Ocean Tides. In *Satellite Altimetry and Earth Sciences: A handbook of Techniques and Applications*, Fu, L. L.; Cazenave, A., Eds. Academic Press: San Diego, CA, 2001; pp 267-301.

75. Hasselman, K.; Barnett, T.; Bouws, E.; Carlson, H.; Cartwright, D.; Enke, K.; Ewing, J.; Gienapp, H.; Hasselman, D.; Kruseman, P.; Meerburg, A.; Muller, P.; Olbers, D.; Richter, K.; Sell, W.; Walden, H., Measurements of wind-wave growth and swell decay during the Joint North Sea Wave Project (JONSWAP). *Deut Hydrogr Z* **1973,** *8*, 1-95.

76. Dean, R. G.; Dalrymple, R. A., *Water Wave Mechanics for Engineers and Scientists*. World Scientific: Singapore, 1991; Vol. 2.

77. Oliver, D. P.; Navarro, D. A.; Baldock, J.; Simpson, S. L.; Kookana, R. S., Sorption behaviour of per- and polyfluoroalkyl substances (PFASs) as affected by the properties of coastal estuarine sediments. *Sci Total Environ* **2020,** *720*, 137263.

78. Li, Y.; Oliver, D. P.; Kookana, R. S., A critical analysis of published data to discern the role of soil and sediment properties in determining sorption of per and polyfluoroalkyl substances (PFASs). *Sci Total Environ* **2018,** *628-629*, 110-120.

79. Ahrens, L.; Norstrom, K.; Viktor, T.; Cousins, A. P.; Josefsson, S., Stockholm Arlanda Airport as a source of per- and polyfluoroalkyl substances to water, sediment and fish. *Chemosphere* **2015,** *129*, 33-8.

80. Lanza, H. A.; Cochran, R. S.; Mudge, J. F.; Olson, A. D.; Blackwell, B. R.; Maul, J. D.; Salice, C. J.; Anderson, T. A., Temporal monitoring of perfluorooctane sulfonate accumulation in aquatic biota downstream of historical aqueous film forming foam use areas. *Environ Toxicol Chem* **2017,** *36* (8), 2022-2029.

81. Houtz, E.; Wang, M.; Park, J. S., Identification and Fate of Aqueous Film Forming Foam Derived Per- and Polyfluoroalkyl Substances in a Wastewater Treatment Plant. *Environmental science & technology* **2018,** *52* (22), 13212-13221.

82. Buck, R. C.; Franklin, J.; Berger, U.; Conder, J. M.; Cousins, I. T.; de Voogt, P.; Jensen, A. A.; Kannan, K.; Mabury, S. A.; van Leeuwen, S. P., Perfluoroalkyl and polyfluoroalkyl substances in the environment: terminology, classification, and origins. *Integr Environ Assess Manag* **2011,** *7* (4), 513-41.

83. Wang, Y.; Arsenault, G.; Riddell, N.; McCrindle, R.; McAlees, A.; Martin, J. W., Perfluorooctane sulfonate (PFOS) precursors can be metabolized enantioselectively: principle for a new PFOS source tracking tool. *Environmental science & technology* **2009,** *43* (21), 8283-9.

84. KHOU Timeline: ITC Chemical Tank Fire in Deer Park. https://www.khou.com/article/news/timeline-itc-chemical-tank-fire-in-deer-park/285-960722df-3907-49c4-91ef-25dc5250dfe1 (accessed February 01, 2020).

85. EWG PFAS Contamination in the U.S. https://www.ewg.org/interactive-maps/2019_pfas_contamination/ (accessed February 01, 2020).

86. Moody, C. A.; Martin, J. W.; Kwan, W. C.; Muir, D. C.; Mabury, S. A., Monitoring perfluorinated surfactants in biota and surface water samples following an accidental release of fire-fighting foam into Etobicoke Creek. *Environmental science & technology* **2002,** *36* (4), 545-51.

87. Moller, A.; Ahrens, L.; Surm, R.; Westerveld, J.; van der Wielen, F.; Ebinghaus, R.; de Voogt, P., Distribution and sources of polyfluoroalkyl substances (PFAS) in the River Rhine watershed. *Environ Pollut* **2010,** *158* (10), 3243-50.

88. Groffen, T.; Wepener, V.; Malherbe, W.; Bervoets, L., Distribution of perfluorinated compounds (PFASs) in the aquatic environment of the industrially polluted Vaal River, South Africa. *Sci Total Environ* **2018,** *627*, 1334-1344.

89. Chen, H.; Han, J.; Zhang, C.; Cheng, J.; Sun, R.; Wang, X.; Han, G.; Yang, W.; He, X., Occurrence and seasonal variations of per- and polyfluoroalkyl substances (PFASs) including fluorinated alternatives in rivers, drain outlets and the receiving Bohai Sea of China. *Environ Pollut* **2017,** *231* (Pt 2), 1223-1231.

90. Cai, Y.; Wang, X.; Wu, Y.; Zhao, S.; Li, Y.; Ma, L.; Chen, C.; Huang, J.; Yu, G., Temporal trends and transport of perfluoroalkyl substances (PFASs) in a subtropical estuary: Jiulong River Estuary, Fujian, China. *Sci Total Environ* **2018,** *639*, 263-270.

91. Hopkins, Z. R.; Sun, M.; DeWitt, J. C.; Knappe, D. R. U., Recently Detected Drinking Water Contaminants: GenX and Other Per- and Polyfluoroalkyl Ether Acids. *J Am Water Works Ass* **2018,** *110* (7), 13-28.

92. Coggan, T. L.; Moodie, D.; Kolobaric, A.; Szabo, D.; Shimeta, J.; Crosbie, N. D.; Lee, E.; Fernandes, M.; Clarke, B. O., An investigation into per- and polyfluoroalkyl substances (PFAS) in nineteen Australian wastewater treatment plants (WWTPs). *Heliyon* **2019,** *5* (8), e02316.

93. Field, J. A.; Seow, J., Properties, occurrence, and fate of fluorotelomer sulfonates. *Crit Rev Envr Sci Tech* **2017,** *47* (8), 643-691.

94. Harding-Marjanovic, K. C.; Houtz, E. F.; Yi, S.; Field, J. A.; Sedlak, D. L.; Alvarez-Cohen, L., Aerobic Biotransformation of Fluorotelomer Thioether Amido Sulfonate (Lodyne) in AFFF-Amended Microcosms. *Environmental science & technology* **2015,** *49* (13), 7666-74.

95. Shaw, D. M. J.; Munoz, G.; Bottos, E. M.; Duy, S. V.; Sauve, S.; Liu, J.; Van Hamme, J. D., Degradation and defluorination of 6:2 fluorotelomer sulfonamidoalkyl betaine and 6:2 fluorotelomer sulfonate by Gordonia sp. strain NB4-1Y under sulfur-limiting conditions. *Sci Total Environ* **2019,** *647*, 690-698.

96. Weiner, B.; Yeung, L. W. Y.; Marchington, E. B.; SD'Agostino, L. A.; Mabury, S. A., Organic fluorine content in aqueous film forming foams (AFFFs) and biodegradation of the foam component 6 : 2 fluorotelomermercaptoalkylamido sulfonate (6 : 2 FTSAS). *Environ Chem* **2013,** *10* (6), 486-493.

97. NASF 6:2 Fluorotelomer Sulfonate (6:2 FTS) TOXICOLOGY AT A GLANCE. https://nasf.org/wp-content/uploads/2019/04/Summary-of-Toxicology-Studies-on-6-2-FTS-and-Detailed-Technical-Support-Documents.pdf (accessed February 01, 2020).

98. Wang, N.; Liu, J.; Buck, R. C.; Korzeniowski, S. H.; Wolstenholme, B. W.; Folsom, P. W.; Sulecki, L. M., 6:2 fluorotelomer sulfonate aerobic biotransformation in activated sludge of waste water treatment plants. *Chemosphere* **2011,** *82* (6), 853-8.

99. Martin, D.; Munoz, G.; Mejia-Avendano, S.; Duy, S. V.; Yao, Y.; Volchek, K.; Brown, C. E.; Liu, J.; Sauve, S., Zwitterionic, cationic, and anionic perfluoroalkyl and polyfluoroalkyl substances integrated into total oxidizable precursor assay of contaminated groundwater. *Talanta* **2019,** *195*, 533-542.

100. Stuchal, L.; Roberts, S. M. *Development of Surface Water Screening Levels for PFOA and PFOS Based on the Protection of Human Health: Prepared for the District and Business Support Program Florida Department of Environmental Protection* University of Florida: Gainsville, FL, 2020.

101. Stahl, L. L.; Snyder, B. D.; Olsen, A. R.; Kincaid, T. M.; Wathen, J. B.; McCarty, H. B., Perfluorinated compounds in fish from U.S. urban rivers and the Great Lakes. *Sci Total Environ* **2014,** *499*, 185-95.

102. Fair, P. A.; Wolf, B.; White, N. D.; Arnott, S. A.; Kannan, K.; Karthikraj, R.; Vena, J. E., Perfluoroalkyl substances (PFASs) in edible fish species from Charleston Harbor and tributaries, South Carolina, United States: Exposure and risk assessment. *Environ Res* **2019,** *171*, 266-277.

103. DSHS, ADV-55 Fish and Shellfish Consumption Advisory for Galveston Bay Estuary. Department of State Health Services, Ed. Texas Department of State Health Services: Austin, TX, 2015.

104. DSHS, Characterization of Potential Adverse health Effects Associated with COnsuming Fish from the San Jacinto River-Houston Ship Channel. Department of State Health Services, Ed. Teaxs Department of State Health Services: Austin, TX, 2013.

105. U.S. EPA *An Examination of EPA Risk Assessment Principles and Practices*; Washington, DC, 2004.

106. Laitinen, J. A.; Koponen, J.; Koikkalainen, J.; Kiviranta, H., Firefighters' exposure to perfluoroalkyl acids and 2-butoxyethanol present in firefighting foams. *Toxicology letters* **2014,** *231* (2), 227-32.

107. Woudneh, M. B.; Chandramouli, B.; Hamilton, C.; Grace, R., Effect of Sample Storage on the Quantitative Determination of 29 PFAS: Observation of Analyte Interconversions during Storage. *Environmental science & technology* **2019,** *53* (21), 12576-12585.

108. Dredger, S. M.; Kothari, A.; Morrison, J.; Sawada, M.; Crighton, E. J.; Graham, I. D., Using participatory design to develop (public) health decision support systems through GIS. *Int J Health Geogr* **2007,** *6*, 53.

109. Dodds, J. N.; Hopkins, Z. R.; Knappe, D. R. U.; Baker, E. S., Rapid Characterization of Per- and Polyfluoroalkyl Substances (PFAS) by Ion Mobility Spectrometry-Mass Spectrometry (IMS-MS). *Anal Chem* **2020,** *92* (6), 4427-4435.

110. Moe, M. K.; Huber, S.; Svenson, J.; Hagenaars, A.; Pabon, M.; Trumper, M.; Berger, U.; Knapen, D.; Herzke, D., The structure of the fire fighting foam surfactant Forafac(R)1157 and its biological and photolytic transformation products. *Chemosphere* **2012,** *89* (7), 869-75.

111. Liu, Y.; Pereira Ados, S.; Martin, J. W., Discovery of C5-C17 poly- and perfluoroalkyl substances in water by in-line SPE-HPLC-Orbitrap with in-source fragmentation flagging. *Anal Chem* **2015,** *87* (8), 4260-8.

112. Janda, J.; Nodler, K.; Scheurer, M.; Happel, O.; Nurenberg, G.; Zwiener, C.; Lange, F. T., Closing the gap - inclusion of ultrashort-chain perfluoroalkyl carboxylic acids in the total oxidizable precursor (TOP) assay protocol. *Environ Sci Process Impacts* **2019,** *21* (11), 1926-1935.

113. Plumlee, G. S.; Morman, G. P.; Meeker, T. M.; Hoefen, P. L.; Hageman, R. E.; Wolf, R. E., 11.7 - The Environmental and Medical Geochemistry of Potentially Hazardous Materials Produced by Disasters. *Treatise on Geochemistry* **2014,** *11*, 257-304.

114. Rieble, D. D.; Hass, C. N.; Pardue, J.; Walsh, W., Toxic and contaminant concerns generated by hurricane Katrina. *J Environ Engin* **2006,** *36* (1), 5-13.

115. Diaz, J. H., The public health impact of hurricanes and major flooding. *J La State Med Soc* **2004,** *156* (3), 145-50.

116. Ahern, M.; Kovats, R. S.; Wilkinson, P.; Few, R.; Matthies, F., Global health impacts of floods: epidemiologic evidence. *Epidemiol Rev* **2005,** *27*, 36-46.

117. Joyce, S., The dead zones: oxygen-starved coastal waters. *Environ Health Perspect* **2000,** *108* (3), A120-5.

118. Euripidou, E.; Murray, V., Public health impacts of floods and chemical contamination. *J Public Health (Oxf)* **2004,** *26* (4), 376-83.

119. Cruz, A. M.; Steinberg, L. J.; Luna, R., Identifying hurricane-induced hazardous material release scenarios in a petroleum refinery. *Nat Hazards Rev* **2001,** *2* (4), 203-210.

120. Krausmann, E.; Mushtaq, F., A qualitative Natech damage scale for the impact of floods on selected industrial facilities. *Nat Hazards* **2008,** *46* (2), 179-197.

121. Mandigo, A. C.; DiScenza, D. J.; Keimowitz, A. R.; Fitzgerald, N., Chemical contamination of soils in the New York City area following Hurricane Sandy. *Environ Geochem Health* **2016,** *38* (5), 1115-1124.

122. Woodruff, J. D.; Irish, J. L.; Camargo, S. J., Coastal flooding by tropical cyclones and sea-level rise. *Nature* **2013,** *504* (7478), 44-52.

123. Peduzzi, P.; Chatenoux, B.; Dao, H.; De Bono, A.; Herold, C.; Kossin, J.; Mouton, F.; Nordbeck, O., Global trends in tropical cyclone risk. *Nature Climate Change* **2012,** *2*, 289.

124. Knutson, T. R.; McBride, J. L.; Chan, J.; Emanuel, K.; Holland, G.; Landsea, C.; Held, I.; Kossin, J. P.; Srivastava, A. K.; Sugi, M., Tropical cyclones and climate change. *Nature Geoscience* **2010,** *3*, 157.

125. Knap, A. H.; Rusyn, I., Environmental exposures due to natural disasters. *Rev Environ Health* **2016,** *31* (1), 89-92.

126. Winsor, M., Timeline of Florence as slow-moving, deadly storm batters Carolinas. *ABC News* 2018.

127. Coyte, R. M.; McKinley, K. L.; Jiang, S.; Karr, J.; Dwyer, G. S.; Keyworth, A. J.; Davis, C. C.; Kondash, A. J.; Vengosh, A., Occurrence and distribution of hexavalent chromium in groundwater from North Carolina, USA. *Sci Total Environ* **2020,** *711*, 135135.

128. Ruhl, L.; Vengosh, A.; Dwyer, G. S.; Hsu-Kim, H.; Deonarine, A., Environmental impacts of the coal ash spill in Kingston, Tennessee: an 18-month survey. *Environmental science & technology* **2010,** *44* (24), 9272-8.

129. U.S. EPA Coal Ash Basics. https://www.epa.gov/coalash/coal-ash-basics (accessed October 12).

130. Dewitt, D., Researcher: Sutton Lake Site Of Numerous Coal Ash Spills. *North Carolina Public Radio* 2019.

131. Ouzts, E. Critics: North Carolina officials 'failing' after Florence coal ash spills *Energy News Network,* [Online], 2018. https://energynews.us/2018/10/16/southeast/critics-north-carolina-officials-failing-after-florence-coal-ash-spills/ (accessed October 12, 2020).

132. Biesecker, M.; Kastanis, A. Hurricane Florence breaches manure lagoon, coal ash pit in North Carolina 2018. https://www.pbs.org/newshour/nation/hurricane-florence-breaches-manure-lagoon-coal-ash-pit-in-north-carolina.

133. U.S. EPA, Soil Sampling Operating Procedure. U.S. Environmental Protection Agency, Ed. U.S. EPA: Athens, GA, 2007.

134. Cantillo, A. Y., Lauenstein, G.G., Performance-Based Quality Assurance—The NOAA National Status and Trends Program Experience. Administration, N. O. a. A., Ed. Silver Spring, MD, 1998.

135. U.S. EPA, National Coastal Condition Assessment Quality Assurance Project Plan United States Environmental Protection Agency, Ed. Washington, DC, 2010.

136. Silva, M. H.; Kwok, A., Open Access ToxCast/Tox21, Toxicological Priority Index (ToxPi) and Integrated Chemical Environment (ICE) Models Rank and Predict Acute Pesticide Toxicity: A Case Study. *Int J Toxicol Envr Health* **2020,** *5* (1), 102-125.

137. Bera, G.; Camargo, K.; Sericano, J. L.; Liu, Y.; Sweet, S. T.; Horney, J.; Jun, M.; Chiu, W.; Rusyn, I.; Wade, T. L.; Knap, A. H., Baseline data for distribution of contaminants by natural disasters: results from a residential Houston neighborhood during Hurricane Harvey flooding. *Heliyon* **2019,** *5* (11), e02860.

138. El-Kady, A. A.; Wade, T. L.; Sweet, S. T.; Sericano, J. L., Distribution and residue profile of organochlorine pesticides and polychlorinated biphenyls in sediment and fish of Lake Manzala, Egypt. *Environ Sci Pollut Res Int* **2017,** *24* (11), 10301-10312.

139. Cook, R. D., Detection of Influential Observations in Linear Regression. *Technometrics* **1977,** *19* (1), 15-18.

140. Wang, Z.; Yang, C.; Parrott, J. L.; Frank, R. A.; Yang, Z.; Brown, C. E.; Hollebone, B. P.; Landriault, M.; Fieldhouse, B.; Liu, Y.; Zhang, G.; Hewitt, L. M., Forensic source differentiation of petrogenic, pyrogenic, and biogenic hydrocarbons in Canadian oil sands environmental samples. *J Hazard Mater* **2014,** *271*, 166-77.

141. Lu, J.; Zhang, C.; Wu, J.; Lin, Y. C.; Zhang, Y. X.; Yu, X. B.; Zhang, Z. H., Pollution, sources, and ecological-health risks of polycyclic aromatic hydrocarbons in coastal waters along coastline of China. *Hum Ecol Risk Assess* **2020,** *26* (4), 968-985.

142. U.S. EPA Regional Screening Levels RSLS Generic Tables. https://www.epa.gov/risk/regional-screening-levels-rsls-generic-tables (accessed July 01, 2020).

143. Nisbet, I. C.; LaGoy, P. K., Toxic equivalency factors (TEFs) for polycyclic aromatic hydrocarbons (PAHs). *Regulatory toxicology and pharmacology : RTP* **1992,** *16* (3), 290-300.

144. E14 Implementation Working Group, ICH E14 Guideline: The Clinical Evaluation of QT/QTc Interval Prolongation and Proarrhythmic Potential for Non-Antiarrhythmic Drugs Questions & Answers (R3). International Council for Harmonisation of Technical Requirements for Pharmaceuticals for Human Use: Geneva, Switzerland, 2015.

145. U.S. EPA, Development of a Relative Potency Factor (Rpf) Approach for Polycyclic Aromatic Hydrocarbon (PAH) Mixtures (External Review Draft). U.S. Environmental Protection Agency: Washington, DC, 2010.

146. U.S. EPA, Provisional Guidance for Quantitative Risk Assessment of Polycyclic Aromatic Hydrocarbons (PAH). U.S. Environmental Protection Agency, Office of Research and Development, Office of Health and Environmental Assessment: Washington, DC, 1993.

147. Vengosh, A.; Cowan, E. A.; Coyte, R. M.; Kondash, A. J.; Wang, Z.; Brandt, J. E.; Dwyer, G. S., Evidence for unmonitored coal ash spills in Sutton Lake, North Carolina: Implications for contamination of lake ecosystems. *Sci Total Environ* **2019,** *686*, 1090-1103.

148. IARC, *Some Non-heterocyclic Polycyclic Aromatic Hydrocarbons and Some Related Exposures*. WHO: Lyon, France, 2010.

149. Myers, J.; Thorbjornsen, K., Identifying metals contamination in soil: A geochemical approach. *Soil Sediment Contam* **2004,** *13* (1), 1-16.

150. Wang, Z. D.; Fingas, M.; Shu, Y. Y.; Sigouin, L.; Landriault, M.; Lambert, P.; Turpin, R.; Campagna, P.; Mullin, J., Quantitative characterization of PAHs in burn

residue and soot samples and differentiation of pyrogenic PAHs from petrogenic PAHs - The 1994 Mobile Burn Study. *Environmental science & technology* **1999,** *33* (18), 3100-3109.

151. USGS, Geochemical and Mineralogical Data for Soils of the Conterminous United States. U.S. Department of the Interior, Ed. U.S. Geological Survey: Reston, VA, 2013; Vol. Data Series 801.

152. National Weather Service Historical Hurricane Florence, September 12 – 15, 2018. https://www.weather.gov/mhx/Florence2018 (accessed December 15).

153. Errett, N. A.; Haynes, E. N.; Wyland, N.; Everhart, A.; Pendergrast, C.; Parker, E. A., Assessing the national capacity for disaster research response (DR2) within the NIEHS Environmental Health Sciences Core Centers. *Environ Health* **2019,** *18* (1), 61.

154. Amolegbe, S. Texas workshop prepares trainees for disaster research *NIEHS Environmental Factor,* [Online], 2019. https://factor.niehs.nih.gov/2019/3/science-highlights/disaster_research/index.htm (accessed April 01, 2020).

155. Schwartz, G. E.; Hower, J. C.; Phillips, A. L.; Rivera, N.; Vengosh, A.; Hsu-Kim, H., Ranking Coal Ash Materials for Their Potential to Leach Arsenic and Selenium: Relative Importance of Ash Chemistry and Site Biogeochemistry. *Environ Eng Sci* **2018,** *35* (7), 728-738.

156. Srivastava, V. K.; Srivastava, P. K.; Misra, U. K., Polycyclic aromatic hydrocarbons of coal fly ash: analysis by gas-liquid chromatography using nematic liquid crystals. *J Toxicol Environ Health* **1985,** *15* (2), 333-7.

157. Kravchenko, J.; Lyerly, H. K., The Impact of Coal-Powered Electrical Plants and Coal Ash Impoundments on the Health of Residential Communities. *N C Med J* **2018,** *79* (5), 289-300.

158. Horney, J. A.; Casillas, G. A.; Baker, E.; Stone, K. W.; Kirsch, K. R.; Camargo, K.; Wade, T. L.; McDonald, T. J., Comparing residential contamination in a Houston environmental justice neighborhood before and after Hurricane Harvey. *PloS one* **2018,** *13* (2), e0192660.

159. Tang, H. P., Recent development in analysis of persistent organic pollutants under the Stockholm Convention. *Trends in Analytical Chemistry* **2013,** *45*.

160. Wang, T.; Wang, Y.; Liao, C.; Cai, Y.; Jiang, G., Perspectives on the inclusion of perfluorooctane sulfonate into the Stockholm Convention on Persistent Organic Pollutants. *Environ Sci Technol* **2009,** *43* (14), 5171-5.

161. Richardson, S. D.; Kimura, S. Y., Water Analysis: Emerging Contaminants and Current Issues. *Anal Chem* **2020,** *92* (1), 473-505.

162. Richmond, E. K.; Grace, M. R.; Kelly, J. J.; Reisinger, A. J.; Rosi, E. J.; Walters, D. M., Pharmaceuticals and personal care products (PPCPs) are ecological disrupting compounds (EcoDC). *Elementa-Sci Anthrop* **2017,** *5*.

163. Omiecinski, C. J.; Vanden Heuvel, J. P.; Perdew, G. H.; Peters, J. M., Xenobiotic metabolism, disposition, and regulation by receptors: from biochemical phenomenon to predictors of major toxicities. *Toxicol Sci* **2011,** *120 Suppl 1*, S49-75.

164. Zacharia, J. T., Degradation Pathways of Persistent Organic Pollutants (POPs) in the Environment. In *Persistent Organic Pollutants*, Donyinah, S. K., Ed. IntechOpen: London, UK, 2019.

165. Vermeulen, R.; Schymanski, E. L.; Barabasi, A. L.; Miller, G. W., The exposome and health: Where chemistry meets biology. *Science* **2020,** *367* (6476), 392-396.

166. Liu, K.; Lee, C.; Singer, G.; Woodworth, M.; Ziegler, T. R.; Kraft, C.; Miller, G. P.; Li, S.; Go, Y. M.; Morgan, E.; Jones, D., Large-scale, enzyme-based xenobiotic identification for exposomics. *Nature Communications* **2021**.

167. Aly, N. A.; Casillas, G.; Luo, Y. S.; McDonald, T. J.; Wade, T. L.; Zhu, R.; Newman, G.; Lloyd, D.; Wright, F. A.; Chiu, W. A.; Rusyn, I., Environmental impacts of Hurricane Florence flooding in eastern North Carolina: temporal analysis of contaminant distribution and potential human health risks. *J Expo Sci Environ Epidemiol* **2021**.

168. Dodds, J. N.; Alexander, N. L. M.; Kirkwood, K. I.; Foster, M. R.; Hopkins, Z. R.; Knappe, D. R. U.; Baker, E. S., From Pesticides to Per- and Polyfluoroalkyl Substances: An Evaluation of Recent Targeted and Untargeted Mass Spectrometry Methods for Xenobiotics. *Anal Chem* **2021,** *93* (1), 641-656.

169. Zhang, X.; Romm, M.; Zheng, X.; Zink, E. M.; Kim, Y. M.; Burnum-Johnson, K. E.; Orton, D. J.; Apffel, A.; Ibrahim, Y. M.; Monroe, M. E.; Moore, R. J.; Smith, J. N.; Ma, J.; Renslow, R. S.; Thomas, D. G.; Blackwell, A. E.; Swinford, G.; Sausen, J.; Kurulugama, R. T.; Eno, N.; Darland, E.; Stafford, G.; Fjeldsted, J.; Metz, T. O.; Teeguarden, J. G.; Smith, R. D.; Baker, E. S., SPE-IMS-MS: An automated platform for sub-sixty second surveillance of endogenous metabolites and xenobiotics in biofluids. *Clin Mass Spectrom* **2016,** *2*, 1-10.

170. Dodds, J. N.; Baker, E. S., Ion Mobility Spectrometry: Fundamental Concepts, Instrumentation, Applications, and the Road Ahead. *J Am Soc Mass Spectrom* **2019,** *30* (11), 2185-2195.

171. Kanu, A. B.; Dwivedi, P.; Tam, M.; Matz, L.; Hill, H. H., Ion mobility-mass spectrometry. *Journal of Mass Spectrometry* **2008,** *43* (1), 1-22.

172. Hoaglund, C. S.; Valentine, S. J.; Sporleder, C. R.; Reilly, J. P.; Clemmer, D. E., Three-dimensional ion mobility/TOFMS analysis of electrosprayed biomolecules. *Anal Chem* **1998,** *70* (11), 2236-42.

173. Wang, X.; Yu, N.; Yang, J.; Jin, L.; Guo, H.; Shi, W.; Zhang, X.; Yang, L.; Yu, H.; Wei, S., Suspect and non-target screening of pesticides and pharmaceuticals transformation products in wastewater using QTOF-MS. *Environ Int* **2020,** *137*, 105599.

174. Grimm, F. A.; Klaren, W. D.; Li, X.; Lehmler, H. J.; Karmakar, M.; Robertson, L. W.; Chiu, W. A.; Rusyn, I., Cardiovascular Effects of Polychlorinated Biphenyls and Their Major Metabolites. *Environ Health Perspect* **2020,** *128* (7), 77008.

175. Baker, E. S.; Clowers, B. H.; Li, F.; Tang, K.; Tolmachev, A. V.; Prior, D. C.; Belov, M. E.; Smith, R. D., Ion mobility spectrometry-mass spectrometry performance using electrodynamic ion funnels and elevated drift gas pressures. *J Am Soc Mass Spectrom* **2007,** *18* (7), 1176-87.

176. Luo, Y. S.; Aly, N. A.; McCord, J.; Strynar, M. J.; Chiu, W. A.; Dodds, J. N.; Baker, E. S.; Rusyn, I., Rapid Characterization of Emerging Per- and Polyfluoroalkyl Substances in Aqueous Film-Forming Foams Using Ion Mobility Spectrometry-Mass Spectrometry. *Environmental science & technology* **2020,** *54* (23), 15024-15034.

177. Convention, S. All POPs listed in the Stockholm Convention. http://www.pops.int/TheConvention/ThePOPs/AllPOPs/tabid/2509/Default.aspx.

178. Xiao, F., Emerging poly- and perfluoroalkyl substances in the aquatic environment: A review of current literature. *Water Res* **2017,** *124*, 482-495.

179. Gluge, J.; Scheringer, M.; Cousins, I. T.; DeWitt, J. C.; Goldenman, G.; Herzke, D.; Lohmann, R.; Ng, C. A.; Trier, X.; Wang, Z. Y., An overview of the uses of per- and polyfluoroalkyl substances (PFAS). *Environ Sci-Proc Imp* **2020,** *22* (12), 2345-2373.

180. OECD, Synthesis Paper on Per- and Polyfluorinated Chemicals (PFCs), Environment, Health and Safety. Environment, Health and Safety Division of the Environment Directorate, OECD: Paris, France, 2013.

181. Kosyakov, D. S.; Ul'yanovskii, N. V.; Anikeenko, E. A.; Gorbova, N. S., Negative ion mode atmospheric pressure ionization methods in lignin mass spectrometry: A comparative study. *Rapid Commun Mass Spectrom* **2016,** *30* (19), 2099-108.

182. Zheng, X.; Dupuis, K. T.; Aly, N. A.; Zhou, Y.; Smith, F. B.; Tang, K.; Smith, R. D.; Baker, E. S., Utilizing ion mobility spectrometry and mass spectrometry for the analysis of polycyclic aromatic hydrocarbons, polychlorinated biphenyls, polybrominated diphenyl ethers and their metabolites. *Anal Chim Acta* **2018,** *1037*, 265-273.

183. EPA, U. Learn about Polychlorinated Biphenyls (PCBs). https://www.epa.gov/pcbs/learn-about-polychlorinated-biphenyls-pcbs#commercial.

184. Aslam, S. N.; Huber, C.; Asimakopoulos, A. G.; Steinnes, E.; Mikkelsen, O., Trace elements and polychlorinated biphenyls (PCBs) in terrestrial compartments of Svalbard, Norwegian Arctic. *Sci Total Environ* **2019,** *685*, 1127-1138.

185. Grimm, F. A.; Hu, D.; Kania-Korwel, I.; Lehmler, H. J.; Ludewig, G.; Hornbuckle, K. C.; Duffel, M. W.; Bergman, A.; Robertson, L. W., Metabolism and metabolites of polychlorinated biphenyls. *Critical reviews in toxicology* **2015,** *45* (3), 245-72.

186. Guvenius, D. M.; Aronsson, A.; Ekman-Ordeberg, G.; Bergman, A.; Noren, K., Human prenatal and postnatal exposure to polybrominated diphenyl ethers, polychlorinated biphenyls, polychlorobiphenylols, and pentachlorophenol. *Environ Health Perspect* **2003,** *111* (9), 1235-41.

187. Herrick, R. F.; Meeker, J. D.; Altshul, L., *Environmental Health Indoor Exposures, Asessments and Interventions*. Apple Academic Press: Oakville, ON, CA, 2016.

188. Espandiari, P.; Glauert, H. P.; Lehmler, H. J.; Lee, E. Y.; Srinivasan, C.; Robertson, L. W., Initiating activity of 4-chlorobiphenyl metabolites in the resistant hepatocyte model. *Toxicol Sci* **2004,** *79* (1), 41-6.

189. Grimm, F. A.; Lehmler, H. J.; He, X.; Robertson, L. W.; Duffel, M. W., Sulfated metabolites of polychlorinated biphenyls are high-affinity ligands for the thyroid hormone transport protein transthyretin. *Environ Health Perspect* **2013,** *121* (6), 657-62.

190. X.H. Lin, J. C. X., A.A. Keller, L. He, Y.H. Gu, W.W. Zheng, D.Y. Sun, Z.B. Lu, J.W. Huang, X.F. Huang, G.M. Li, Occurrence and risk assessment of emerging contaminants in a water reclamation and ecological reuse project. *Science of the Total Environment* **2020,** *744*.

191. Hube, S.; Wu, B., Mitigation of emerging pollutants and pathogens in decentralized wastewater treatment processes: A review. *Sci Total Environ* **2021,** *779*, 146545.

192. Vajda, A. M.; Barber, L. B.; Gray, J. L.; Lopez, E. M.; Bolden, A. M.; Schoenfuss, H. L.; Norris, D. O., Demasculinization of male fish by wastewater treatment plant effluent. *Aquat Toxicol* **2011,** *103* (3-4), 213-21.

193. Guiloski, I. C.; Ribas, J. L. C.; Piancini, L. D. S.; Dagostim, A. C.; Cirio, S. M.; Favaro, L. F.; Boschen, S. L.; Cestari, M. M.; da Cunha, C.; Silva de Assis, H. C., Paracetamol causes endocrine disruption and hepatotoxicity in male fish Rhamdia quelen after subchronic exposure. *Environ Toxicol Pharmacol* **2017,** *53*, 111-120.

194. Lv, Y. Z.; Yao, L.; Wang, L.; Liu, W. R.; Zhao, J. L.; He, L. Y.; Ying, G. G., Bioaccumulation, metabolism, and risk assessment of phenolic endocrine disrupting chemicals in specific tissues of wild fish. *Chemosphere* **2019,** *226*, 607-615.

195. Plasencia, M. D.; Isailovic, D.; Merenbloom, S. I.; Mechref, Y.; Novotny, M. V.; Clemmer, D. E., Resolving and assigning N-linked glycan structural isomers from ovalbumin by IMS-MS. *J Am Soc Mass Spectrom* **2008,** *19* (11), 1706-15.

196. Isailovic, D.; Kurulugama, R. T.; Plasencia, M. D.; Stokes, S. T.; Kyselova, Z.; Goldman, R.; Mechref, Y.; Novotny, M. V.; Clemmer, D. E., Profiling of human serum glycans associated with liver cancer and cirrhosis by IMS-MS. *J Proteome Res* **2008,** *7* (3), 1109-17.

197. Sim, W. J.; Lee, J. W.; Lee, E. S.; Shin, S. K.; Hwang, S. R.; Oh, J. E., Occurrence and distribution of pharmaceuticals in wastewater from households, livestock farms, hospitals and pharmaceutical manufactures. *Chemosphere* **2011,** *82* (2), 179-86.

198. Zhang, W.; Pang, S.; Lin, Z.; Mishra, S.; Bhatt, P.; Chen, S., Biotransformation of perfluoroalkyl acid precursors from various environmental systems: advances and perspectives. *Environ Pollut* **2021,** *272*, 115908.

199. Schaefer, C. E.; Choyke, S.; Ferguson, P. L.; Andaya, C.; Burant, A.; Maizel, A.; Strathmann, T. J.; Higgins, C. P., Electrochemical Transformations of Perfluoroalkyl Acid (PFAA) Precursors and PFAAs in Groundwater Impacted with Aqueous Film Forming Foams. *Environmental science & technology* **2018,** *52* (18), 10689-10697.

200. Liu, J. X.; Avendano, S. M., Microbial degradation of polyfluoroalkyl chemicals in the environment: A review. *Environment International* **2013,** *61*, 98-114.

201. Singh, R. K.; Fernando, S.; Baygi, S. F.; Multari, N.; Thagard, S. M.; Holsen, T. M., Breakdown Products from Perfluorinated Alkyl Substances (PFAS) Degradation in a Plasma-Based Water Treatment Process. *Environmental science & technology* **2019,** *53* (5), 2731-2738.

202. Aly, N. A.; Luo, Y. S.; Liu, Y.; Casillas, G.; McDonald, T. J.; Kaihatu, J. M.; Jun, M.; Ellis, N.; Gossett, S.; Dodds, J. N.; Baker, E. S.; Bhandari, S.; Chiu, W. A.; Rusyn, I., Temporal and spatial analysis of per and polyfluoroalkyl substances in surface waters of Houston ship channel following a large-scale industrial fire incident. *Environ Pollut* **2020,** *265* (Pt B), 115009.

203. Miller, A.; Yeskey, K.; Garantziotis, S.; Arnesen, S.; Bennett, A.; O'Fallon, L.; Thompson, C.; Reinlib, L.; Masten, S.; Remington, J.; Love, C.; Ramsey, S.; Rosselli, R.; Galluzzo, B.; Lee, J.; Kwok, R.; Hughes, J., Integrating Health Research into Disaster Response: The New NIH Disaster Research Response Program. *Int J Environ Res Public Health* **2016,** *13* (7).

204. Burnum-Johnson, K. E.; Zheng, X.; Dodds, J. N.; Ash, J.; Fourches, D.; Nicora, C. D.; Wendler, J. P.; Metz, T. O.; Waters, K. M.; Jansson, J. K.; Smith, R. D.; Baker, E. S., Ion Mobility Spectrometry and the Omics: Distinguishing Isomers, Molecular Classes and Contaminant Ions in Complex Samples. *Trends Analyt Chem* **2019,** *116*, 292-299.

205. Valdiviezo, A.; Aly, N. A.; Luo, Y. S.; Cordova, A.; Casillas, G.; Foster, M.; Baker, E. S.; Rusyn, I. R., Analysis of per- and polyfluoroalkyl substances in Houston Ship Channel and Galveston Bay following a large-scale industrial fire using ion-mobility-spectrometry-mass spectrometry. *Journal of Environmental Sciences* **2021,** *115*, 350-362.

APPENDIX A

SUPPLEMENTARY MATERIAL FOR CHAPTER II

Appendix A.1: LC-MS detection and quantitation of the PFAS compounds in standards and environmental water samples from HSC/GB. (A) LC-MS chromatograms of a synthetic PFAS mixture containing 29 chemicals. (B) LC-MS chromatogram of PFAS substances in sample collected on March 22, 2019 at location SCW2 that was closest to the ITC incident. (C) LC-MS chromatogram of PFAS substances in sample collected on July 23, 2019 at location SCW2. Calibration curves for representative (D) perfluorinated compounds and (E) fluorotelomer compounds. The y-axis in all plots represents the relative abundance of each compound and was used to calculate the concentrations (in ng/mL).

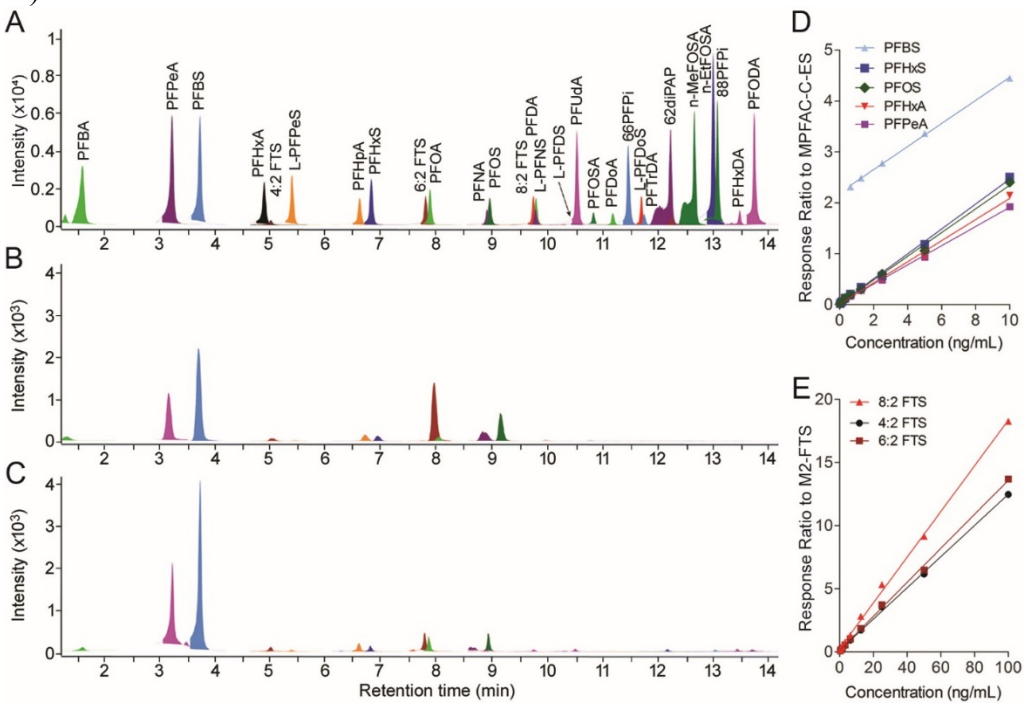

Appendix A.2: Temporal patterns of each PFAS at each open water (A) or shore-accessible (B) locations, with significant peaks identified as described in Methods. For monotonic trends, peak is identified as the first time-point and the p-value corresponds to the slope coefficient for a linear trend model. For non-monotonic visual trends, the peak is identified as where the slope changes direction using a change point test for the mean difference between adjacent time-points, and the p-value corresponds to the change point confidence level.

Appendix A.3: PFAS Concentrations Over Sampling Period

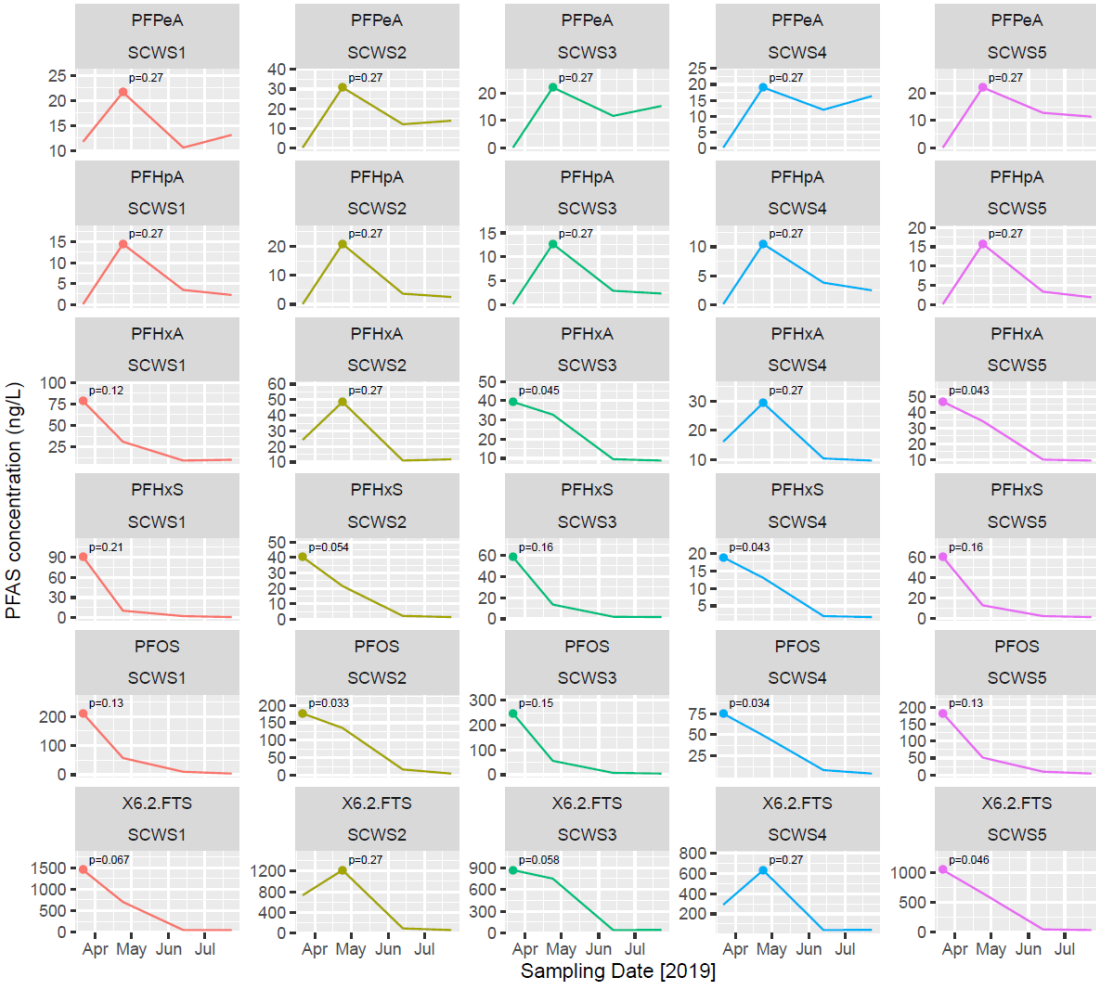

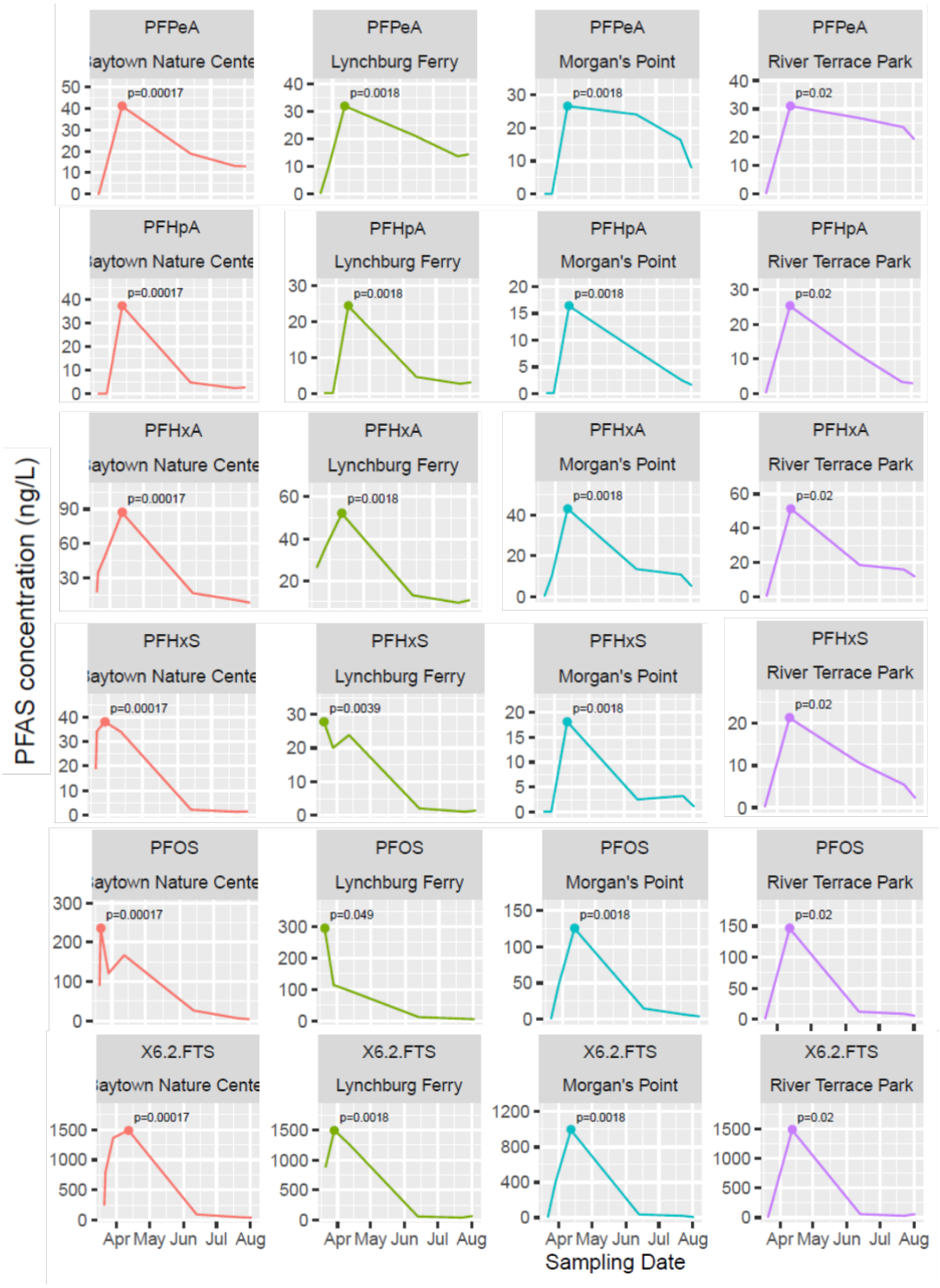
PFPeA
Lynchburg Ferry
Morgan's Point
River Terrace Park
PFHpA
PFHxA
PFHxS
PFOS
X6.2.FTS
p=0.00017
p=0.0018
p=0.02
p=0.0039
p=0.049
PFAS concentration (ng/L)
Apr May Jun Jul Aug
Sampling Date

Appendix A.4: Grid outlines for modeling. (A) Grid over the Gulf of Mexico. (B) Grid over the Texas shelf. (C) Grid over the Galveston Bay. (D) Grid over the Houston Ship Channel.

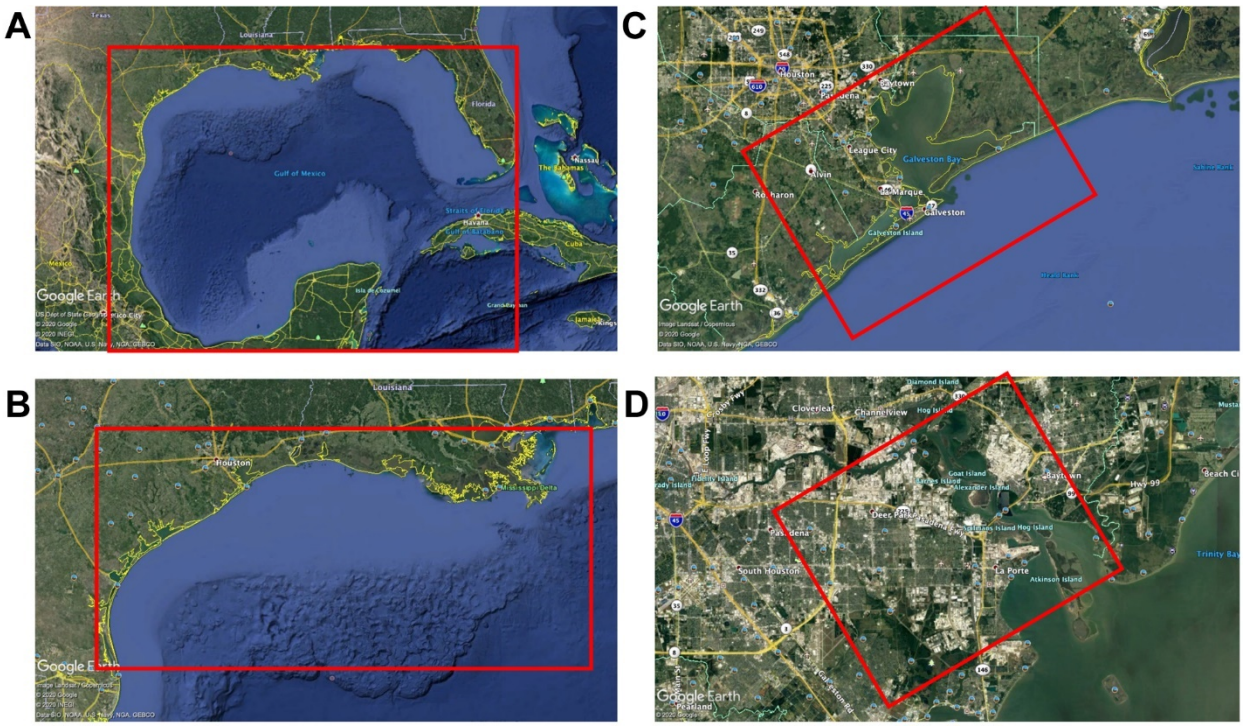

Appendix A.5: Detailed comparison of PFAS concentration measurements with water standards and guideline values from Table 2. For each sub-panel (A-P) that represents a different PFAS as shown above the graphs, sample concentrations are plotted by location, separated into three time periods. Samples are color-coded by whether they exceed any regulatory limits (lighter = below the limit, darker = above the limit). Regulatory limits are shown as lines, with line color indicating the boundaries of the limits (min=green, max=red), and line style (solid=drinking water, dotted=fish consumption, dashed=recreational swimming/wading) indicating their basis on different exposure scenarios.

A.

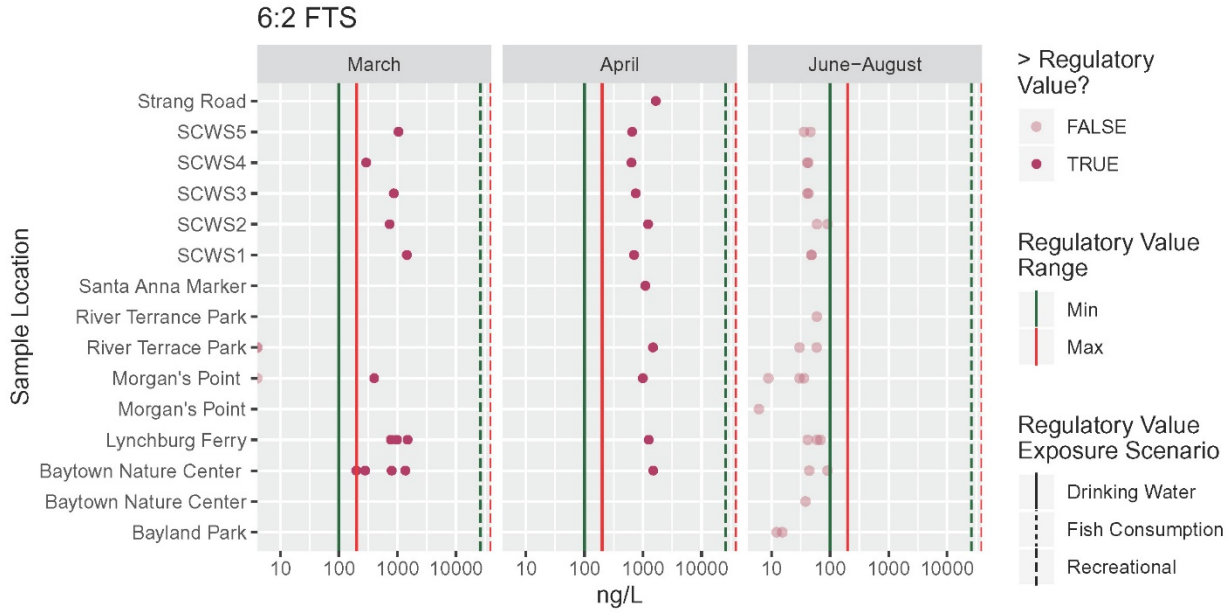

B.

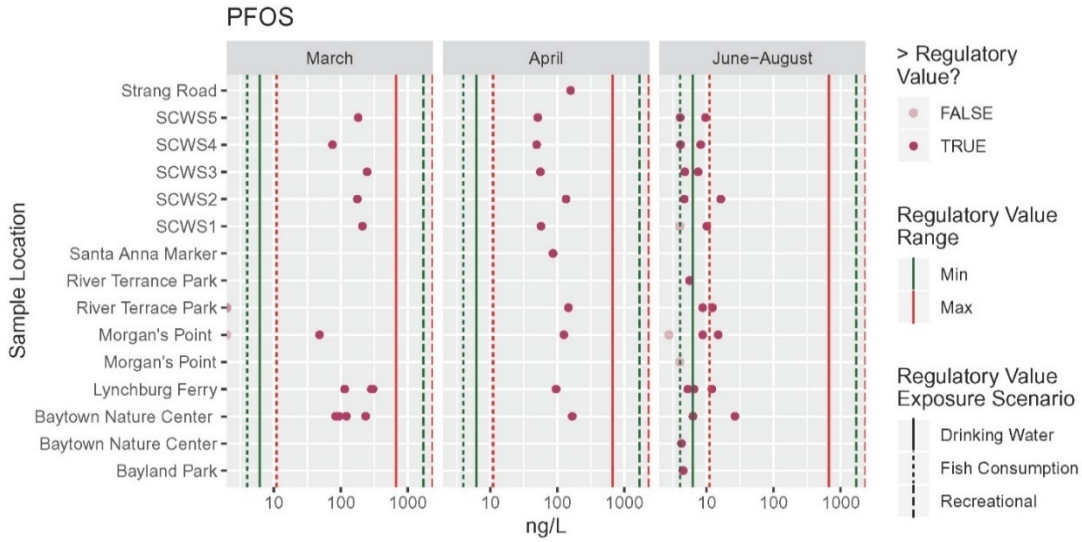

C

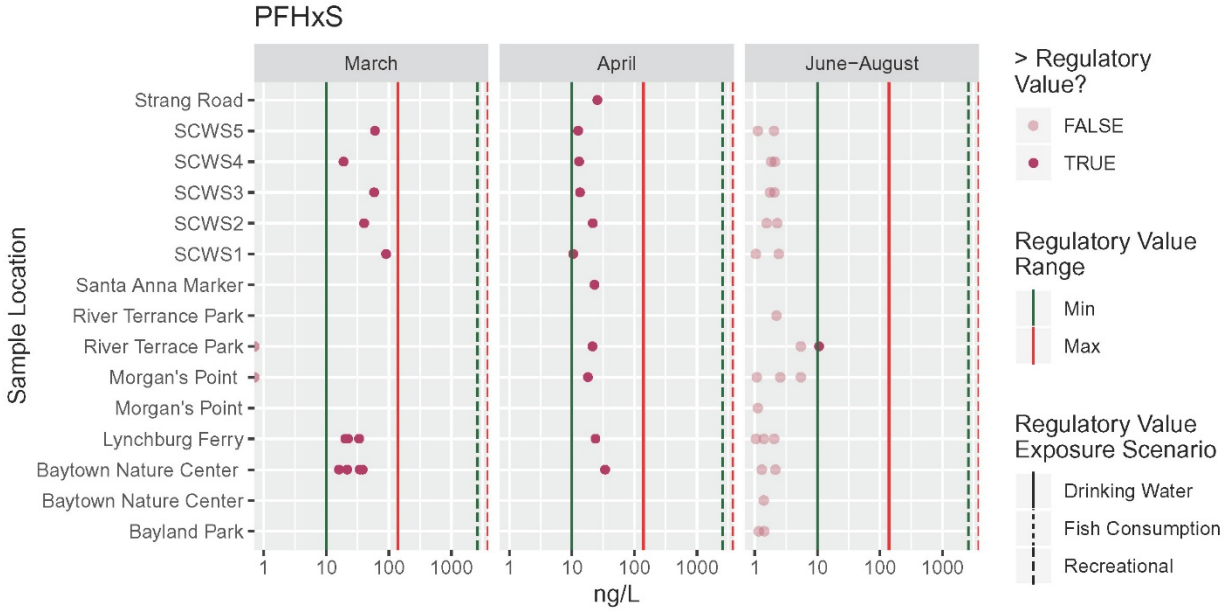
PFHxS
March
April
June–August
Strang Road
SCWS5
SCWS4
SCWS3
SCWS2
SCWS1
Santa Anna Marker
River Terrance Park
River Terrace Park
Morgan's Point
Morgan's Point
Lynchburg Ferry
Baytown Nature Center
Baytown Nature Center
Bayland Park
Sample Location
1
10
100
1000
ng/L
> Regulatory Value?
FALSE
TRUE
Regulatory Value Range
Min
Max
Regulatory Value Exposure Scenario
Drinking Water
Fish Consumption
Recreational

D.

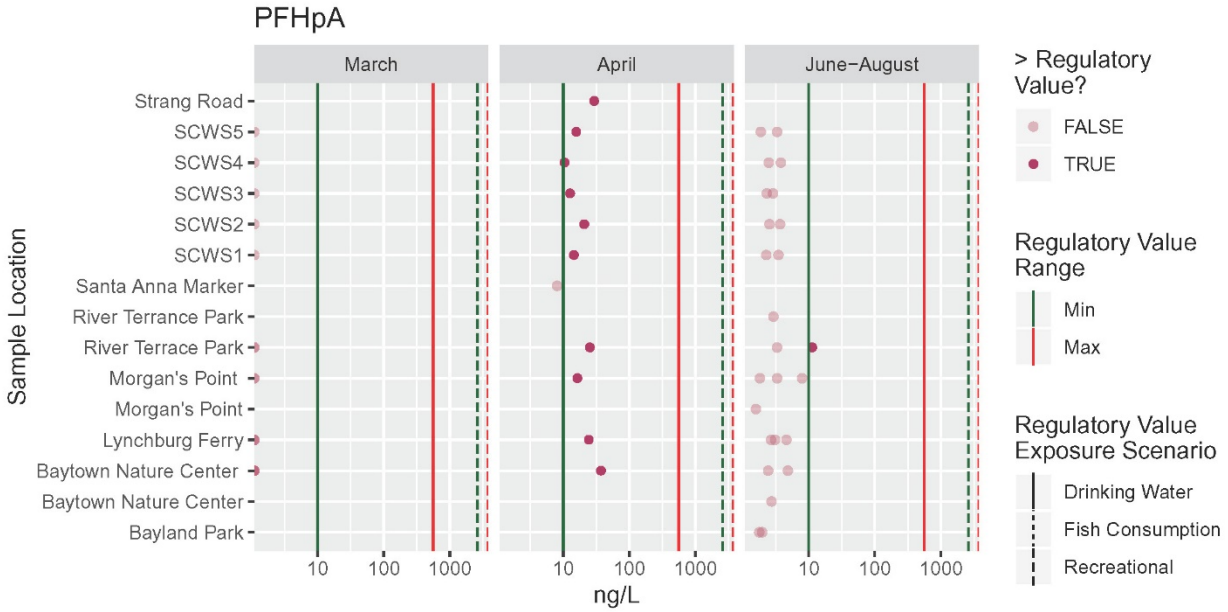
PFHpA
March
April
June–August
Strang Road
SCWS5
SCWS4
SCWS3
SCWS2
SCWS1
Santa Anna Marker
River Terrance Park
River Terrace Park
Morgan's Point
Morgan's Point
Lynchburg Ferry
Baytown Nature Center
Baytown Nature Center
Bayland Park
Sample Location
10
100
1000
ng/L
> Regulatory Value?
FALSE
TRUE
Regulatory Value Range
Min
Max
Regulatory Value Exposure Scenario
Drinking Water
Fish Consumption
Recreational

E

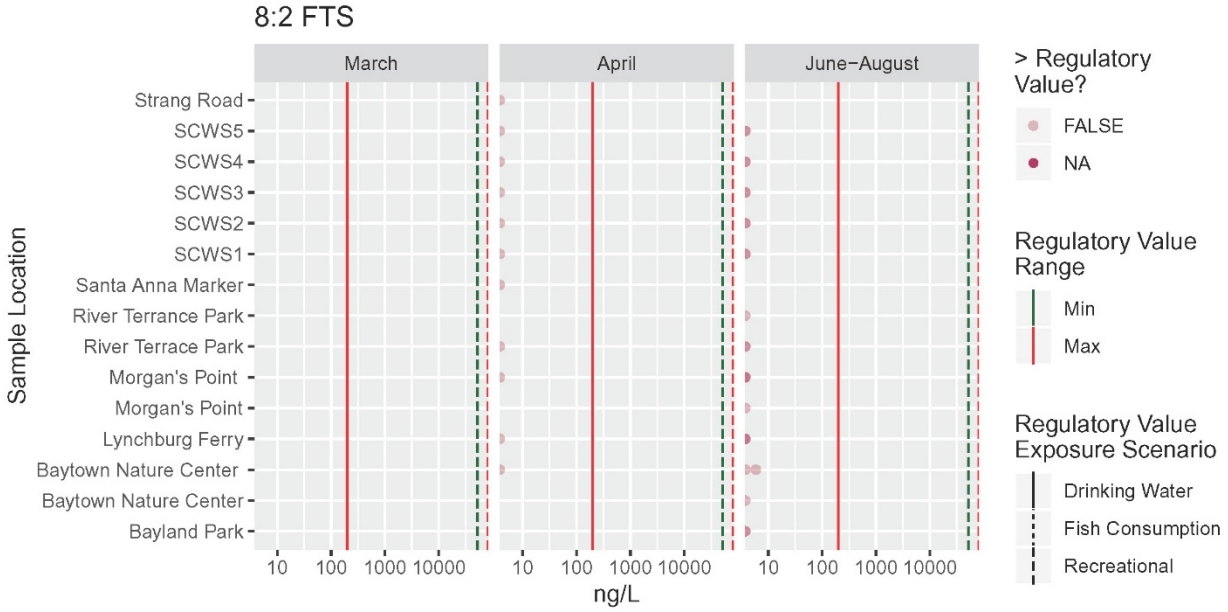
8:2 FTS
March
April
June–August
Strang Road
SCWS5
SCWS4
SCWS3
SCWS2
SCWS1
Santa Anna Marker
River Terrance Park
River Terrace Park
Morgan's Point
Morgan's Point
Lynchburg Ferry
Baytown Nature Center
Baytown Nature Center
Bayland Park
Sample Location
10 100 1000 10000
ng/L
> Regulatory Value?
FALSE
NA
Regulatory Value Range
Min
Max
Regulatory Value Exposure Scenario
Drinking Water
Fish Consumption
Recreational

F.

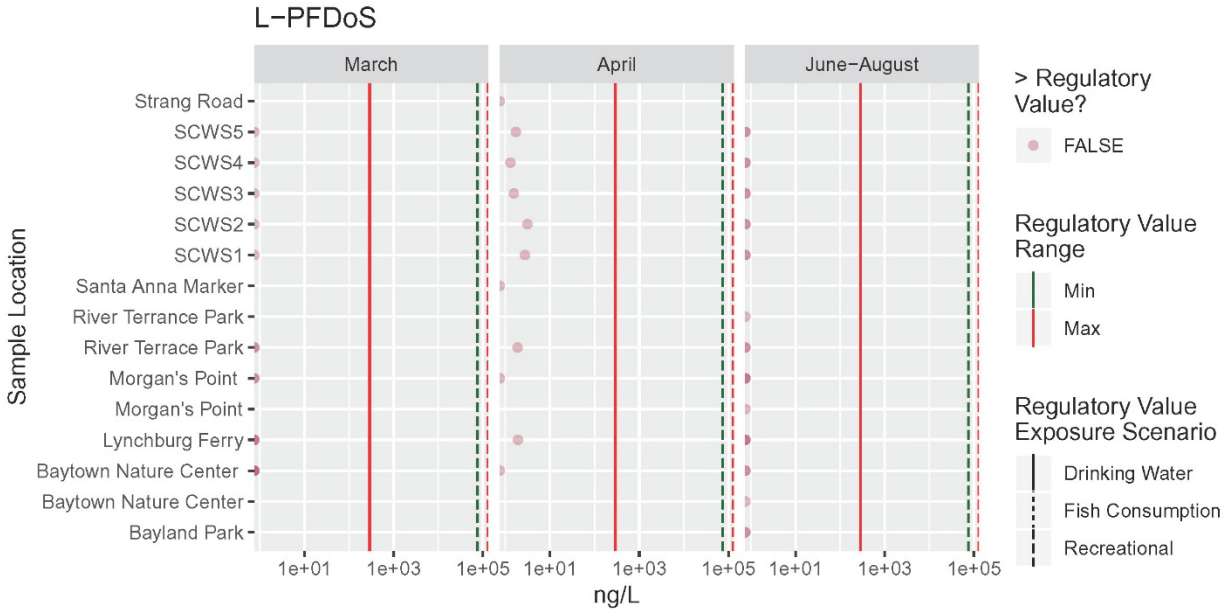
L–PFDoS
March
April
June–August
Strang Road
SCWS5
SCWS4
SCWS3
SCWS2
SCWS1
Santa Anna Marker
River Terrance Park
River Terrace Park
Morgan's Point
Morgan's Point
Lynchburg Ferry
Baytown Nature Center
Baytown Nature Center
Bayland Park
Sample Location
1e+01 1e+03 1e+05
ng/L
> Regulatory Value?
FALSE
Regulatory Value Range
Min
Max
Regulatory Value Exposure Scenario
Drinking Water
Fish Consumption
Recreational

G.

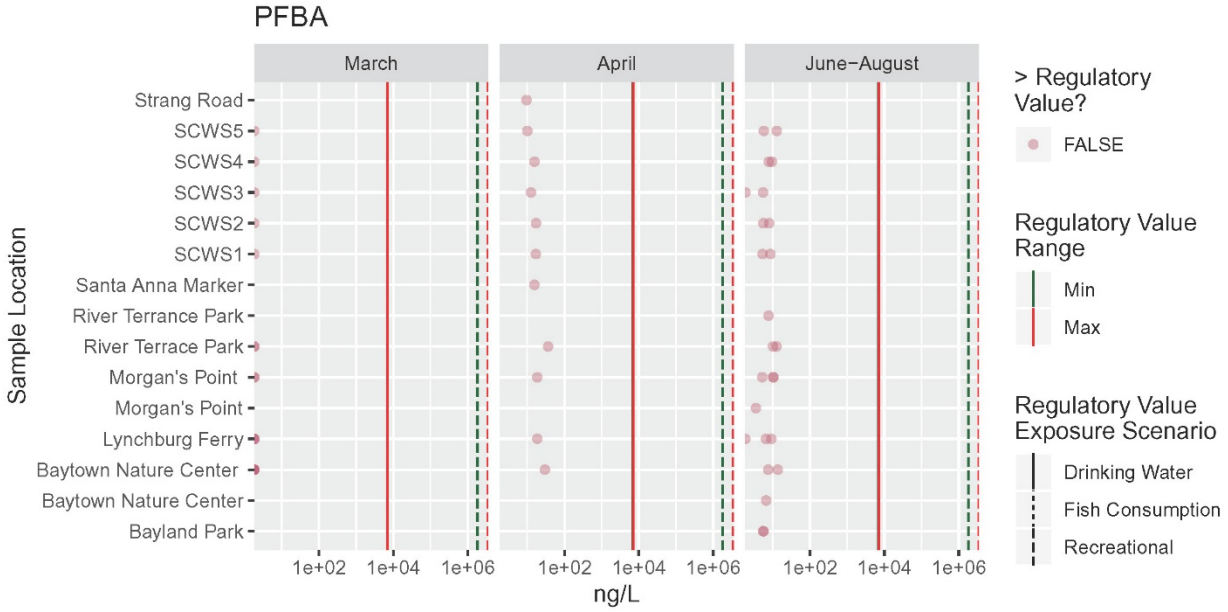
PFBA
March
April
June–August
Strang Road
SCWS5
SCWS4
SCWS3
SCWS2
SCWS1
Santa Anna Marker
River Terrance Park
River Terrace Park
Morgan's Point
Morgan's Point
Lynchburg Ferry
Baytown Nature Center
Baytown Nature Center
Bayland Park
Sample Location
1e+02
1e+04
1e+06
ng/L
> Regulatory Value?
FALSE
Regulatory Value Range
Min
Max
Regulatory Value Exposure Scenario
Drinking Water
Fish Consumption
Recreational

H.

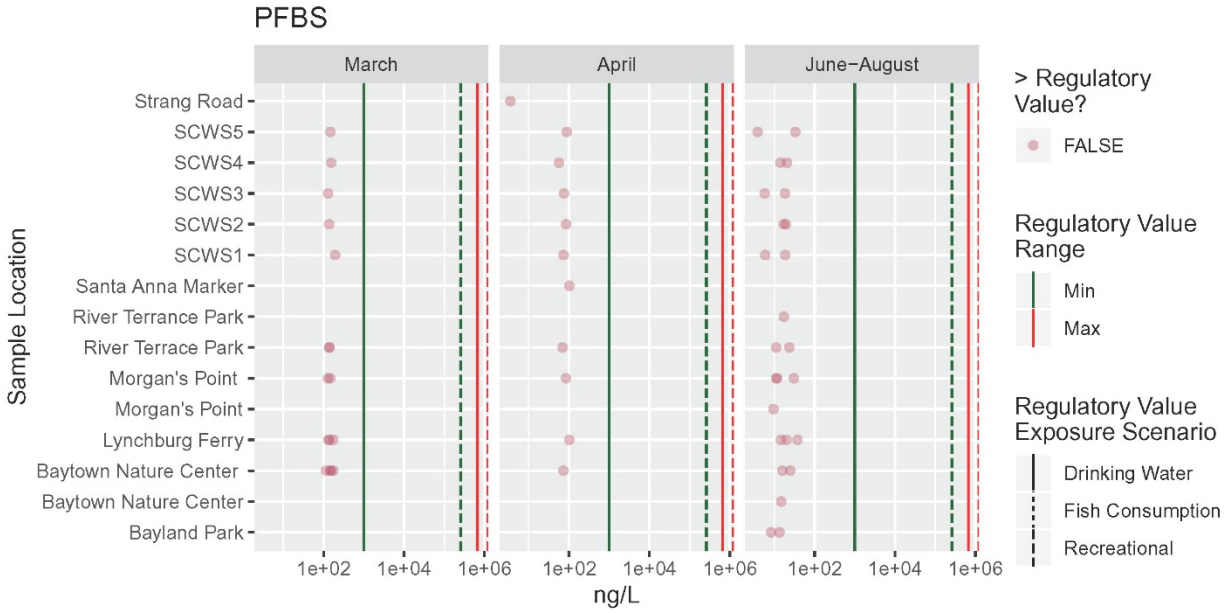
PFBS
March
April
June–August
Strang Road
SCWS5
SCWS4
SCWS3
SCWS2
SCWS1
Santa Anna Marker
River Terrance Park
River Terrace Park
Morgan's Point
Morgan's Point
Lynchburg Ferry
Baytown Nature Center
Baytown Nature Center
Bayland Park
Sample Location
1e+02
1e+04
1e+06
ng/L
> Regulatory Value?
FALSE
Regulatory Value Range
Min
Max
Regulatory Value Exposure Scenario
Drinking Water
Fish Consumption
Recreational

I.

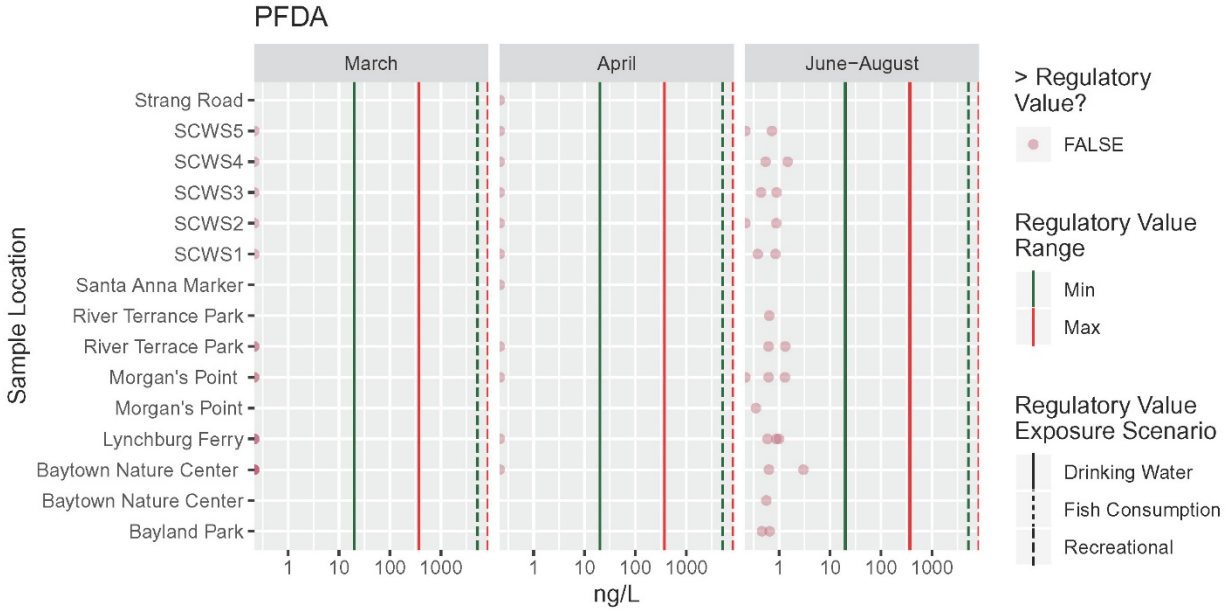
PFDA
March
April
June–August
Strang Road
SCWS5
SCWS4
SCWS3
SCWS2
SCWS1
Santa Anna Marker
River Terrance Park
River Terrace Park
Morgan's Point
Morgan's Point
Lynchburg Ferry
Baytown Nature Center
Baytown Nature Center
Bayland Park
Sample Location
1 10 100 1000
ng/L
> Regulatory Value?
FALSE
Regulatory Value Range
Min
Max
Regulatory Value Exposure Scenario
Drinking Water
Fish Consumption
Recreational

J.

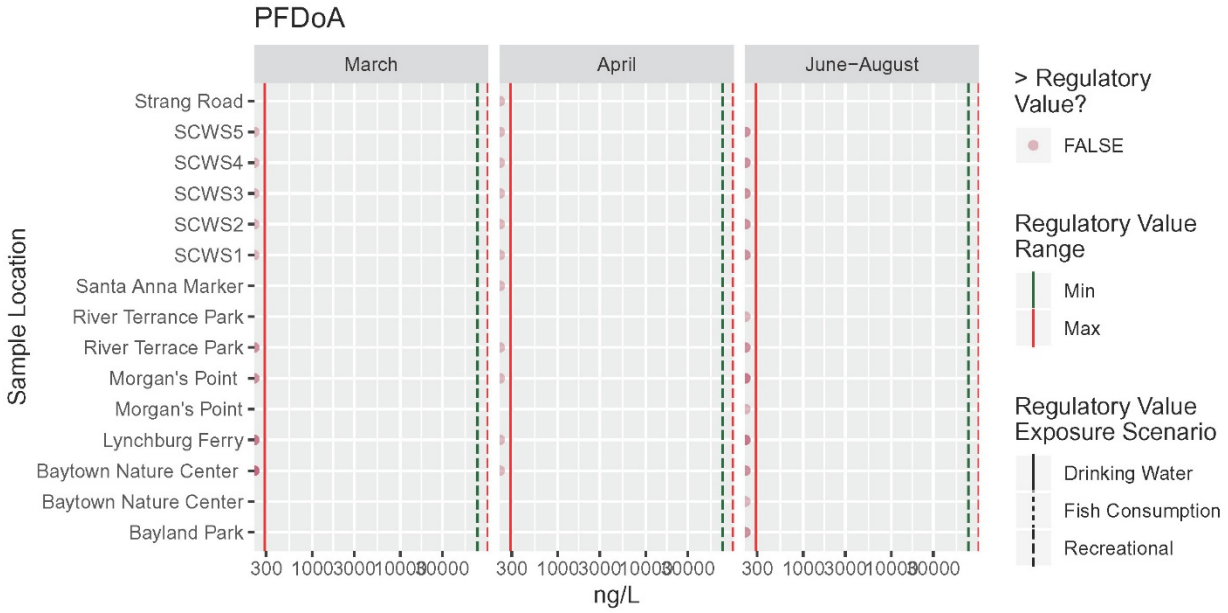
PFDoA
March
April
June–August
Strang Road
SCWS5
SCWS4
SCWS3
SCWS2
SCWS1
Santa Anna Marker
River Terrance Park
River Terrace Park
Morgan's Point
Morgan's Point
Lynchburg Ferry
Baytown Nature Center
Baytown Nature Center
Bayland Park
Sample Location
300 1000 3000 10000 30000
ng/L
> Regulatory Value?
FALSE
Regulatory Value Range
Min
Max
Regulatory Value Exposure Scenario
Drinking Water
Fish Consumption
Recreational

K.

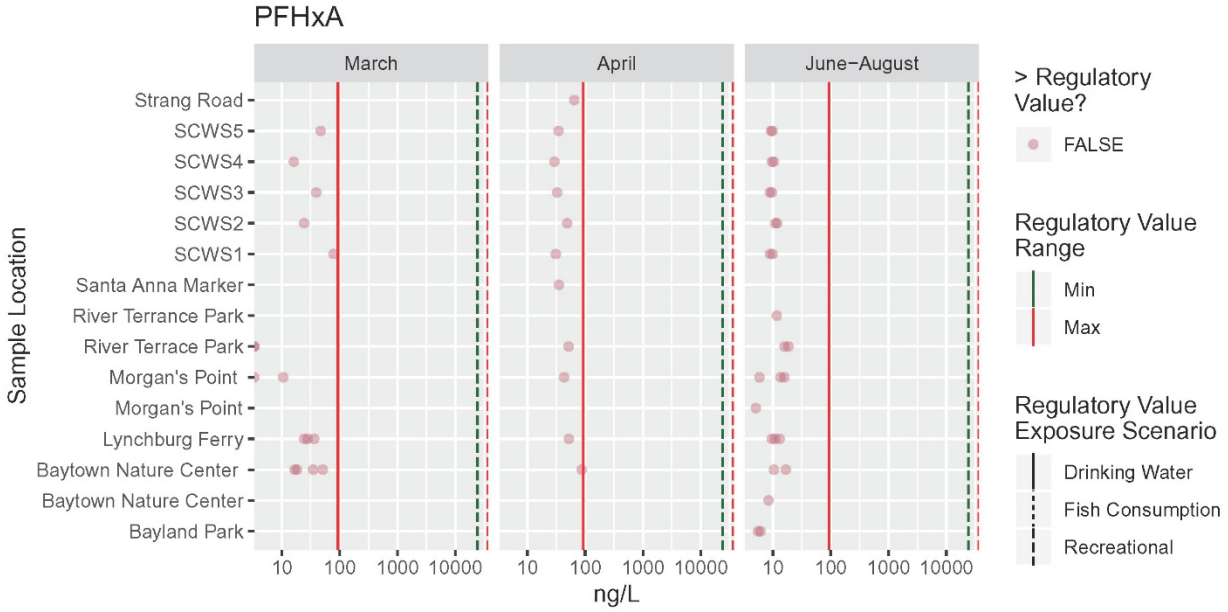
PFHxA
March
April
June–August
Strang Road
SCWS5
SCWS4
SCWS3
SCWS2
SCWS1
Santa Anna Marker
River Terrance Park
River Terrace Park
Morgan's Point
Morgan's Point
Lynchburg Ferry
Baytown Nature Center
Baytown Nature Center
Bayland Park
Sample Location
10 100 1000 10000
ng/L
> Regulatory Value?
FALSE
Regulatory Value Range
Min
Max
Regulatory Value Exposure Scenario
Drinking Water
Fish Consumption
Recreational

L.

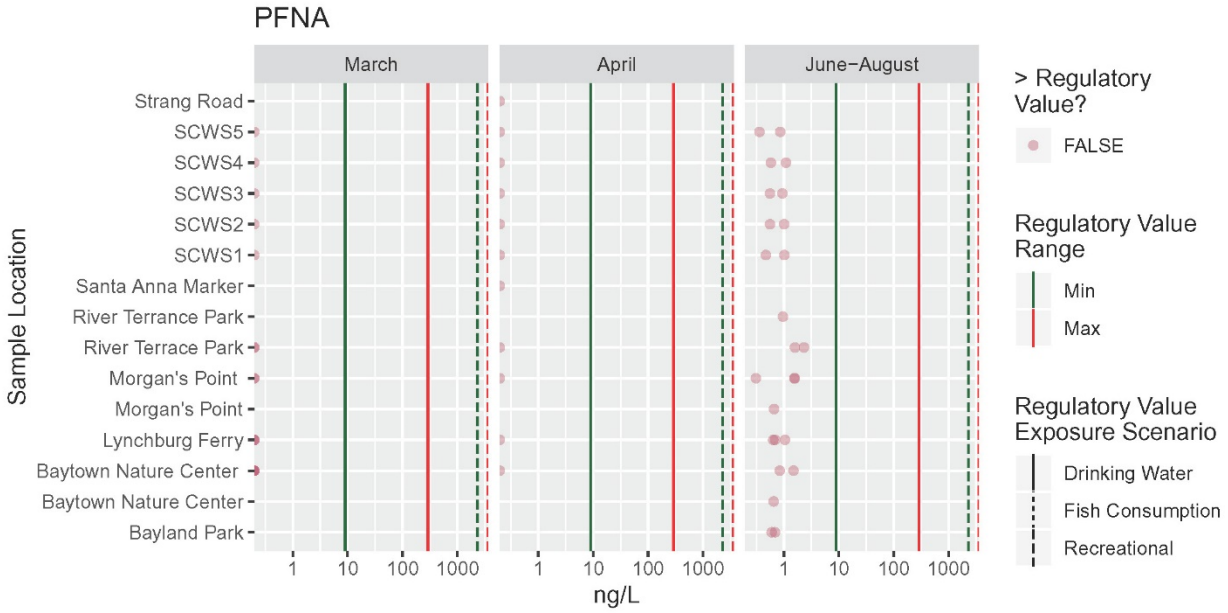
PFNA
March
April
June–August
Strang Road
SCWS5
SCWS4
SCWS3
SCWS2
SCWS1
Santa Anna Marker
River Terrance Park
River Terrace Park
Morgan's Point
Morgan's Point
Lynchburg Ferry
Baytown Nature Center
Baytown Nature Center
Bayland Park
Sample Location
1 10 100 1000
ng/L
> Regulatory Value?
FALSE
Regulatory Value Range
Min
Max
Regulatory Value Exposure Scenario
Drinking Water
Fish Consumption
Recreational

M.

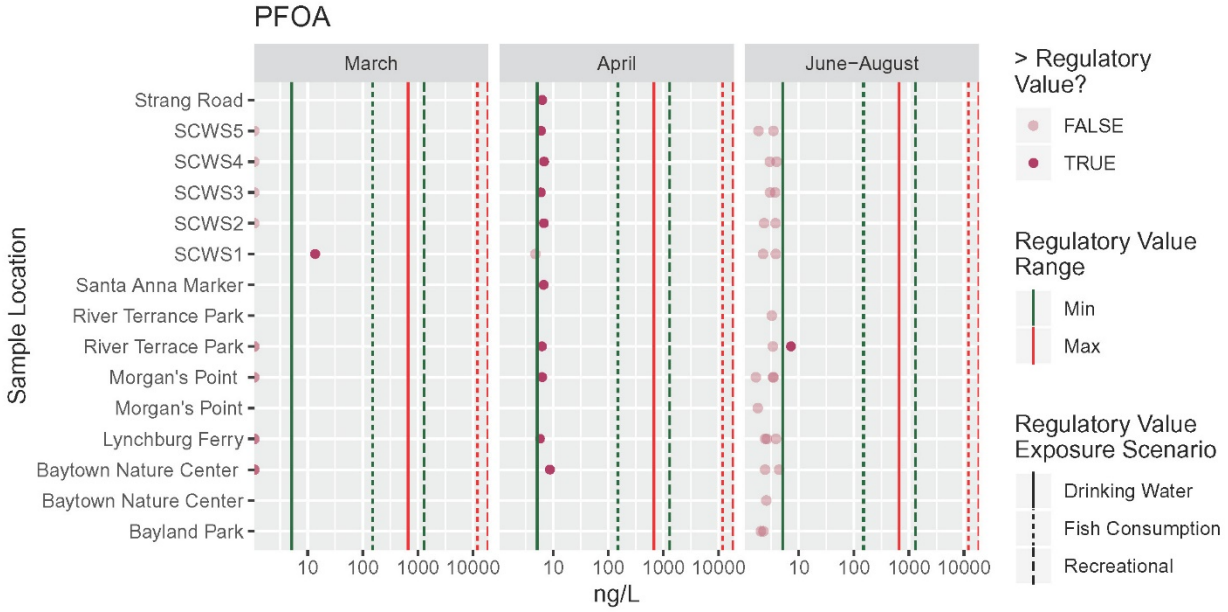
PFOA
March
April
June–August
Strang Road
SCWS5
SCWS4
SCWS3
SCWS2
SCWS1
Santa Anna Marker
River Terrance Park
River Terrace Park
Morgan's Point
Morgan's Point
Lynchburg Ferry
Baytown Nature Center
Baytown Nature Center
Bayland Park
Sample Location
10
100
1000
10000
ng/L
> Regulatory Value?
FALSE
TRUE
Regulatory Value Range
Min
Max
Regulatory Value Exposure Scenario
Drinking Water
Fish Consumption
Recreational

N.

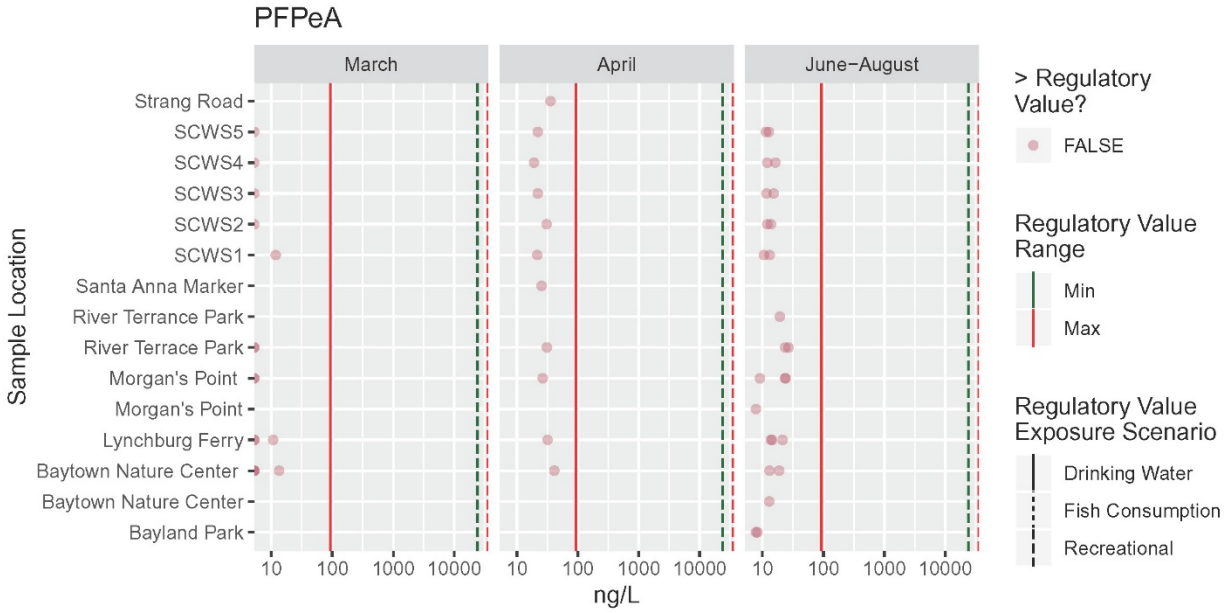
PFPeA
March
April
June–August
Strang Road
SCWS5
SCWS4
SCWS3
SCWS2
SCWS1
Santa Anna Marker
River Terrance Park
River Terrace Park
Morgan's Point
Morgan's Point
Lynchburg Ferry
Baytown Nature Center
Baytown Nature Center
Bayland Park
Sample Location
10
100
1000
10000
ng/L
> Regulatory Value?
FALSE
Regulatory Value Range
Min
Max
Regulatory Value Exposure Scenario
Drinking Water
Fish Consumption
Recreational

O.

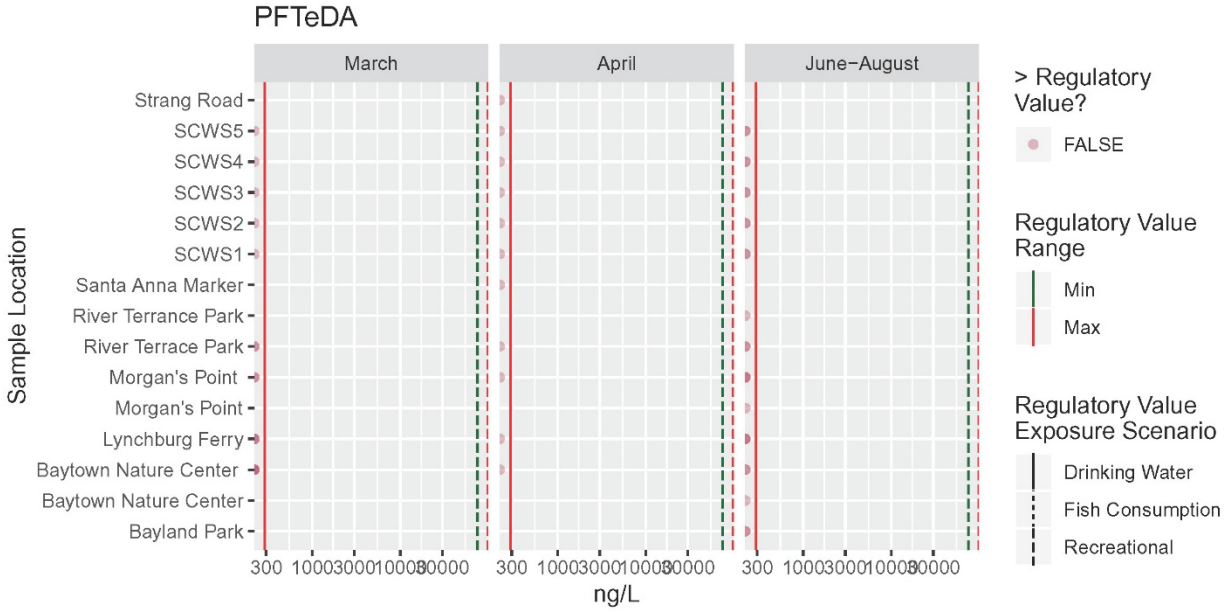

P.

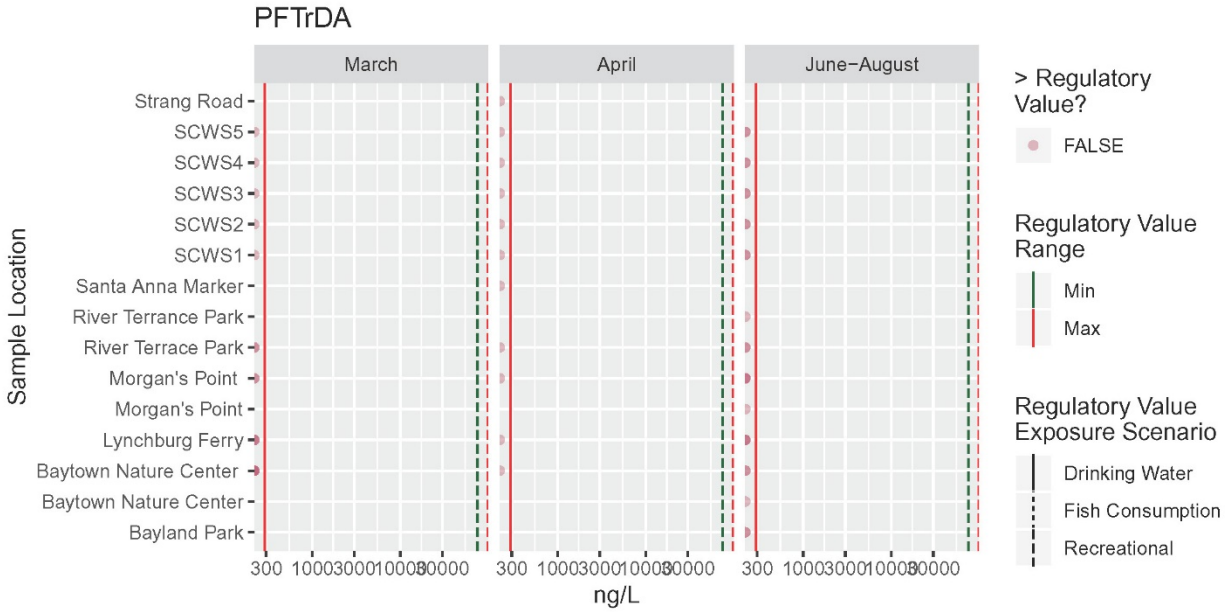

Appendix A.6. Additional Supplemental Tables

Please refer to the online excel file to retrieve Appendix A.6.

ST1: AFFFs that were reported to be used at the ITC incident in March 2019

ST2: PFAS data for HSC/GB for March 21, 2019 as reported by US EPA

ST3: Raw data for PFAS analyses in HSC/GB

ST4: PFAS Reference materials

ST5: Materials used in sample extraction

ST6: LC-MSMS method acquisition details

ST7: Representative data on the linear range and R2 for each tested compound's calibration curves

ST8: Replication of the duplicate samples

ST9: Method precision as determined by repeated injections of standards

ST10: Grid parameters for the four nested grids used with the Delft3D model

ST11: Geographical locations of the "drogue" movements with tide input into the model

ST12: Geographical locations of the "drogue" movements with tide and wind input into the model

APPENDIX B

SUPPLEMENTARY MATERIAL FOR CHAPTER III

Appendix B.1. Additional Supplemental Figures

Please refer to the online PDF file to retrieve Appendix B.1.

Appendix B.1. Additional Supplemental Tables

Please refer to the online excel file to retrieve Appendix B.2.

ST1: Overview of sampling locations, dates and analysis type

ST2: Sample Locations and Dates

ST3: Raw Data for PAH

ST4: Raw data for pesticides, industrial chemicals and PCB

ST5: Raw data for metals.

ST6: QC Data for PAH and Organics

ST7: QC Data for Metals

ST8: Cook's Distance results for each sample and metal.

ST9: Pyrogenic Index (PI) and PAH Source Apportionment Ratios

ST10: Non-cancer and cancer risk values for organic compounds

ST11: PAH BaP TEF, non-cancer and cancer risk values for organic compounds

ST12: Enrichment Factors for metals

ST13: Metals Normalized to Al

ST14: Coal Ash, Superfund and Toxic Release Inventory Locations

APPENDIX C

SUPPLEMENTARY INFORMATION CHAPTER IV

Appendix C.1. IMS-MS Instrument Settings

ESI Ionization Settings:
Gas temperature: 325 C
Drying Gas: 10 l/min
Nebulizer: 60 psi
Sheath Gas Temperature: 400 C
Sheath Gas Flow: 12 l/min

ESI Acquisition Setttings:
Frame Rate: 5.6 frames/ sec
IM Transient Rate: 2 IM transients/ frame
Max Drift Time: 60 ms
TOF Transient Rate: 503 transients/ IM transients
IM Trap
Trap Fill Time: 20000 us
Trap Release Time: 300 us

APPI Ionization Settings:
Gas temperature: 300 C
Vaporizer: 300 C
Drying Gas: 8 l/min
Nebulizer: 20 psi
VCap: 3000 V

APPI Acquisition:
Frame Rate: 0.9 frames/ sec
IM Transient Rate: 18 IM transients/ frame
Max Drift Time: 60 ms
TOF Transient Rate: 503 transients/ IM transients
IM Trap
Trap Fill Time: 20000 us
Trap Release Time: 300 us

Advanced Parameters:
IM Front Funnel – High Pressure Funnel Delta: 150 V
IM Front Funnel – High Pressure Funnel RF: 150 V
IM Front Funnel – Trap Funnel Delta: 180 V
IM Front Funnel – Trap Funnel RF: 150 V
IM Front Funnel – Trap Funnel Exit: 10 V
IM Trap – Trap Entrance Grid Low: 97 V
IM Trap – Trap Entrance Grid Delta: 10 V
IM Trap – Trap Entrance: 91 V
IM Trap – Trap Exit: 90 V
IM Trap – Trap Exit Grid 1 Low: 87.2 V
IM Trap – Trap Exit Grid 1 Delta: 4 V
IM Trap – Trap Exit Grid 2 Low: 86.6 V
IM Trap – Trap Exit Grid 2 Delta: 8.5 V
IM Drift Tube – Drift Tube Entrance Voltage: 1700 V
IM Drift Tube – Drift Tube Exit Voltage: 250 V
IM Rear Funnel – Rear Funnel Entrance: 240 V
IM Rear Funnel – Rear Funnel RF: 150 V
IM Rear Funnel – Rear Funnel Exit: 43 V
IM Rear Funnel – IM Hex Delta: -8 V
IM Rear Funnel – IM Hex RF: 600 V
IM Rear Funnel – IM Hex Entrance: 41 V
IM – IM Hex Delta Delta: 0 V
IM – Collision Cell Delta Delta: 0 V
IM – IBC Delta Delta: 0 V

Appendix C.2. List of Chemicals with calculated CCS and m/z values

Please refer to the online excel file to retrieve Appendix C.2.